

**PHARMACOKINETICS,
BIO- DISTRIBUTION AND DOSIMETRY OF SOME WIDELY USED
RADIOPHARMACEUTICALS IN NUCLEAR MEDICINE UNDER
BANGLADESH CONDITION**



**A THESIS SUBMITTED TO
BANGLADESH UNIVERSITY OF ENGINEERING AND
TECHNOLOGY
FOR THE DEGREE OF MASTER OF PHILOSOPHY
IN
PHYSICS**

**BY
NAUREEN MAHBUB RAHMAN**

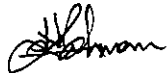
**DEPARTMENT OF PHYSICS
BANGLADESH UNIVERSITY OF ENGINEERING AND
TECHNOLOGY**

December, 2001



Certificate

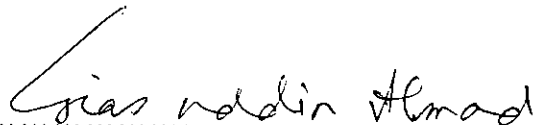
This is to certify that this research work presented herein is original. This thesis or any part of it has not been submitted for the award of any other degree or diploma.



.....
(Naureen Mahbub Rahman)



.....
(Dr. M.A. Karim)
Co-Supervisor



.....
(Prof. Dr. Gias Uddin Ahmad)
Supervisor

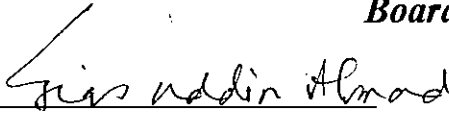
**BANGLADESH UNIVERSITY OF ENGINEERING AND TECHNOLOGY
DHAKA
DEPARTMENT OF PHYSICS**





Certification of Thesis work


The thesis titled "PHARMACOKINETICS, BIO-DISTRIBUTION AND DOSIMETRY OF SOME WIDELY USED RADIOPHARMACEUTICALS IN NUCLEAR MEDICINE UNDER BANGLADESH CONDITION" submitted by NAUREEN MAHBUB RAHMAN, Roll No: 9414006P, Session: 1993-94-95 has been accepted as satisfactory in partial fulfillment for the requirement for the degree of Master of Philosophy on January 30, 2002.

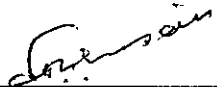
Board of Examiners

1. 
Dr. Gias uddin Ahmad (Supervisor) Chairman
Professor
Department of Physics, BUET

2. 
Dr. M. A. Karim (Co-Supervisor) Member
Director
Institute of Nuclear Medicine
BSM Medical University, Shahbag
Dhaka

3. 
Dr. Nazma Zaman Member (Ex-officio)
Professor and Head
Department of Physics, BUET

4. 
Dr. Momimul Huq Member
Professor
Department of Physics, BUET

5. 
Dr. S. R. Husain Member (External)
Chief Medical Physicist
Delta Medical Center Ltd. (Oncology Unit)
Mirpur, Dhaka

DEDICATED

TO

MY PARENTS

Acknowledgement

I express my profound indebtedness and gratitude to my supervisor Dr. Gias uddin Ahmad, Professor, Department of Physics, Bangladesh University of Engineering and Technology (BUET) for his constant guidance. I am sincerely grateful to him for his untiring help and advice while preparing this manuscript and overall encouragement throughout the period of study.

Sincere thanks are offered to my co-supervisor Dr. M.A. Karim, Director, Institute Nuclear Medicine (INM) of BAEC, Dhaka for his moral support and assistance during my research work.

I gratefully acknowledge and offer thanks to Mr. Nurul Islam, Senior Scientific Officer, Institute Nuclear Medicine (INM), BAEC, Dhaka, for his constant help and guidance throughout the period of this research.

I am grateful to Prof. Dr. Nazma Zaman, Head, Department of Physics, BUET, for her inspiration during the tenure of the study. I extend gratitude to my teachers Dr. A. Asgar, Dr. Mominul Huq and Dr. Md. A.H. Bhuiyan, Professors, Department of Physics, BUET; Dr. Jiban Podder, Ms. Dil Afroze Ahmed, Dr. F.A. Khan, Ms. Fahima Khanam, Associate Professors, Department of Physics, BUET; Dr. Md. Nazrul Islam, Dr. A.K.M. Akter Hossain, Dr. Md. Mostak Hossain Assistant Professors, of the Department of Physics, BUET, and Dr. Fatema Nasreen of Physics Department Eden Girls College, Dhaka and also to my friends Mrs. Afia Begum and Mr. Ashraf, Lecturers, Department of Physics, BUET for their encouragement and assistance during the tenure of this research work.

Sincere thanks are also extended to Dr. Fauzia Moslem and Dr. Lutfun Nisa Chief Medical Officers; Dr. Sufia Yasmeen, Dr. Faridul Alam, Dr. Mahbubul Haque, Principle Medical Officers; Mrs. Kamila Afroj, Senior Scientific Officer; Dr. Mizanul Hasan, Dr. Nurun Nahar, Dr. Fatima Sultana Haque, Dr. Jesmina Ara Haque, Senior Medical Officers, of INM, BAEC, Dhaka, for their suggestions and co-operation while conducting this work.

I am grateful to the authorities of Bangladesh University Grants Commission, Dhaka, for allowing me to conduct this research work whilst in-service. Further, thanks are offered to Dr. Matiur Rahman Mian, Director, Institute of Scientific Instrumentation (ISI), Dhaka for encouragement and moral support during the period of this work.

I express heartfelt indebtedness to Mr. A.K.M. Mushifur Rahman, Assistant Engineer, Local Government and Engineering Department (LGED), for his help in completing the calculations contained in the thesis.

Thanks are due to Engg. Mr. Sharif, Systems Manager, Siemens International, Bangladesh for providing the specifications of Siemens Gamma Camera which was used in this study and to Mrs. Nurjahan of INM for help in collecting the data of patients, Mr. Alauddin, Librarian of INM and also to my student Mr. Mamunur Rashid, Sub Asst. Engg, Maintenance Division, BIRDEM and Mr. Aziz Ahmed for their help in performing the research work.

I am grateful to the authority of Bangladesh University of Engineering and Technology for giving me necessary permission and providing financial support for carrying out this research work.

It is, however, impossible to express gratitude to one's kith and kin but it is no exaggeration to say that without the guidance, valuable suggestions, understanding and constant encouragement of my parents Dr.S.M.Rahman and Dr.(Mrs) Sultana Ahmed, my husband Mr. A.K.M.Mushfiqur Rahman, my sister Miss. Shahreen M. Rahman, and my uncle Mr.G.M.Ahmed and my brother-in-law Mr. Mizanur Rahman this piece of research work would never have been completed.

Naureen M.Rahman
Department of Physics
BUET, Dhaka-1000
December, 2001

ABSTRACT

The present study was carried out with forty patients, twenty each, for kidney and liver and were categorized in three different age groups of 21-30 years, 31-40 years and 41-50 years. The radiopharmaceuticals, ^{99m}Tc -DTPA for target organ kidney and ^{99m}Tc -Tin Colloid for target organ liver were used as the injected radiopharmaceuticals. Besides the target organs kidney and liver, other surrounding organs' distribution was also measured.

^{99m}Tc -DTPA (Diethylene-Triamine-Pentaacetic Acid) was introduced in individual human bodies to study the renal function and ^{99m}Tc -Tin Colloid was introduced to study the liver function in-terms of biodistribution and also in-terms of measuring the cumulative activity, the dose absorbed by different organs of the body and also by the radiation absorbed dose in the whole body. For interpretation of the clinical findings pharmacokinetic studies were also performed in kidneys of twenty patients of different age group. Data of pharmacokinetic distribution of radiation dose from Tc-99m DTPA were measured in twenty individuals who had undergone diagnostic process.

The biodistribution of Tc-99m DTPA was found highest in lungs followed by kidneys. In lungs it varied from 9.31% to 13.26% and in kidney biodistribution ranged from 5.68% to 10.28. The lowest biodistribution was recorded in bones of the body which indicated that the radiopharmaceutical did not move sufficiently through the more solid part of the body. The biodistribution of ^{99m}Tc -Tin Colloid was highest in liver which ranged between 46.06% and 70.22%, the average value being 62.58%. It is observed that, most of the radiopharmaceutical remained concentrated in the liver, which indicates the high affinity of the radiopharmaceutical to the organ. The lowest biodistribution was recorded in the

small intestine (SI) which shows a lower affinity of the radiopharmaceutical to the small intestine.

In case of kidney, the highest amount of ^{99m}Tc -DTPA was absorbed in the target organ kidney which ranged from 0.132 to 0.293 rads, the average value being 0.182 rad. Lowest absorption was recorded in thyroid. This indicated that, the movement of the radiopharmaceutical varied according to the position of the organ from the source organ. In case of liver, The highest amount of radiopharmaceutical was absorbed in the target organ liver, the average value was 1.2445 rads. Lowest absorption was recorded in bladder.

The radiation absorbed dose in the kidney ranged from 0.0383 to 0.06952 rad per mCi. The mean value was 0.048 rad/mCi. Some variations were observed in radiation absorbed dose of twenty patients but these variation is not very significant .The variation may be due to the difference in age group of patients. The 20 patients were grouped into three categories, 5 being in the 21-30 years age group, 8 in the 31-40 years age group and 7 in the 41-50 years age group. The radiation absorbed dose is higher in patients of lower age group of 21-30 years, followed by middle age group of 31-40 years. The lowest absorbed dose was observed in older age group of 41-50 years.

The radiation absorbed dose in the liver of the twenty patients ranged between 0.1909 rads/ mCi to 0.2816 rads/mCi, the mean value being 0.2482 rads/mCi. A little variations were observed in radiation absorbed dose in twenty patients due to the difference in age group of patients. Among all of them, 37% of patients showed highest radiation absorption who are in the younger group. This was followed by middle aged patient group which is 33% and the older group include only 30%. This study indicates that the radiation absorption was higher in young age patients who are normally much healthier and stronger.

The radiation absorbed dose in adults for Tc-99m DTPA and also for Tc-99m Tin Colloid was very much within the limit as reported in world

literature. Dose estimates for the patients, studied at different times included in this study are in reasonable accord for individual organ doses between different patients.

The biodistribution of ^{99m}Tc -DTPA and dose absorbed in kidney alone/5mCi of the injected dose was also compared. It is obtained that there is similarity in the trend of biodistribution and dose absorbed by kidney. The patient who showed higher biodistribution, had higher dose absorption in kidney and vice-versa. This was same for the comparison between biodistribution of the radiopharmaceutical and the dose absorption in liver alone due to the injected dose of 5mCi.

A study was undertaken to observe the radioactivity remaining in the body and its clearance with time. It is found that the three half-lives of the radiopharmaceutical was observed at 9,90 and 600 min in case of all the samples taken after 3,5,7 and 11th min of infusion. This indicates that the remaining activity of the radiopharmaceutical becomes negligible after 10 hrs of infusion and thereafter the activity becomes gradually cleared. So the patients are free of any hazardous effect of the radiopharmaceuticals. The obtained result for both the radiopharmaceutical was very much within the limit as reported before. They are obviously in agreement with the result obtained by other investigators.

TABLE CONTENTS

	Pages
Acknowledgements	iii
Abstract	vi
Contents	ix
List Of Tables	x
List Of Figures	xii



CONTENTS

1. CHAPTER -1 INTRODUCTION	1
1.1. General	2
1.2. Radioactivity	7
1.3. Biological Effect of Radiation	15
1.4. The Era of Nuclear Medicine	20
1.5. Aims and Objectives	25
2. CHAPTER -2 LITERATURE REVIEW	27
2.1. Introduction	28
2.2. Review	28
3. CHAPTER -3 EXPERIMENTAL DETAILS	49
3.1. Introduction	50
3.2. Equipment setup	63
3.3. Radiopharmaceuticals	82
3.4. Anatomical Portray of the Organ Understudy	96
3.5. Methodology of the Proposed Topic	99
3.6. Experimental Procedure	111
4. CHAPTER -4 RESULTS AND DISCUSSION	116
4.1. Introduction	117
4.2. Results of Target Organ Kidney	118
4.3. Results of Target Organ Liver	140
4.4. Discussion	153
5. CHAPTER - 5 CONCLUSION	155
6. CHAPTER - 6 REFERENCES	158
7. CHAPTER - 7 APPENDIX	170

LIST OF TABLES

Sl.No.	Table No.		Pages
1.	3.1	Characteristics of commonly used radionuclide	84
2.	3.2	Radionuclide generators used in nuclear medicine	88
3.	3.3	Renal radiopharmaceutical	92
4.	3.4	Absorbed Dose Per Unit Cumulative Activity (Rad/ μ Ci-hrs) For ^{99m}Tc	101
5.	4.1	Biodistribution of the radiopharmaceutical in different organs (target organ: kidney)	119
6.	4.2	Cumulative activity of the radiopharmaceutical in different organs (target organ: kidney)	121
7.	4.3	Absorbed dose of the radiopharmaceutical in different organs (target organ: kidney)	124
8.	4.4	Radiation absorbed dose of the radiopharmaceutical in patients (target organ: kidney)	126
9.	4.5	Radiation absorbed dose by kidney Vs biodistribution of kidney	130
10.	4.6	Pharmacokinetic study of ^{99m}Tc DTPA (after 3 rd minute of infusion)	132
11.	4.7	Pharmacokinetic study of ^{99m}Tc DTPA (after 5 th minute of infusion)	134

Contd...

Sl.No.	Table No		Pages
12.	4.8	Pharmacokinetic study of ^{99m}Tc DTPA (after 7 th minute of infusion)	136
13.	4.9	Pharmacokinetic study of ^{99m}Tc DTPA (after 11 th minute of infusion)	138
14.	4.10	Biodistribution of the radiopharmaceutical in different organ (target organ: liver)	141
15.	4.11	Cumulative activity of the radiopharmaceutical in different organs (target organ: liver)	144
16.	4.12	Absorbed dose of the radiopharmaceutical in different organs (target organ: liver)	145
17.	4.13	Radiation absorbed dose of the radiopharmaceutical in patients (target organ: liver)	147
18.	4.14	Radiation absorbed dose by liver Vs biodistribution of liver	150

LIST OF FIGURE

Sl.No.	Figures	Pages
1.	1.1 Major pathway of radionuclides to man in the event of an uncontrolled release of radioactivity	3
2.	1.2.1 Uranium-238 decay series	4
3.	1.2.2 Thorium-232 decay series	5
4.	1.2.3 Actinium decay series	6
5.	1.3.1 Radioactive decay scheme for Alpha decay of ^{226}Ra	8
6.	1.3.2 Radioactive decay scheme for Negatron decay of ^{137}Cs	8
7.	1.3.3 Simplified decay scheme for ^{99}Mo	9
8.	1.3.4 Radioactive decay scheme for ^{60}Co	9
9.	1.3.5 Radioactive decay scheme for Positron Decay of ^{22}Na	10
10.	1.3.6 Iodine-131 transformation(decay) scheme	10
11.	1.4 Development of cell injury	19
12.	1.5 Schematic diagram illustrating the absorption of energy from radiation resulting in biological damage	21
13.	3.1 Measured current Versus applied voltages for ionization detectors	53
14.	3.2 Single probe rectilinear scanner illustrating the component parts of typical system	61
15.	3.3 A schematic electronic diagram of a CRT- Cathode Ray Tube, PHA- Pulse-Height Analyzer, PM- Photomultiplier Tube	64
16.	3.4 A typical gamma camera	66
17.	3.5 Different designs of collimators	67
18.	3.6 Schematic illustration of four typical collimator types used in nuclear medicine	68

Contd..

Sl.No	Figures	Pages
19.	3.7	Basic principle of photomultiplier (PM) tube. 70
20.	3.8	Arrangement of seven photomultiplier (PM) tubes to produce X and Y, location of the X- Ray interaction in the detector, X+, X-, Y+ and Y- pulse are obtained by the outputs of all PM tubes weighted by capacitors for the location of each PM tubes in relation to the site of X-Ray interaction. 71
21.	3.9	A three- head Single Photon Emission Computed Tomography camera, TRIAD model 74
22.	3.10	Basic principle of reconstruction of an image by back projection technique 76
23.	3.11	An illustration of the back projection technique using the data from an acquisition matrix into a reconstruction matrix 78
24.	3.12	(a) Isomeric transition of ^{99m}Tc ten percent of decay follows internal conversion 87
25.		(b) Internal conversion process 87
26.	3.13	Cross-sectional drawing of A $^{99}\text{Mo} - ^{99m}\text{Tc}$ generator 89
27.	3.14	Build up and decay of ^{99m}Tc generator eluted on days 0, 1.4, 2 and 4 89
28.	3.15	Diagram of coronal section of right kidney 96
29.	3.16	Liver in normal position relative to rib cage, diaphragm, stomach, and pancreas 98
30.	3.17	Absorbed dose delivered to target organ from one or more source organs containing radioactivity is calculated by absorbed fraction dosimeter method 99

Contd..

Sl.No	Figures	Pages
31.	3.18 Representation of an “Average Man” used for MIRD dose calculations and tables.	102
32.	3.19 Hypothetical time activity curve for radioactivity in a source organ.	103
33.	3.20 (a) Photograph of static study of kidney	117
34.	3.20 (b) Photograph of static study of kidney	117
35.	3.20 (c) Photograph of static study of kidney	113
36.	3.20 (d) Photograph of dynamic study of kidney	113
37.	3.20 (e) Photograph of static study of liver	114
38.	3.20 (f) Photograph of static study of Liver	114
39.	3.20 (g) Photograph of dynamic study of kidney	115
40.	4.1 Graph of biodistribution of the radiopharmaceutical Different Organs (target Organ: kidney)	120
41.	4.2 Graph of radiation absorbed dose of the radiopharmaceutical in a patient according to Different Age Group	127
42.	4.3 Graph of radiation absorbed dose of the radiopharmaceutical in a patient according to Different Age Group	128
43.	4.4 Graph of radiation dose absorbed by kidney Vs Biodistribution of Kidney	130
44.	4.5 Graph of pharmacokinetic study of Tc ^{99m} DTPA (in left kidney)	133
45.	4.6 Graph of pharmacokinetic study of Tc ^{99m} DTPA (in right kidney)	135

Cont...

Sl.No	Figures		Pages
46.	4.7	Graph of pharmacokinetic study of Tc ^{99m} DTPA (comparison between left and right kidney)	137
47.	4.8	Graph of pharmacokinetic study of Tc ^{99m} DTPA (average between left and right kidney)	139
48.	4.9	Graph of biodistribution of different organs (target organ: liver)	142
49.	4.10	Graph radiation absorbed dose in a patient according to different age group (target organ: liver)	148
50.	4.11	Graph radiation absorbed dose in a patient according to different age group (target organ: liver)	149
51.	4.12	Graph of radiation absorbed dose by liver Vs biodistribution of radiopharmaceutical within the liver	151

CHAPTER 1

INTRODUCTION

CHAPTER 1

INTRODUCTION

1.1 General

All particulate and electromagnetic radiations interact with the atom of the absorber while passing through it, producing ionization and excitation of the absorber atoms. These radiations are known as ionizing radiations. From the very beginning of the creation of the earth, man is continuously being exposed to ionizing radiation, from natural background radiation to all artificial sources of radiation (Figure: 1.1).

Nearly three thousand nuclides are known, of which approximately 2700 are radioactive nuclides and the rest are stable^[1]. The natural background radiation originates from these terrestrial and extra-terrestrial radionuclides. These radionuclides are the member of three natural radioactive series-Thorium, Uranium and Actinium along with their progeny (Figure: 1.2.1, 1.2.2, 1.2.3). Another series is Neptunium (^{237}Np , $T_{1/2}$ 2.2×10^6 yr.) with its fifteen daughters arising from artificial origin which is also a major contributor of the background radiation occurring naturally. Besides these, there are a few non-series single natural radionuclides like ^3H , ^{14}C , ^{40}K and ^{87}Rb which contributes a noticeable amount of dose to man, both internally and externally; the gaseous radioactive elements in the atmosphere like Thoron, Radon etc. and Cosmic rays also add to it. Majority of the radionuclides is artificially produced in the cyclotron and reactor. Some short-lived radionuclides are also available from the radionuclides-generator. The origin of the artificial radioactivity are nuclear explosion tests, reprocessing of nuclear fuels, uses of radioisotopes in medicines, agricultural research, sea bed disposal (Estonia, Kara Sea, Russian Lake etc.), accidental occurrence in nuclear facilities (Kystym 1957, Windscale

1957, Three-Mile Island 1976, Chernobyl 1987 etc), radioactive laboratories and test of nuclear weapons.

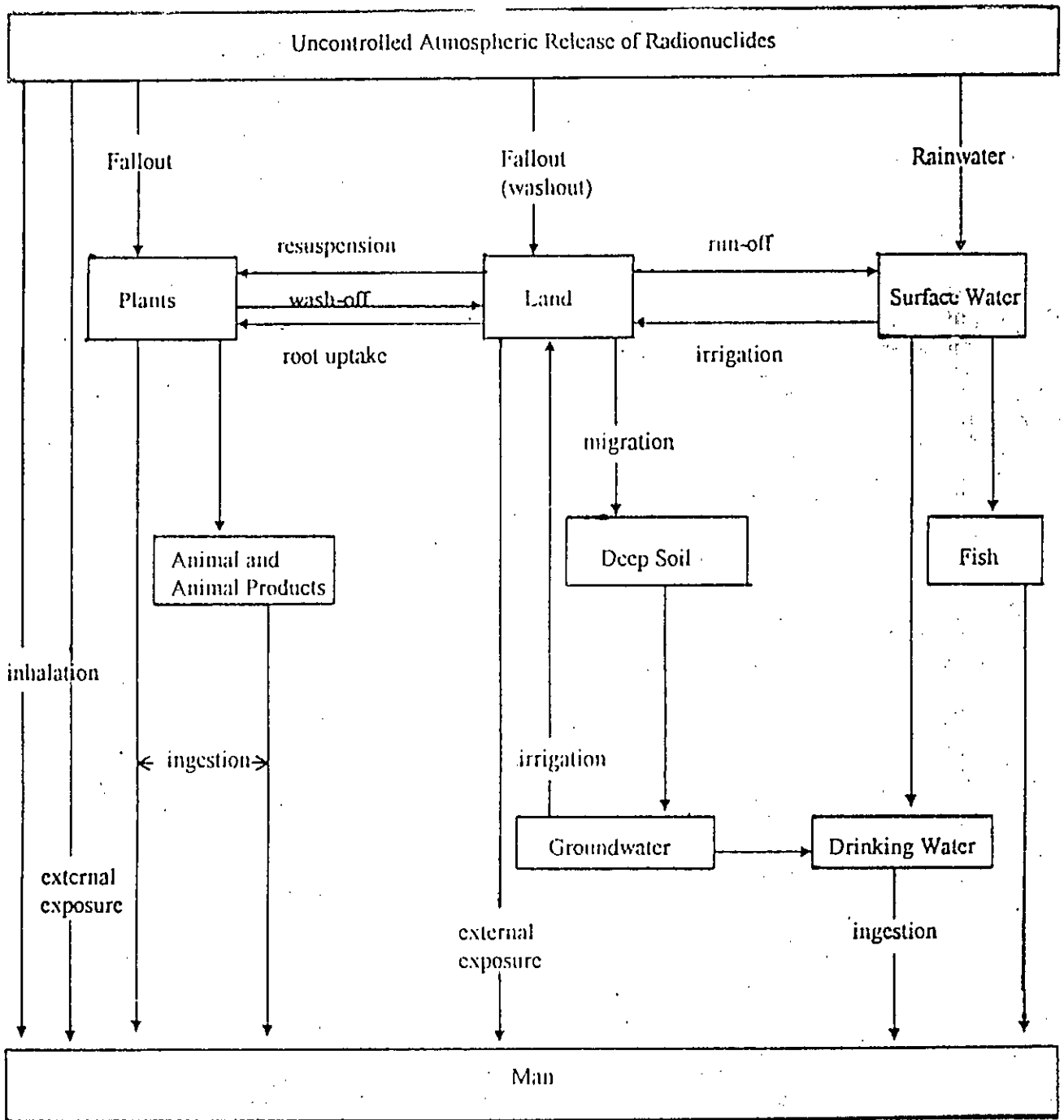


Figure 1.1 Major Pathways of Radionuclides To Man in The Event of An Uncontrolled Release of Radioactivity^[87]

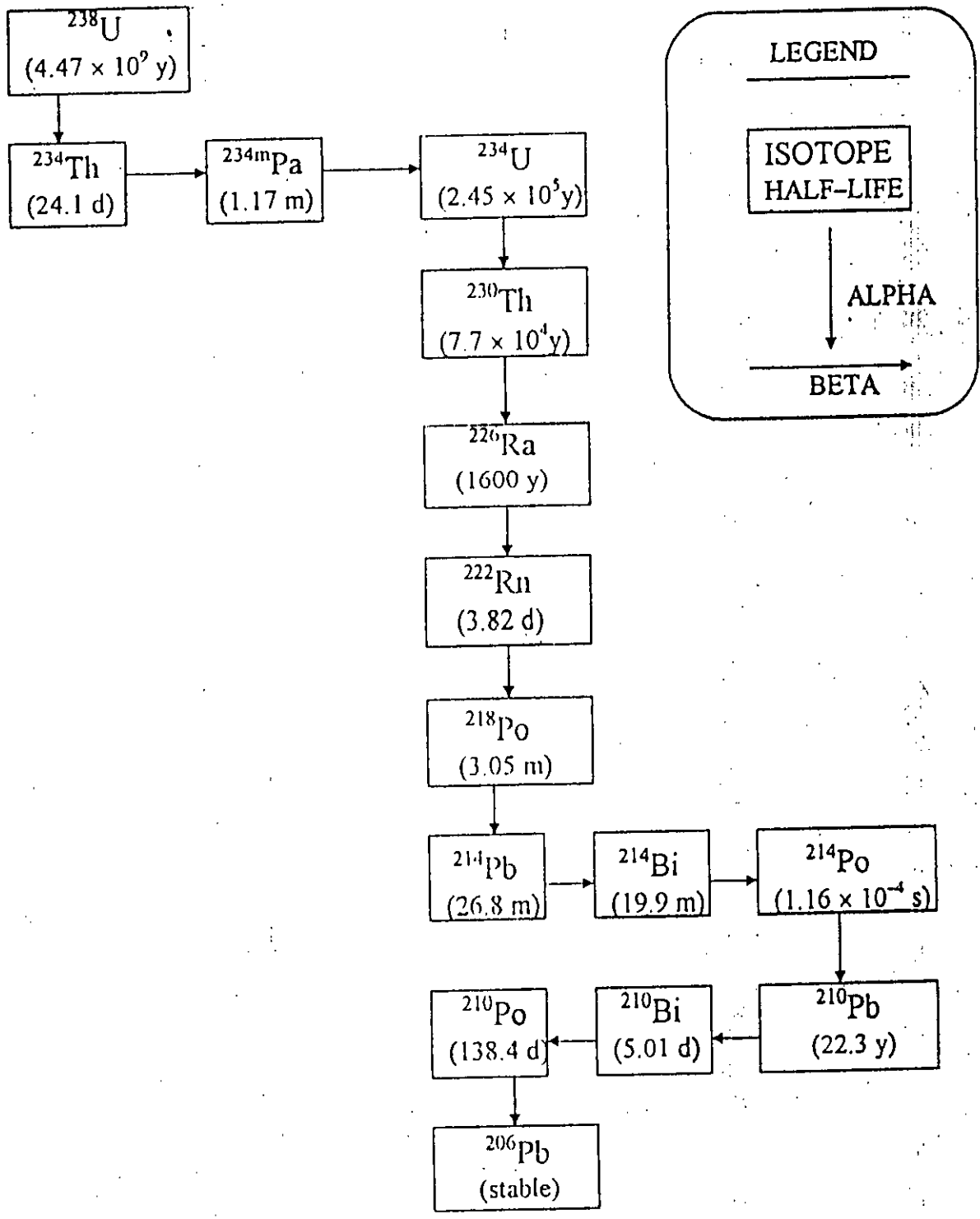


Figure 1.2.1 Uranium-238 Decay Series

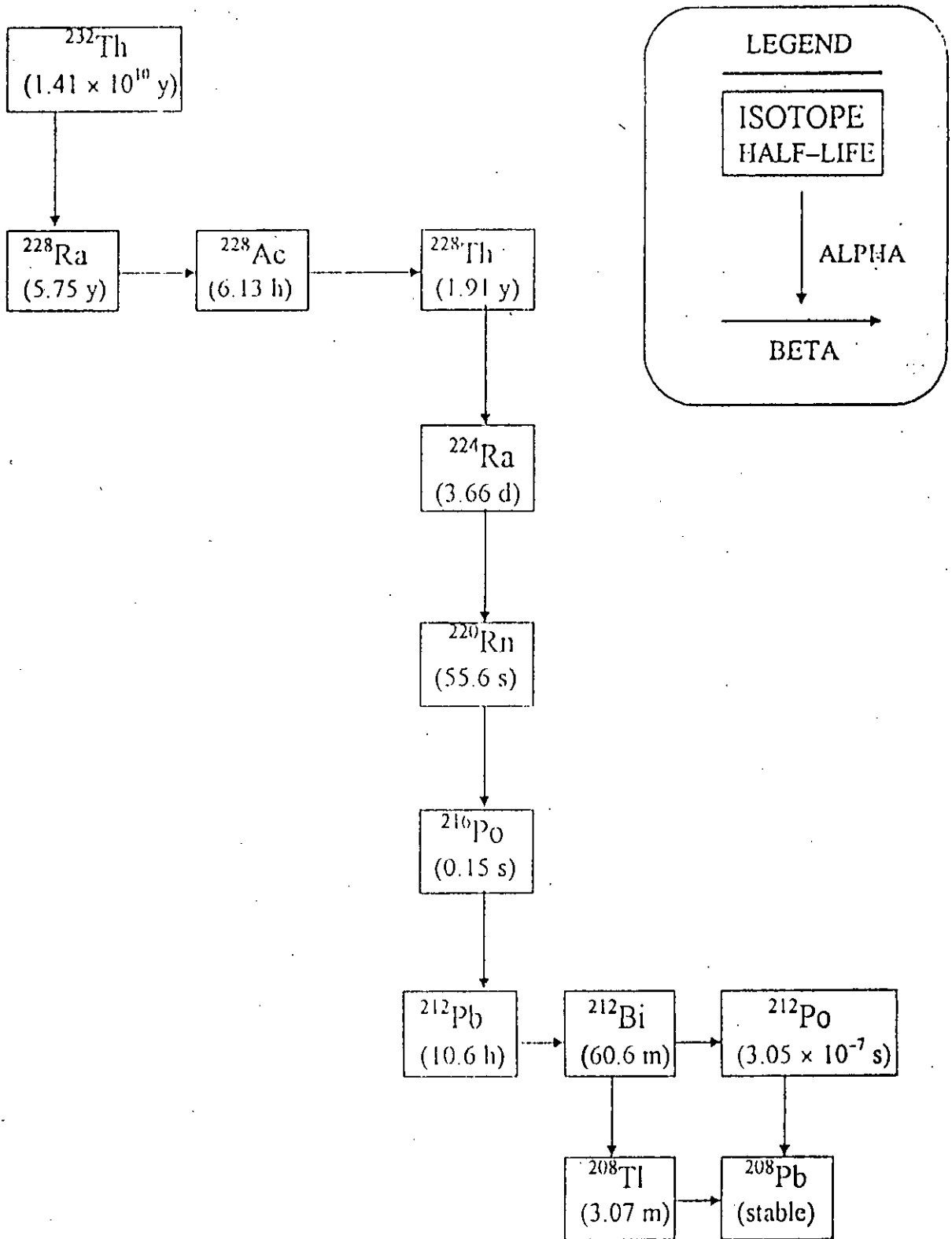


Figure 1.2.2 Thorium-232 Decay Series

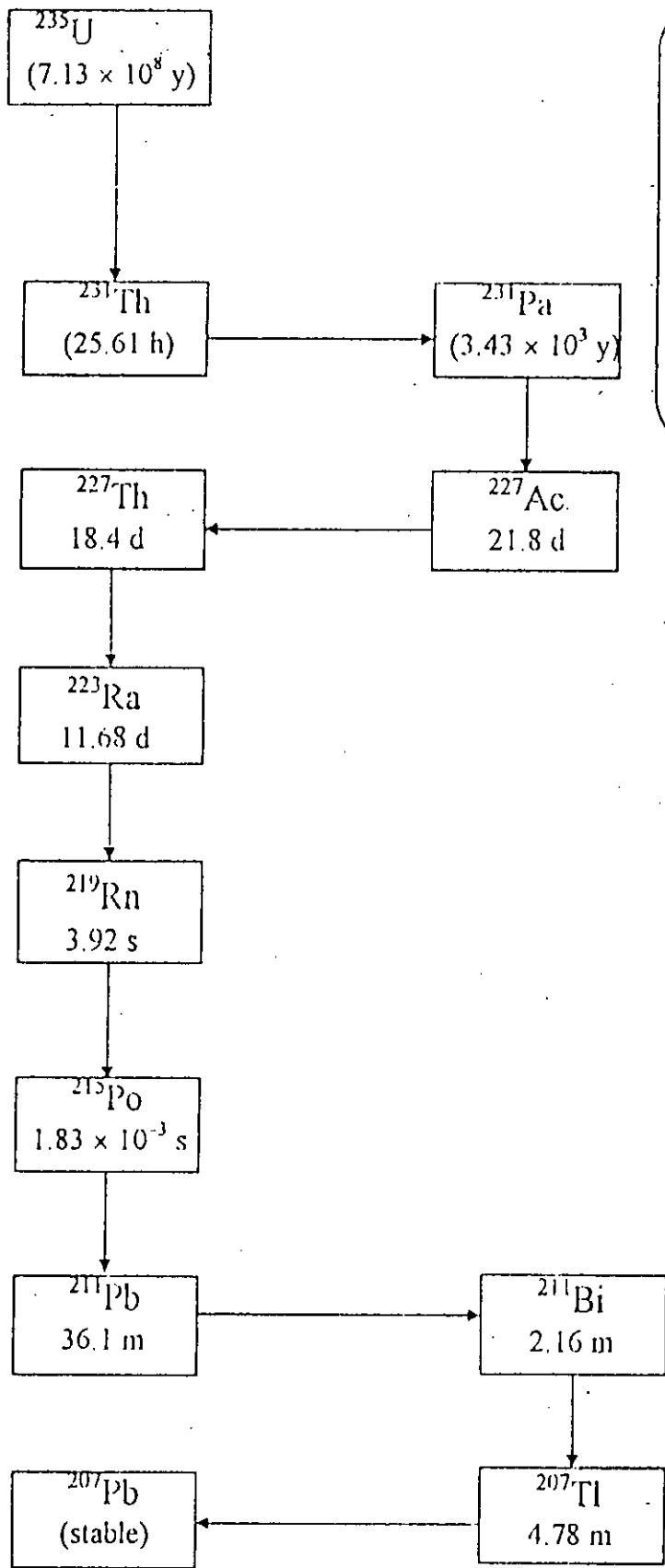


Figure 1.2.3 Actinium Decay Series

1.2 Radioactivity

Radioactivity may be defined as spontaneous nuclear transformation that result in the formation of new element^[2]. All these transformations are accomplished by various mechanisms, like alpha particle emission, beta particle and positron emission and orbital electron capture, gamma ray emission, isomeric transition etc. Each of the reaction may or may not be accompanied by gamma radiation (Figure: 1.3.1, 1.3.2, 1.3.3, 1.3.4, 1.3.5, 1.3.6).

Radioactivity and radioactive properties of nuclides are determined by nuclear considerations only and are independent of chemical and physical states of radioisotope. The exact mode of radioactive transformation depends only on two factors (i) the particular type of nuclear instability i.e. whether the neutron to proton ratio is either too high or too low for the particular nuclide under consideration and (ii) on the mass-energy relationship among the parent nucleus, daughter nucleus and the emitted particle.

The alpha particle:

The alpha particle is highly energetic helium nucleus. When the neutron to proton ratio in a radioactive isotope is too low the nucleus of the radioisotope emits alpha particle. Alpha particle is positively charged massive particle. It has got two protons and two neutrons as its constituent. In alpha transition the atomic and mass numbers are conserved. So it follows that, the emission of α -particle results in a daughter whose atomic number is two less than that of the parent, also, whose mass number is four less than that of the parent. With one exception, $^{147}_{62}\text{Sn}$, naturally occurring α -emitters are found only among elements of atomic number greater than 82.

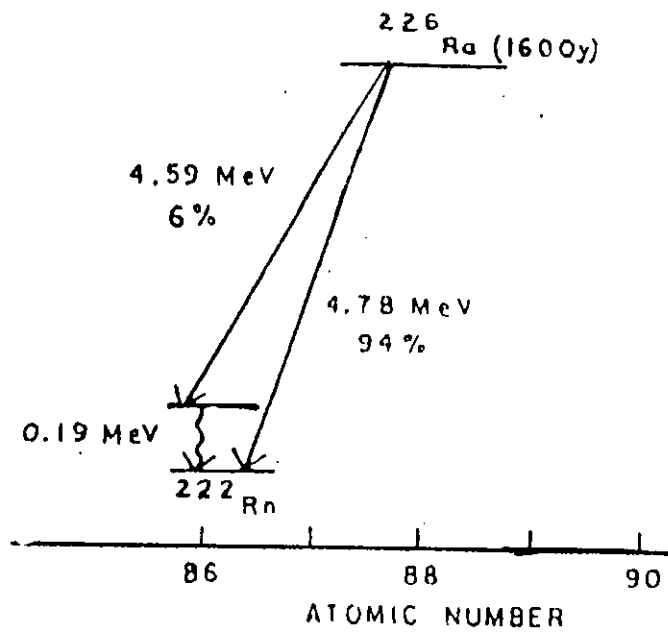


Figure 1.3.1 Radioactive Decay Scheme for Alpha Decay of ^{226}Ra

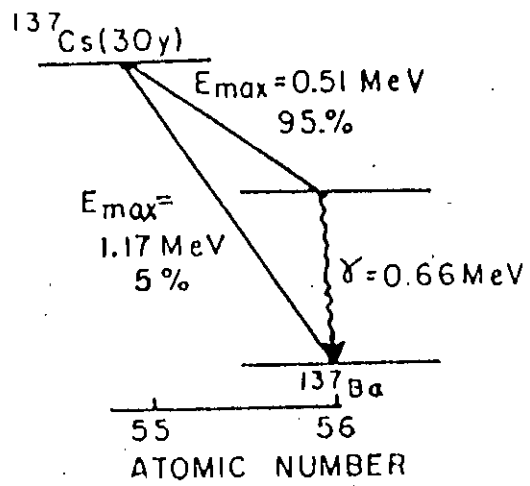


Figure 1.3.2 Radioactive Decay Scheme for Negatron Decay of ^{137}Cs

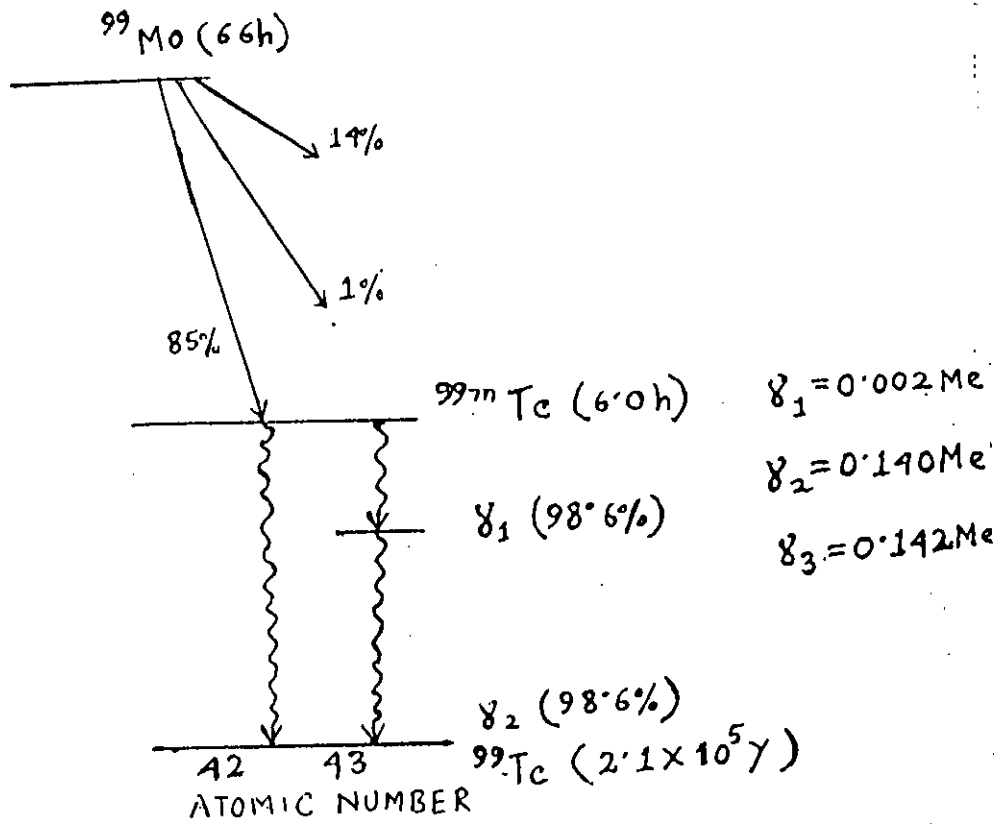


Figure 1.3.3 Simplified Decay Scheme for ^{99}Mo

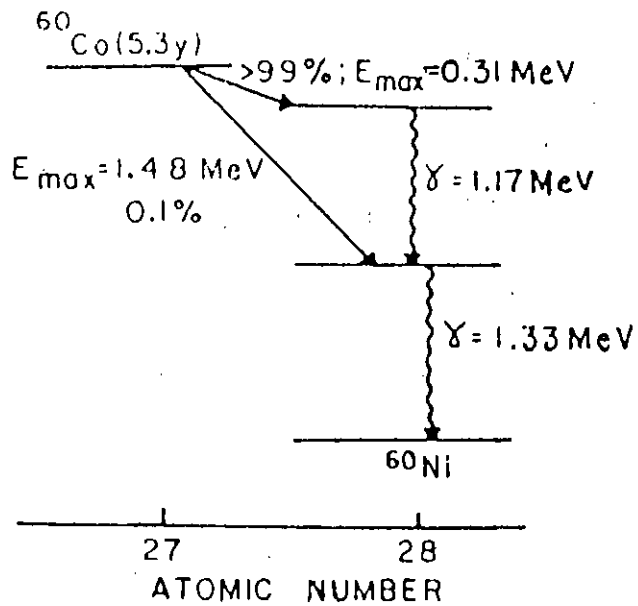


Figure 1.3.4 Radioactive Decay Scheme for ^{60}Co

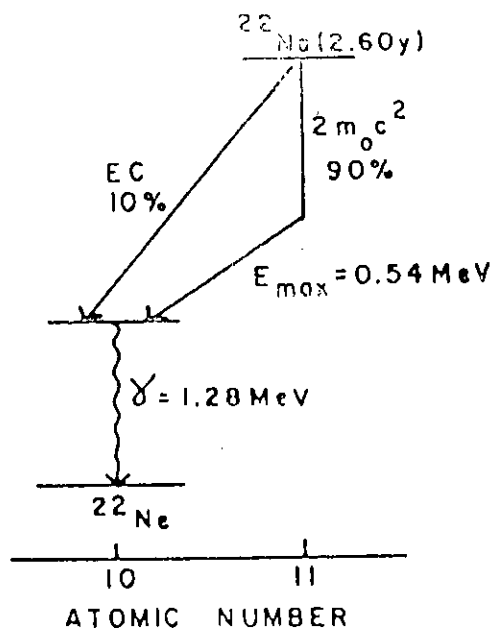


Figure 1.3.5 Radioactive Decay Scheme for Positron Decay of ^{22}Na

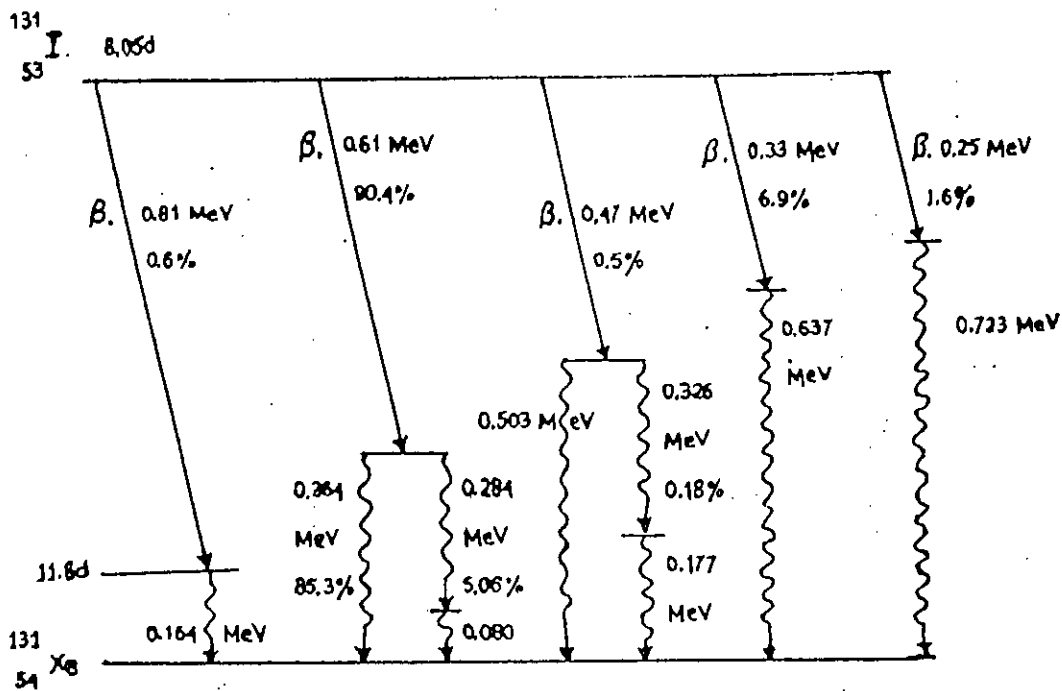


Figure 1.3.6 Iodine-131 Transformation (Decay) Scheme

For α -emission to be observed from the high atomic numbered naturally occurring elements, theoretical consideration demand that an alpha particle have a kinetic energy greater than 3.8 MeV, which has been verified experimentally. α -particles are essentially mono energetic, though spectrograms show discrete energy groupings, with a little energy difference among the different groups. Alpha rays are extremely limited in their ability to penetrate matter. Even in air, the most energetic α -particles from the radioactive substances travels only a few centimeters and in tissue, this range is measured in microns. The dead outer layer of skin is thick enough to absorb all the α -radiation of the radioactive materials. Hence, alpha radiation emitted from a source outside the body is not considered as radiation hazard. So it has got a lesser impact in the field of nuclear medicine. But, this alpha radiation is highly toxic when it irradiates the inner part of the body from the internal deposition of radioisotopes, as in this case, the shielding effects of the dead outer layer of skin is absent and the energy of α -radiation is dissipated in the living tissue.

The beta particle:

A *beta particle* is an ordinary electron, ejected from the nucleus of a beta-unstable radioactive atom. It has a single negative electrical charge and a very small mass. It is postulated that, β -particle is formed at the instant of the transformation of a neutron into a proton and electron. A β -decay occurs among those isotopes that have a surplus of neutrons. For a beta emission to be energetically possible, the exact nuclear mass of the parent must be greater than the sum of the exact masses of the daughter nucleus plus the beta particle. ^{32}P , ^3H , ^{14}C , ^{90}Sr , ^{90}Y are several beta emitting isotopes known as pure β - emitters. There are also some other which are known as beta-gamma emitter e.g. ^{203}Hg . In these cases, β -particle is followed by a γ -ray. β -particles were thought to be mono-energetic. But these are found to be

emitted with a continuous energy distribution ranging from zero to the theoretically expected value, based on mass-energy considerations for the particular β - transition. Generally, the average energy of a beta radiation from most beta-active radioisotopes are about 30%-40% of the maximum energy. Beta radiations, because of its ability to penetrate tissue to varying depths, depending on the energy of the beta particle, may be an external radiation hazard. But the exact degree of hazard depends on the beta-emitting isotope and varies, for case individuals. Even then the β -particles themselves present special detection and measurement problems for application in nuclear medicine. The beta rays whose energies are less than 200 KeV such as those from Tritium, ^{35}S , and ^{14}C , has a very limited penetrability. For these reasons, these are not considered as external radiation hazards. However, β -rays produces a highly penetrating X-rays known as *Bremsstrahlung*. These are emitted when high-speed charged particles suffer a rapid acceleration. Bremsstrahlung photons have a continuous energy distribution, ranges downward from a theoretical maximum, equal to the maximum kinetic energy of the β -Particle. It is assumed that, all the Bremsstrahlung photons are of lower energy. So it can be said that, beta radiation may indirectly result in an external radiation hazard through the production of Bremsstrahlung. Any beta-emitting isotope is potentially hazardous whenever it is deposited in the body in amounts exceeding those thought to be safe.

The positron:

A positron is a beta particle, which is positively charged. In the instances, when the neutron to proton ratio is low and the emission of alpha is not possible energetically, the nucleus attains stability by emitting a positron. A positron in every respect is same as the negative beta particle or

an ordinary electron^[11]. It has only transitory existences. As a result of the interaction between cosmic ray and the atmosphere, the positron occurs in the nature. But it disappears in a matter of microseconds after the formation. The positron combines with an electron, and the two particles are annihilated, giving rise to two gamma-ray photons whose energies are equal to the mass equivalent to the positron and electron^[12]. ²²Na, an useful isotope for biomedical research is an example of positron emitter. Positron emitters are useful in nuclear medicine because two photons are generated per nuclear decay event. The exact directional relationship between the annihilation photons are useful as it permits the use of "Coincidence Counting" techniques. Since positrons are nothing but electrons, the radiation hazards from the positron themselves is very much alike to the hazard from the β -particles. The origination of γ -radiation from the annihilation of the positron makes all positron-emitting isotopes potentially external radiation hazards.

All sorts of radioactive decay is associated with either *the capture or emission of an electron and as a result of it a neutrino* must be emitted to conserve the energy. When an atom is being transformed by orbital electron capture, an X-ray, characteristic of daughter element is emitted as an electron from an outer orbit, falls into the energy level occupied by the electron which had been captured. These X-ray photons of the characteristic X-ray are emitted after the nucleus captures the orbital electron. When the absorbed radiation dose from internally deposited isotopes are calculated, this low energy characteristic X-rays resulting from decay by orbital electron capture, should be considered.

The gamma rays:

Gamma rays are monochromatic electromagnetic radiation. It is emitted from the nuclei of an excited atom following radioactive transformation. The attenuation of gamma radiation is qualitatively different from that of either alpha or beta ray. The corpuscular radiations like α -or β -ray have definite and precise ranges in material, and thus can completely be absorbed whereas, the intensity of γ -radiation maintains an inversely proportional relationship with the thickness of its absorber. As X-rays are indistinguishable from gamma ray, all characteristic X-rays that arises from the extra-nuclear structure of many radioisotopes are considered as radiation hazards. The gamma rays arising from the mutual annihilation of positrons and negatrons are usually associated with the isotopes that emit positron. The general rule in health physics is to associate positron emission with gamma radiation in all occurrences involving radiation hazard evaluation.

The daughter nucleus of a radioactive parent may be formed in a long-lived metastable or isomeric state, as opposed to an excited state. The decay of metastable or isomeric state, by the emission of a gamma ray is known as *an isomeric transition*. An alternative to X-ray emission, which is especially frequent among the metastable states, is decay by internal conversion. During these processes, the nucleus decays by transferring energy to an orbital electron, which is ejected instead of X-ray. It is assumed that, the gamma ray is absorbed internally by collision with an orbital electron. This ejected electron is known as conversion electron. Similar to β -decay, the internal conversion results in the emission of electrons. The important differences are (i) in β -decay, the electron originates from the nucleus, whereas in internal conversion it originates from an electron orbit and (ii) β -particles are emitted with a continuous spectrum of energies, whereas conversion electron's have a discrete series of energies determined

by the difference between the X-ray energy and orbital electron binding energies ^[13]. Metastable radionuclides are playing a vital role in the field of nuclear medicine. Because of their relatively longer life times, these metastable radionuclides can be separated from their radioactive parent and obtain a relatively pure source of gamma rays. Metastable radionuclides are not purely "Pure Gamma Emitter" as it always emits a certain number of conversion electrons. Various radiations interact with matter by these mechanisms. Energy is transferred from radiation to matter with which the radiation interacts. Every matter consists of an atomic nuclei and extra nuclear electrons. Normally radiation interacts with either or both of these constituents of matter. The probability of occurrence of any specific type of interaction and hence the penetrating power of several radiation, depends on the type and energy of the radiation as well as on the nature of absorbing medium. In all instances, the excitation and ionization of absorber atoms results from their interaction with the radiation. Ultimately the energy is transferred to tissue / cell of the absorber medium.

1.3 BIOLOGICAL EFFECT OF RADIATION

The discovery of X-rays in 1895 and natural radioactivity in 1896, leads the way of understanding that, ionizing radiation is harmful to molecular, cellular and organ system level. Ionizing radiation normally causes ionization in matter through which it passes and is able to damage extensively the molecular structure of the matter either as a result of direct energy transfer to it's atoms or molecules or as a result of the secondary electrons released by ionization. The ultimate effect is alternation of the living cell. The effect of ionizing radiation on biological tissue is very serious. The interaction between the radiation and the biological cell is followed by harmful effects of radiation. These biologic effects are the

result of chain reactions initiated by the interaction with the atoms of low atomic number (C, H, O, and N) which constitute organic matter ^[3]. Cell is the basic biologic unit. The biologic cell of typical type contains a large amount of water (approximately 70%), some special types of macromolecules and other elements. More precisely a typical cell is a sac of fluid, or cytoplasm, enclosed by chromosomes which include the more essential component of life, deoxyribonucleic acid or DNA; that carries the life sustaining information ^[4]. Normally the molecules of the biological tissue are in covalent bonding. When an ionizing radiation passes through biological molecules, the covalent bond, especially those of water are split to form free ions, free radicals and finally H_2O_2 and consequently biochemical changes occur in the body which may later show up in the form of clinical symptoms ^[5]. The biologic effects of ionizing radiation are conveniently divided into two classes, namely somatic and genetic ^[6]. From the acute or/and chronic exposure, these effects normally do occur. However, the effects of radiation on biological matter are dependent on! (i) the energy and the type of radiation, (ii) the dose rate, (iii) the volume irradiated and (iv) the sensitivity of the tissue ^[7].

Somatic Effects:

The somatic effects arise from the damage to the ordinary cells of the body and affect only the radio-exposed individual ^[6]. This effect may occur irrespective of acute irradiation or chronic irradiation. These effects are also dependent on (i) the degree of oxidation, and hence temperature of the exposed part of the body, (ii) the metabolic state, and hence the diet, (iii) the irradiated person's sex; and (iv) the body color ^[8]. Somatic effects leads the way of inhibition of mitosis, chromosome aberration and breakage and finally the occurrence of death of cell.

Genetic Effects:

When there is an occurrence of damage or mutation or alternation in the chromosome structure due to the irradiation of germ cells (sperm or ovum) in the individual, this affects the descendents of the irradiated person. This sort of effect is known as genetic or hereditary effects. This effect may be observed through generation after generation. The natural radiation leads the path of a genetic mutation. Any unrepaired DNA mutations in germinal cells that are non-lethal for the cell could in principle be transmitted to subsequent generations and becomes manifest as hereditary disorders in the descendents of the radio-exposed individual ^[4]. There is no threshold of exposure at which radio-exposed individual has a definite probability of producing a mutagenic effect ^[3]. However, the natural background radiation is responsible for, from 4% to 10% of all naturally occurring genetic mutations ^[9].

Short term Effects:

These are somatic effects. Manifestation of few week's exposure or an acute exposure of above 1 Gy delivered between a few minutes to a few hours are the cause of this type of effect. Acute whole body radiation overexposure affects all the organs and systems of the body. Since all the organs and organ systems are not equally sensitive to radiation, the pattern of response or disease syndrome, in overexposed individual depends on the magnitude of the dose. The immediate effects manifest as: Chromosome aberration, blood changes, nausea and vomiting, diarrhoea, loss of appetite, malaise and fatigue, epilation, skin erythems, sterility, etc and death ^[10].

Delayed Effects:

The delayed effects of radiation may be due either to a single large overexposure or continuing low-level exposure^[9]. Continuous overexposure can be due to the exposure to external radiation fields, or can result from inhalation or ingestion of a radioisotope. This exposure then becomes fixed in the body – (i) through chemical reaction with the tissue protein or (ii) because of the chemical similarity of the radioisotope with normal metabolites and may be systemically observed within certain organs and tissues. For both the cases, there is a chance that the internally deposited radioisotope may continue to irradiate the tissue for a longer time. According to minimum threshold dose and probability of effects by that dose, these delayed effects of radiation on human cell are classified into two groups –

(a) *Stochastic Effects* – This manifest themselves long after the exposure and include increased risk of cancer and, by implication from studies on animals, of hereditary disorder^[2]. For such type of effect, no threshold dose has been defined. These effects may occur at any dose, the probability of manifestation increases with absorbed dose^[10]. Stochastic effects can be reduced in frequency by lowering the dose but even then the effect can not be avoided entirely as they are assumed to occur with low frequency at low doses.

(b) *Non- stochastic or deterministic Effect*- These effects result from high dose exposures and in this case, the threshold dose for occurrence can be defined. This effect is avoided in normal radiation protection procedures by limiting doses to below the threshold dose levels. Among the delayed consequences of overexposure the followings are of concern (i) cancer, (ii) malfunctioning or loss of function of tissue in organ, (iii) genetic effects, (iv) shortening of life span and (v) cataracts (Figure: 1.4)

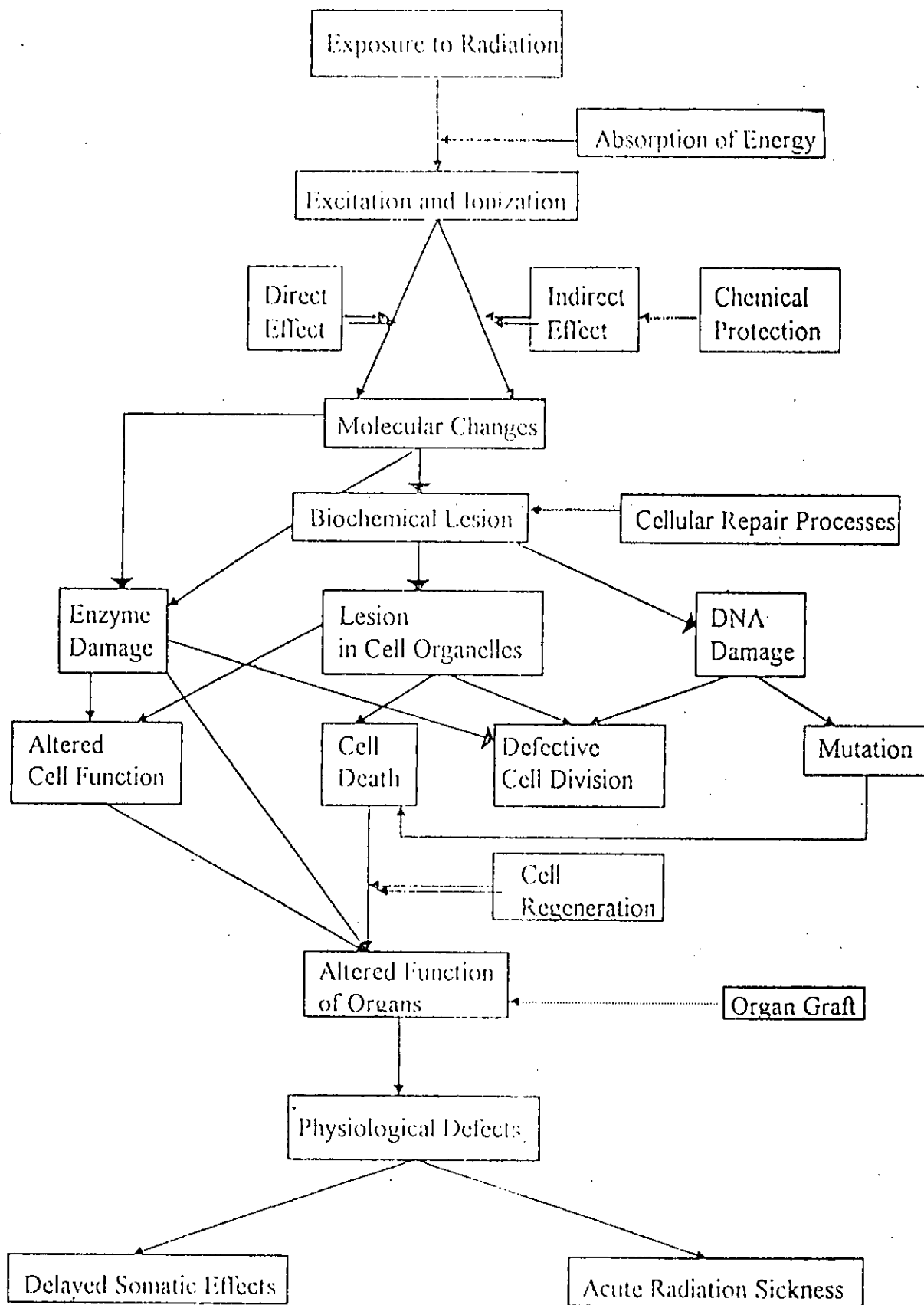


Figure 1.4 Development of Cell Injury ^[09]

1.4 THE ERA OF NUCLEAR MEDICINE

Radiation ranks among the most thoroughly investigated etiologic agents associated with disease [2]. The definite diagnosis of diseases is obtainable using the non-traumatic as well as non-invasive methodology (Figure: 1.5). The rapid and often dramatic development in the field of radiation biology is possible by the strong support of nuclear medicine, which have provided the diagnostic methods that are approaching the ideal. Nuclear medicine acts as the bridge between a particular clinical problem and relevant test with radionuclides. Nuclear medicine began its journey as a minor technical tool used in few branches of medicine. However, all over the world, it has now become established as a clinical discipline in its own right. Nuclear medicine, now-a days, can be defined as that branch of medicine concerned with the application of tracer principle to clinical medicine and biomedical research [14]. Nuclear medicine is growing rapidly for last few decades. This expansion has been greatly contributed by the technical developments in nuclear physics research.

Nuclear medicine arrived on the world scene in the 1960s^[15]. Since then, radionuclides were being used in medicine quite seriously and usefully, developing surely and slowly with increasing radionuclide availability and with each new advance in electronics and radiopharmaceutical manipulation. The development of nuclear medicine started in the 1940s^[16]. The 1940s provided the era of Geiger-counters and differential uptake of the biological-radioactive elements, ^{131}I and ^{32}P , for therapy and diagnosis^[15]. During the '50s, scintillation detectors, some manual scanning and practice of tagging biological compounds with radionuclides such as ^{51}Cr labeled red blood cells and ^{60}Co leveled vitamin B_{12} , were introduced^[15,17,18]. 1960s is the age of automatic rectilinear scanner which emerged concurrently with the short-lived radionuclides.

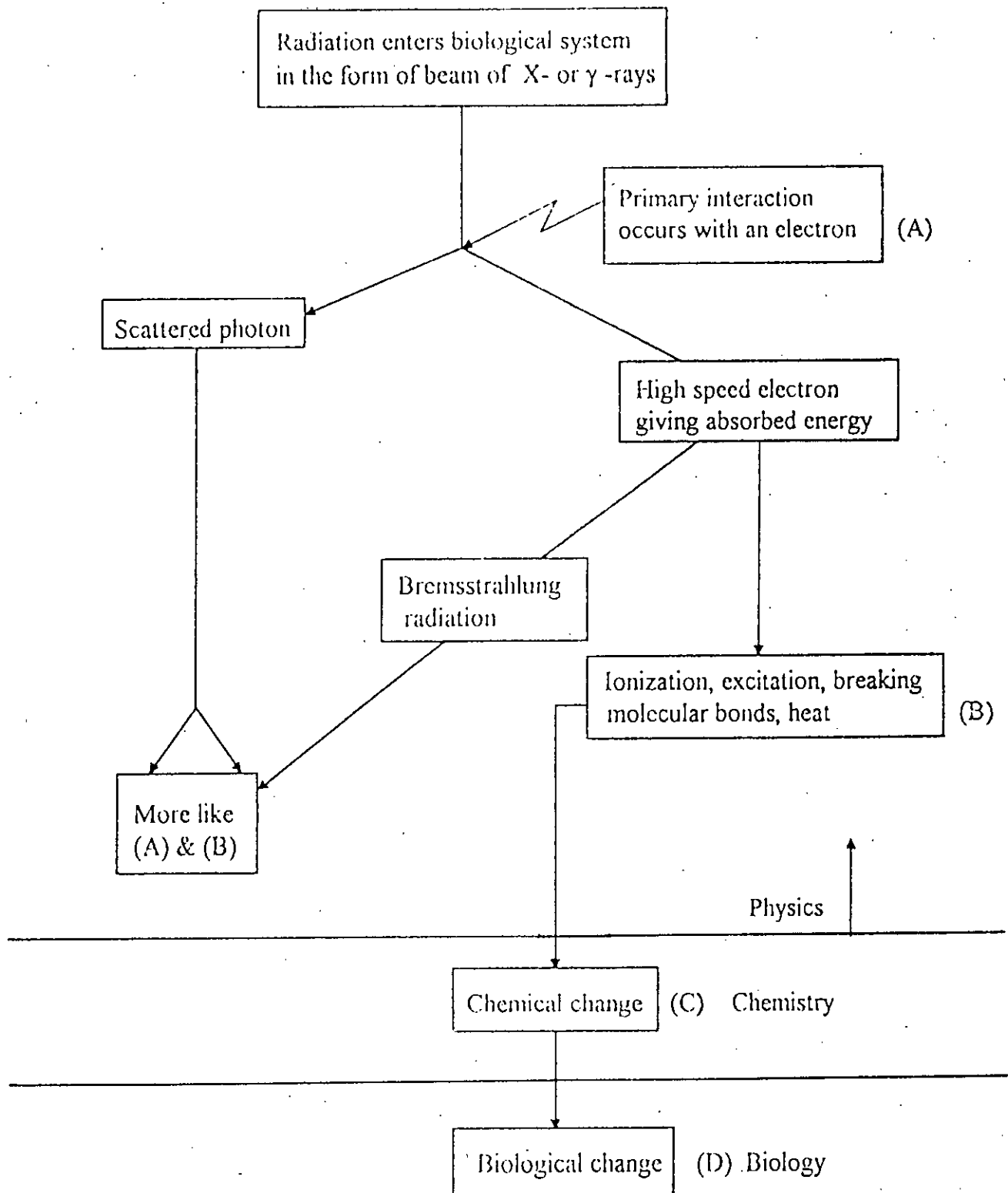


Figure 1.5 Schematic Diagram Illustrating The Absorption of Energy from Radiation Resulting in Biological Damage⁽⁸⁸⁾

The radionuclides were characterized by relatively high energy and thus the rectilinear scanner with its thick crystal and special collimators provided an excellent imaging device. Pulse height analysis, allowing simultaneous measurement of multiple radio-nuclides further widened the field; while radiochemical manipulation became an important area of investigation to extend the usefulness of scanners ^[15]. Although the scintillation camera is the primary imaging device of virtually all modern nuclear medicine laboratories, a limited number of scanners continued to be used till 1980s.

In 1960, an alternative type of scintillation camera, known as autofluoroscope was introduced ^[19,20]. But it was not very popular device like scintillation camera. The introduction of Technetium-99m by Harper et al ^[21], dramatically changed the requirements for imaging device. The desirability of the scintillation camera for imaging was enhanced further by the wide range of ^{99m}Tc-labeled radiopharmaceuticals that were developed in the late 1960s and throughout the 1970s. Laboratory investigations, like radioimmunoassay also started to be a major part in the diagnostic armamentarium in the 1970s. Radiopharmaceuticals can be utilized up to the optimum point for the diagnostic and therapeutic nuclear medicine procedure. For these reasons, ^{99m}Tc-DTPA ^[22] and ^{99m}Tc -glucoheptonate^[23] for brain and renal imaging, ^{99m}Tc-MAA ^[24] for pulmonary perfusion studies, ^{99m}Tc-tagged polyphosphates^[25] and diphosphonates^[26] for bone imaging, ^{99m}Tc-sulfer colloid^[27] for liver imaging and ^{99m}Tc-labeled hepatobiliary tract imaging^[28] became popular imaging agent in the decade of 70s. In this decade, modification in collimator design, crystal characteristics and number and types of photomultiplier tubes of scintillation camera, and the use of solid state circuitry made it (the camera) a superior imaging device both electronically and physically. In mid '70s, the positron emission tomography was modified to multicrystal **positron**

emission transaxial tomography system (PETT), which contributes a lot to show a great potential for positron emission tomography in the evaluation of metabolism within organ of interest. During this period, the combination of conventional scintillation camera, a computer and a special collimator appears and shows a promising future of nuclear medicine. This successful interfacing gives rise to digital nuclear medicine. In the later part of the last century, computerized tomography (CT), digital radiology and nuclear magnetic resonance arrived on the scene. These are now serving as complements to nuclear medicine procedures in the diagnostic processes. Hence nuclear medicine is serving as the primary method of establishing functional information. The functional information is being widely utilized in the section of diagnostic nuclear medicine and helps in managing a broad spectrum of diseases. The therapeutic nuclear medicine utilizes the damaged part of cell/tissue of the targeted radiation and deals with the recovery.

Nuclear medicine strongly supports the use of radiopharmaceuticals, as it's most important tool, because of the fact that radiopharmaceuticals meet the criteria of sterility and apyrogenicity so that those can be safely administered to humans for the purpose of diagnosis, therapy and research^[29]. The whole basis of nuclear medicine imaging is that a radioactive isotope is introduced into the particular part of the body, under investigation. This isotope introduction can be done in two ways, either (i) directly into the bloodstream or (ii) in a particular organ of the body that has an affinity for one element. In most cases, neither of these two is possible. However, the radioactive substance can be attached to a chemical, which would be chosen according to its preferential absorption by the respective part of the body. Hence, the chemicals to which radioactive labels can be attached by substituting chemical's own one or more atoms, are called as radiopharmaceuticals^[30]. Though, the absorption of the energy from ionizing

radiations can cause damage to living tissue^[13], it has proved itself to be very successful in the study of a particular physiological function of an organ or tissue, or in the localization of specific disease and shows encouraging results. The uptake of radiopharmaceuticals depends on some aspects of normal or disordered function of the organ under investigation. The amount of radiopharmaceutical administered to the patient is a very small amount, which would produce no detectable amount of pharmacological effect. In the therapeutic nuclear medicine also, the desired response is produced by targeted delivery of radiation rather than a pharmaceutical response. It is a basic necessity that, for diagnostic nuclear medicine, the used radionuclides should produce a useful clinical information with minimum exposure of patient to radiation. These radionuclides are normally of short half-lives as is compatible with time needed to complete the investigation. These are gamma emitters, which are of high enough energy, able to detect even the deep-seated tissues, but not high enough up to that extent which would make detection difficult. ^{99m}Tc is regarded as the most important radionuclide in the field of nuclear medicine. It is a generator produced radionuclide. Besides this, there are various radionuclides which are nuclear medically important for diagnosis purpose, such as Hydrogen-3, Carbon-11 and 14, Nitrogen-13, Oxygen-15, Cobalt-57, Gallium-67 and 68, Iodine-123 and 131 and 125, Cesium-137 etc^[13,31]. For therapeutic nuclear medicine the requirement is for emission of particulate radiation with tissue penetration equal to the dimensions of the lesion and with a half-life that minimizes the patient's period of hospitalization.

It has already been known that, any amount of exposure from ionizing radiation, irrespective of their origin and reason of use, produces an amount

of biological effect. In spite of its harmful effect, various radionuclides are being widely used in the nuclear medicine centers and modern private clinics all over the country to derive maximum benefit for mankind, maintaining the level of exposure as low as practicable and consistent with the requirements of treatment and diagnosis. It is a common practice, in radioisotope therapies, to calculate an average dose to tissue, from the activity and mass of the tissue specimen. This approach is practical but not accurate if the radionuclide distribution in tissue specimen is not uniform^[32],^{33, 34]}. However radionuclides are rarely uniformly distributed in tissue and tissue response is seldom-linear^[33]. There is a wide applicability of radiopharmaceuticals in therapy but it has a limitation for diagnostic application because of the potential hazard for the patient.

1.5 AIMS AND OBJECTIVES

The importance of many physical aspects of radionuclide distribution pertaining to radiopharmaceuticals are known. The need for the exact and precise information in distribution of dose decays in close proximity to every cell is highly essential for accurate assessment of cellular doses. This also ensures a precise therapeutic perception and reduces excess potential risks to patients. For assessing the radiation effects on an organ, the amount of radiation energy deposited in that organ is calculated^[33]. The calculation of this deposited radiation energy by the internally administered radionuclides is determined by performing internal radiation dosimetry. The distribution of radioactivity within an organ may be inhomogeneous. Bio-distribution calculations can not completely remove all the uncertainties in dose specification for that organ. For these complications and variables, radiation doses are being calculated. Extensive pharmacokinetic study will then contribute to the interpretation of all the clinical findings^[35].

Under the circumstances stated above, the present study is totally new in the research field of Bangladesh and has been performed with the following aims and objectives:

- ◆ To study radiation absorbed doses by organs (kidney and liver).
- ◆ To determine the distribution of doses of radiation to organs i.e. the study of bio-distributions.
- ◆ To study the pharmacokinetics of the used radiopharmaceutical within kidney.

The present work attempts to determine the absorbed dose of a radiopharmaceutical widely used in the field of nuclear medicine and the distribution of the same in respective organs of the body. Following the findings, the pharmacokinetic study of radiopharmaceutical within kidney was also a point of observation. From the resultant observation the effect of the widely used radiopharmaceutical in human body can be explained. A few works has been done in this spectrum outside Bangladesh that are mentioned in the references. So this work obviously would open a new era in the research field of nuclear medicine in Bangladesh. Observed results would also find a chance to be compared itself with the traditional and permissible doses of radiopharmaceutical, to see whether they are justified for the people of a developing country like Bangladesh or not. It is important to mention that, there is a wide scope to do comprehensive research in this field.

CHAPTER 2

Literature Review

CHAPTER 2

Literature Review

2.1 INTRODUCTION

The radiation sources and the radioisotopes are now being widely used in medicine, in sterilization of the medical products and appliances. The use of different types of ionizing radiation for diagnostic and therapeutic purpose causes hazard to the biologic tissue. As the deleterious effects of radiation became known, it became necessary to keep the radiation exposure below the maximum permissible dose so as not to cause any biological damage. Scientists throughout the world used different techniques to investigate the various biological effects of radiation on different organs of the body. Methods and results of some of the recent works, that are relevant to the present work, are described below in brief:

2.2 REVIEW

M. Juweid et al^[36] assessed the biodistribution, pharmacokinetics and dosimetry of ^{188}Re -labeled MN-14, an IgG anti-carcinoembryonic antigen monoclonal antibody (MAb), in patients in advanced gastrointestinal cancer. Eleven patients were administered radioactive doses of directly labeled ^{188}Re -MN-14 IgG, ranging from 20.5mci to 161.0mc: (2.0mg-4.9mg). Ten of these patients received two or three MAb infusions given three to four days apart, delivering total doses of 30mci/m²- 80mci/m². External scintigraphy was used to evaluate the MAb biodistribution, and quantitative external scintigraphic methods are used to determine the organ and tumor radiation doses. The result showed that the biodistribution studies indicate the enhanced ^{188}Re -MN-14 uptake in the liver, spleen and kidneys,

compared to that of ^{131}I -MN-14. The biologic $T_{1/2}$ values for ^{188}Re -MN-14 in blood and whole body (in hours) were found as 8.2 ± 4.1 ($n=7$) and 107.8 ± 104.2 ($n=9$), respectively (mean \pm s.d.). The radiation absorbed doses (cGy/mCi) delivered to the total body, red marrow, lungs, liver, spleen, and kidneys were obtained 0.5 ± 0.05 , 3.6 ± 1.6 , 2.0 ± 0.8 , 5.9 ± 2.5 , 7.1 ± 1.9 and 8.5 ± 2.8 respectively. Red marrow suppression was the only dose limiting toxicity (DLT) observed. The maximum tolerance dose of fractionated doses of ^{188}Re -MN-14 was estimated to be 60mCi/m^2 .

M. Baldwin et al ^[37] studied that SPECT imaging with ^{123}I -labeled methyl 3β -(4-iodophenyl) trapan-2 β -carboxylate (^{123}I β -CIT) in nonhuman primates showing brain striate activity which primarily reflects binding to the transporter. For accurate determination of the organ time- activity data, the biodistribution and calculation of radiation absorbed dose of ^{123}I β -CIT were measured. The whole body transmission images were obtained with a scanning line source for attenuation correction of the emission images. It was found that the peak brain uptake represented 14% of the injected dose with 2% of the activity approximately overlying the striatal region. Highest radiation doses were found to the lung (0.1mGy/MBq , 0.38 rads/mCi) and liver (0.087mGy/MBq , 0.32 rads (mCi)). It was concluded that Iodine ^{123}I - β -CIT is a promising SPECT agent for imaging of the dopamine transporter in humans with favorable dosimetry and high brain uptake.

B.L Holman et al ^[38] investigated the biodistribution, dosimetry and clinical evaluation of Technetium-99m Ethyl Cysteinate Dimer(ECD) in normal subjects and in-patients with chronic cerebral infarction. Sixteen normal subjects were injected with $\approx 10\text{mCi}$, of $^{99\text{m}}\text{Tc}$ ECD. The anterior and the posterior single-pass whole body images were obtained at multiple times

after injection. They found that the blood clearance of the radiotracer was rapid, falling to $10.0 \pm 6.6\%$ and $4.9 \pm 1.1\%$ of the injected dose at 2 and 60min respectively. The brain uptake obtained was $6.4 \pm 2.1\%$ of the injected dose 5min after injection. The urinary bladder was found to be the critical organ. Technetium-99m-ECD on SPECT study was performed with a rotating gamma camera in ten of sixteen normal subjects and thirty-four patients with clinical and CT evidence of chronic stroke. It was noticed that thirty- three of the thirty-four patient (97.1%) had focal [^{99m}Tc] ECD abnormalities based on visual inspection of the SPECT images. They found, high quality Technetium-99m ECD SPECT images as a result of the optimal physical and biological characteristics of the tracer and shows promise for the evaluation of patients suffering from stroke.

C. Rosette et al^[39] performed study on human biodistribution, dosimetry and clinical use of technetium (iii)-99m-Q12. They found that technetium (iii)-99m-Q12, trans-(1,2-bis (dihydro-2,2,5,5 tetramethyl-3 (2H) furanone-4-methyleneimino)ethanc)bis (tris(3-methoxy-1 propyl)-phosphine) technetium (iii)-99m which is a nonreducible complex of Tc (iii), exhibits good heart uptake (2.2%) of injected dose at 1hr post injection under resting conditions and no detectable myocardial washout or redistribution up to 5hr post injection. They also found that the biodistribution is characterized by very rapid hepatic biliary clearance which allows effective myocardial imaging at times as short as 15 min post injection. Blood and plasma clearances and myocardial uptake are rapid, while lung uptake is found to be minimal .The heart-to- lung and heart-to-liver ratios are observed higher at stress than at rest . These ratios are found to be independent of time elapsed between injection and image acquisition and of whether the patient is fasted

or fed after tracer administration. On this basis they reported that $^{99m}\text{Tc-Q12}$ appears to be promising myocardial perfusion imaging agent.

M. Nakajo et al ^[40] evaluated the biodistribution and in vivo kinetics of Iodine-131 lipiodol infused via the hepatic artery of patient with hepatic cancer. The study was performed to estimate the potential of internal radiotherapy of hepatic cancer in five patients. It was observed that the Iodine-131 lipiodol can be used as an intra-arterial infusion agent to treat certain vascular hepatic cancer.

C.M. Thonoor et al ^[41] studied the biodistribution and radiation dosimetry of radioiodinated-SCH 23982, a potential dopamine D-1 receptor imaging agent. Their study indicates that [^{123}I] SCH 23982 is a suitable agent for imaging the D-1 dopamine receptor in the human brain by single photon emission computed tomography. They have calculated the internal radiation absorbed dose to nine source organs, total body, the Gastrointestinal (GI) tract, gonads and red bone marrow for the human using the physical decay data for ^{123}I . The critical organ was found to be the lower large intestine which received 1.1 rad /mCi of administered dose and the total body dose was 63 m rad /mCi.

F.J. Wackers et al ^[42] assessed the biodistribution, dosimetry and safety of new myocardial imaging agent, Technetium-99m Hexakis-2-Methoxyisobutyl Isonitrile (HEXAMIBI) in 17 normal volunteers at rest and in exercise. It was observed that Technetium-99m HEXAMIBI clears rapidly from the blood with good myocardial uptake and the myocardial to background ratios were favourable for myocardial imaging. It was also

found that the myocardial images were of good quality and appeared less granular with sharper myocardial walls compared to ^{201}Tl images.

P. D. Mozley et al ^[43] performed biodistribution and dosimetry of a Technetium-99m labeled Tropane for imaging dopamine transporter. They found that there were no pharmacological effects of the radiotracer [$^{99\text{m}}\text{Tc}$] TRODAT-1. Image analysis showed that the kidneys excreted between 20% and 32% of the injected dose during the first 22-28 hours post administration, after which no additional activity could be recovered in urine. It is also observed that, the dose estimates were significantly higher in women than in men because the females who participated in this study were taller and heavier than reference woman. Nevertheless, the dose limiting organ in both men and women was the liver which received an average of 0.046 mGy /MBq (0.17 rads/mCi, range 0.14-0.22 rad). Finally it could be stated that , TRODAT selectively bind the dopamine transporter in the brain and body . Pharmacological side effects are negligible and its radiation dosimetry profile is highly favorable .

S. Vallabhajosula et al ^[44] investigated $^{99\text{m}}\text{Tc}$ -ethyl cysteinate dimer (ECD), a new derivative of DADT (Lipophilic neutral $^{99\text{m}}\text{Tc}$ Complex of diaminedithiol) which showed high brain uptake in non-human primates. The invivo kinetics and biodistribution were studied in 16 normal human subjects. Dynamic images of brain obtained for 10 minutes, following an intravenous administration of [$^{99\text{m}}\text{Tc}$] ECD showed that, maximum $^{99\text{m}}\text{Tc}$ brain activity reacted within 1 minute and remained near the level for the next 10 minutes. The blood clearance of the tracer was found to be very rapid and the activity remaining in blood after 5min was <10%. Within 2hr, 50% of $^{99\text{m}}\text{Tc}$ activity was excreted in urine. Anterior and posterior total –

body images were obtained at 5,30,60 min, 2,4,24 and 48 hr using a moving table at 20cm/min. Percent injected dose was calculated for different organs and tissue. The brain uptake was $6.5 \pm 1.9\%$ at 5 min. post injection and remained relatively constant over several hours. Two-compartment analysis of brain time-activity curve showed that 40% of brain activity washed out faster ($T_{1/2}=1.3$ hr) while the remaining 60% had a slower clearance rate ($T_{1/2}=42.3$ hr). Some of the tracer was excreted through the hepatobiliary system. Lung uptake and retention of [^{99m}Tc]ECD was negligible. Radiation dosimetry was found favorable for the administration of up to 20-40mC of [^{99m}Tc] ECD. They have concluded that [^{99m}Tc] ECD is rapidly extracted and retained by the brain providing favorable condition for single photon emission computed tomography imaging .

M. Stabin et al ^[45] studied the radiation dosimetry for Technetium-99m-MAG₃, Technetium-99m-DTPA and Iodine-131-OIH based on human biodistribution studies. Radiation dose estimates were performed using standard MIRD technique. Average residence times in urinary bladder, kidney and the remainder of the body were used to predict radiation dose equivalents and effective dose equivalents for the three agents. The doses for DTPA and MAG₃ were very similar and much lower on an per unit injected activity than OIH. The effective dose equivalents were 3.3m Sv/370 MBq of for ^{99m}Tc -DTPA, 3.7mSV/370MBq for ^{99m}Tc -MAG₃ and 0.99m Sv/11.1MBq for ^{131}I -OIH for bladder voiding every 4.8hr.

Andrew Taylor Jr. and Dennis Eshima ^[46] observed the effects of altered physiologic states on clearance and biodistribution of Technetium-99m Mercaptoacetyltriglycine ([^{99m}Tc -] MAG₃), Iodine-131 OIH and Iodine-125 lothalamate. They studied that ([^{99m}Tc] MAG₃) which is a new renal

radiopharmaceutical with biologic property similar to iodine-131 orthoiodohippuric acid ($[^{131}\text{I}]\text{-OIH}$), may be used as a replacement for $[^{131}\text{I}]\text{OIH}$ and /or $[^{99\text{m}}\text{Tc}]\text{DTPA}$. To have this finding they have compared the effects of several potential adverse clinical conditions on the clearance and biodistribution of MAG_3 , OIH and a GFR marker.

B. C. Lentle et al^[47] studied the variables in radiotracer kinetics and distribution. In their findings, they have described, that, the injection of the radiotracer might result in scintigraphic images that are either normal or abnormal. In the later case disease will be present. Since tracer method reflects subtle alternation in physiology, scintigraphs may reveal not only disease but treatment, drug toxicity and medical interventions. In addition, factors in the habits and lifestyle of patients will also result in changes that may be recognised scintigraphically. The authors wish to describe in the findings that some of the types of changes in radiopharmaceutical distribution that are due to influences other than direct diseases. They have also provided perspective concerning the types of altered biodistributions that may be encountered in clinical practice.

H.M. Deloar et al^[48] verified accuracy of the TLD method. Under the standard protocol for 2-[F-18] fluora-2-deoxy-D-glucose ($^{18}\text{F}\text{-FDG}$), whole body PET experiments and simultaneous body surface dose measurements by TLDs were performed on six normal volunteers. The use of the body surface dose measured with TLDs, the cumulated activity of nine source organs overestimated with a mathematical unfolding technique for three different initial guesses. The accuracy of the results obtained by the TLD method was investigated by comparison with the actual cumulated activity of the same/source organs measured by whole body PET (Positron Emission

Tomography). The cumulated activities of the source organs obtained by the TLD method and whole body PET show a significant correlation (correlation coefficient, $R > 0.98$, level of confidence, $P < 0.001$) with each other. The mean effective dose equivalents in this study are 3.2×10^{-2} mSv/MBq obtained from the TLD method and 2.9×10^{-2} mSv/MBq obtained from whole body PET. They have finally concluded that, there is a good agreement between the result of the TLD method and whole body PET. Because of the simplicity and cost effective-ness of the TLD method, this could be used in estimating internal absorbed dose for any kind of radiopharmaceutical.

Glenn D. Flux et al^[49] investigated a method of dosimetry that quantifies the three dimensional absorbed dose distribution resulting from an intralesional administration of a radio labeled monoclonal antibody, allowing for both spatial and temporal heterogeneity of distribution of the radionuclide and without the need for a calibration scan. They have developed a mathematical model to describe the distribution of activity as a function of time resulting from infusion at a single point within the solid component of a tumor. The parameters, required for this model, are either known directly or may be obtained from SPECT images data registered to computer tomography. Convolution of this distribution with a point-source kernel, enabled the three-dimensional absorbed dose distribution to be obtained. This method was applied to a set of patient-data acquired in the course of a clinical study and dose-profiles and dose-volume histograms were also produced. They found that the three dimensional distribution of dose was significantly non-uniform. The initial results suggests that this method offers a means of determining the absorbed dose distribution within a tumor resulting from intralesional infusion. Furthermore it enabled,

individual patient treatment planning and optimization of the parameters that are within the clinician's control.

T. Smith et al ^[50] evaluated the radiation dosimetry of Technetium-99m-DMSA in children aged from 5wks to 14.8 years, who were undergoing routine diagnostic investigation of renal impairment. The organ dose were calculated using MIRDOSE 3 with biokinetic data, and effective doses and effective dose equivalents were also estimated. They obtained that the effective doses estimated by interpolation by inverse weight between pediatric anthropomorphic phantoms differed by up to 46% from those based on discrete phantoms which showed less variation. In children with normal bilateral renal function, the mean effective dose per administered activity was 0.91 ± 0.08 mSv. Renal pathology reduces the effective dose, on average, by 15% of the value for normal patient. It is observed that over the pediatric age range, the uniformity of effective dose values was improved by scaling the administered activity according to body surface area rather than body weight.

S.M. Goddu et al ^[51] calculated the cellular dosimetry that is important in both diagnostic and therapeutic nuclear medicine. Experimental range-energy relations for electrons and alpha particles, along with derived geometric reduction factors were used to calculate cellular absorbed fractions for these radiations. The resulting absorber fractions are employed to calculate cellular S-value for several radionuclides. They found that cellular sources with energies ranging from 0.1 keV to 1MeV, distributed uniformly in the source region. These are calculated for several target ←source combinations including cell←cell, cell←cell surface, nucleus← nucleus, nucleus ←cytoplasm and nucleus ←cell surface. Similar

type of data are collected for mono-energetic alpha particle sources with energies ranging from 3 to 10 MeV. S-values are also conveniently tabulated for ^{32}P , ^{35}S , ^{86}Rb , ^{89}Sr , ^{90}Y , $^{114\text{m}}\text{In}$, ^{131}I , Anger electron emitters ^{51}Cr , ^{67}Ga , $^{99\text{m}}\text{Tc}$, ^{111}In , ^{123}I , ^{125}I , ^{201}Tl , ^{203}Pb and the alpha emitters ^{210}Po . In addition to this, S-values are obtained for radionuclides in the ^{212}Pb decay series, including ^{212}Pb , ^{212}Bi and ^{212}Po . The absorbed fractions and the S-value both are supplied for a number of different size cells and cell nuclei. With the absorbed fractions and S-value it is obtained that along with experimentally determined information on biokinetics and subcellular distribution of radionuclides, the cellular self-absorbed dose can be conveniently calculated.

G.M. Makrigiorgoes et al ^[52] have investigated the limitations of conventional Internal dosimetry at the cellular level. A theoretical examination of the validity at the cellular level of assumption used in classical internal dosimetry has been undertaken. It was observed that when selective intracellular uptake of a radiolabeled compound occurs in specific cells within a cell cluster, conventional dosimetry underestimates the radiation dose delivered to the labeled cells by two fold to more than 25fold if the emitted electrons have ranges of a few micrometers or less, i.e., energies smaller than ≈ 10 keV. It was found that under same conditions, conventional dosimetry overestimates (20% to 50%) the electron radiation dose to the non-labeled cells of the cell cluster. It was also observed that inclusion of photons in the calculation of the total dose to individual cells does not alter significantly the conclusions of this investigation.

R.W. Howel et al ^[53] evaluated the design and performance characteristics of an experimental Cesium-137 irradiator to simulate internal radionuclide

dose rate pattern. When radionuclides are administered internally, the biological effect can depend on the total absorbed dose and the rate at which it is delivered. A ^{137}Cs irradiator was designed to deliver dose-rate pattern that simulate those encountered in radionuclide therapy. An 18-Ci ^{137}Cs irradiator was fitted with a computer controlled mercury attenuator for the purpose, that facilitated changes in dose-rates. The absorbed dose and dose rate were calibrated with MOSFET dosimeters customized for low dose-rates. It is obtained from the investigation that, the initial dose-rates ranging from 0.01-30cGy/hr can be delivered depending on the location of the cage in the irradiator and the thickness of the mercury in the attenuator system. To demonstrate the irradiation system's capability and to deliver dose-rate patterns encountered in the radionuclide therapy, a simulation was performed where the dose-rate initially increased exponentially followed by an exponential decrease. It is obtained that the irradiator system is well-suited to expose small animals to any dose-rates pattern, thereby facilitating calibration of biologic dosimeters (e.g. cell survival, chromosome aberrations) which can be used to measure the absorbed dose to a target tissue after administration of radionuclide.

K. S. Kolbert et al ^[54] investigated the implementation and evaluation of patient specific three-dimensional internal dosimetry. Normally the calculation of absorbed dose in target region from a source region rely on a standard "reference man" geometry and assume an uniform distribution of radiolabel. But this approach is acceptable at the low level of radioisotopes administered for the most diagnostic purposes, the generality of the calculations is not adequate for doses at the higher levels required for therapy and is not extendible to tumor dosimetry. For the reason, they have developed an integrated system which utilizes patient's anatomy and

radionuclide distribution in the calculation of absorbed dose-rate or total dose to any user-defined target region. Images of radionuclide distribution (PET/SPECT) are registered to anatomic images (CT/MRI) and then entered into three dimensional internal dosimetry system (3D-ID) where regions of interest are defined. Dose calculations are performed by the mathematical convolution between user- specified, dose point kernel with the activity in source volume over the target volume. The resulting dose-rate distribution was scaled by cumulated activity to yield absorbed dose. In addition to calculating the mean dose, dose- volume histograms were generated which plot absorbed dose with respect to percent of volume. The method was evaluated using selected standard man phantom organs. The dose estimates for two patients were included to illustrate differences between patient-specific and MIRD based calculations. This also provides an alternative approach to image display and three dimensional internal dose calculations. The representation of absorbed dose to a target volume provides valuable information in assessing tumor control probability and normal tissue toxicity.

H.B. Giap et al ^[55] developed SPECT based three-dimensional treatment planning system for radioimmunotherapy. In radioimmunotherapy, there were two major obstacles in developing the method of determining accurate dose estimates. These were (i) difficulty in obtaining an accurate patient-specific three-dimensional activity map *invivo*, and (ii) calculation of the resulting absorbed dose. The authors proposed a method for three dimensional internal dosimetry that integrates the three dimensional activity map from SPECT, with a dose-point kernel convolution technique, to provide the three-dimensional distribution of absorbed dose. The accurate activity quantitation was achieved with appropriate methods. The count

density map from SPECT images was converted into an activity concentration map with a calibration phantom approach. This map was then convolved with an ^{131}I dose-point kernel and three dimensional fast Fourier transform to yield three-dimensional distribution of absorbed dose, which was under processing, to provide the absorbed dose distribution in regions of interest. The accuracy of quantitative SPECT was validated to be within 16%. Calculation of penetrating radiation absorbed dose was verified with thermoluminescent dosimeter measurements to be within 8%. With standard organs and configuration, absorbed dose calculated in this method was in good agreement with MIRD formalism (less than 14%). This newly developed method overcomes the limitations of planar imaging techniques and the current routine implementation of the MIRD formalism. The result can be processed to provide the absorbed dose distribution in regions of interest and parameters for treatment optimization. Absorbed dose distribution from any plane can be graphically displayed in various ways.

G. Sgouros et al ^[56] described a calculation approach that provides the spatially varying radiation absorbed dose, presented as isodose contours, superimposed on CT images, from non-uniform and /or irregular cumulated activity distributions. The CT images are obtained from magnetic tape and are displayed on a high resolution color graphic display monitor. Source tissue geometrics are defined on a series of contiguous CT images automatically or manually, thereby a three dimensional representation of the various source volumes of activity were obtained. Dose calculations are performed using a radionuclide-specific absorbed dose point kernel in the form of a look up table. This method yields spatially varying dose delivered to tumor and normal tissue volumes from a patient-specific cumulated activity distribution in a clinically implantable manner. This label of

accuracy in determining normal tissue and tumor dose may prove valuable in the evaluation and implementation of radionuclides and radiolabeled compounds for therapeutic purpose.

Graham et al ^[57] calculated the estimated dosimetry in subjects undergoing imaging studies for defining the radiation risk of ¹¹C-glucose PET imaging. They obtained the time-dependent radioactivity concentrations in normal tissue in thirty-three subjects after intravenous injection of ¹¹C -glucose by PET imaging. They calculated the radiation absorbed doses according to the procedures of the Medical Internal Radiation Dose (MIRD) committee along with the variation in dose based on the calculated standard deviation of activity distribution observed in the individual patients.

John et al ^[58] established a relationship between the bone marrow absorbed dose and the toxicity .The relationship is expressed as the percentage decrease in the peripheral blood platelet count. The MIRD model was used to calculate the bone marrow absorbed dose. Patients suffering from metastatic prostate cancer, undergoes investigation using the noninvasive and pharmacokinetic methods. The mean bone marrow absorbed dose using the noninvasive and pharmacokinetic methods were in a close range to each other.

O, Connor et al ^[59] estimated the dosimetry and biodistribution of an Iodine-123-labeled somatostatin analog in patient with neuroendocrine tumors. Region of interest in the analysis of the whole-body image was to determine organ and tumor dose. The gallbladder wall received highest dose of 0.48 rad /mCi , while other organs receiving doses of 0.12 rads /mCi or less. Tumors could be identified in the work. Calculations with ¹³¹I instead of

¹²³I indicated that the gallbladder wall would receive 2 rad /mCi and the average tumor doses would range from 0.9 to 5.0 rad/mCi. They conclude that ¹²³I -octreotide can be established as a useful agent for the visualization of neuroendocrine tumors.

Votaw et al ^[60] calculated the radiation dose to 26 organs and the whole body from [¹²³I] epidepride, The dosimetry calculations used a combination of in vivo uptake and biodistribution data from one rhesus monkey and seven humans to estimate residence times in eight organs. The computer program MIRDOSE 2 was used to calculate the dosimetry. Results indicate that 75% of the radioactivity is cleaned through the urinary tract while the remaining radioactivity clears through the gallbladder and intestinal tract.

Cheryl et al ^[61] measured external exposure rates of 27 patients using a calibrated ionization survey meter. The exposure rates were measured at the time of release from the hospital and 2-7 days post-hospital discharge. Measurements were taken at 1,0.6 and 0.3 meters from the patient's upright body axis (stomach to thyroid). Vertical movement of the survey instrument was utilized to obtain the maximum reading each time. All patients had exposure rates <2mR/hr at 1meter at 2-4 day post-hospital discharge, 88% (21/24) had exposure rates <2mr/hr at 0.6 meter at 2-4 days post-hospital discharge.

C.Nicholl et al ^[62] observed, the pharmacokinetics of Iodine-123-IMBA for melanoma imaging. They tried to describe the synthesis of radioiodinated IMBA, N-(2-diethylaminoethyl) -3-[¹²³I /¹³¹I] iodo-4-methoxybenzamide 8, -its organ distribution, its comparison with BZA and other benzamides, and demonstrate the scintigraphic efficacy of the title compound with three

melanoma patients. They observed that due to rapid background clearance and high melanoma affinity, IMBA showed high tumor contrast at 4hr after injection which makes it a promising new radiopharmaceutical for the scintigraphic detection of melanoma metastases.

B. Bubeck et al^[63] studied the pharmacokinetic of Technetium-99m-Mercaptoacetylglycylglycine (^{99m}Tc-MAG₃) in human, to replace O-iodohippurate (OIH) for renal function studies. For interpretation of clinical findings, extensive pharmacokinetic studies were performed on patients. These showed that, ^{99m}Tc-MAG₃ compared with OIH, has a higher plasma-protein binding, an essentially higher intravascular concentration, a smaller volume of distribution with practically identical biologic half-lives and a correspondingly lower clearance. The steady-state measurement showed high clearance of OIH than of ^{99m}Tc-MAG₃ (n-124). Competitive inhibition of tubular transport system by p-aminohippurate (PAH) (20 patients) revealed a distinctly higher suppression of ^{99m}Tc-MAG₃ clearance than OIH which indicates lower affinity of the ^{99m}Tc complex to the tubular cell. The plasma extraction efficiencies of both the agents did not indicate an extra-renal elimination of ^{99m}Tc-MAG₃. They conclude that, this new radiopharmaceutical is a pragmatic alternative to OIH and offer advantages not only for scintigraphic imaging but is also suited for quantitative renal function studies.

H. Herzog et al^[64] measured the pharmacokinetics of Yttrium-86 radiopharmaceuticals with PET and radiation dose calculation of analogous Yttrium-90 radiotherapeutics to demonstrate the quantitative in vivo assessment of human. The technique is illustrated in a patient with disseminated bone metastases from breast cancer who, was injected with

100MBq of ^{86}Y -citrate, an analog of the commercially available radiotherapeutic ^{90}Y -citrate. Whole-body biodistribution was measured with PET camera 4, 10, 21, 28 and 45 hr post-injection. Uptake data were determined from reconstructed transverse PET images by region of interest in normal bone tissue, liver and metastases. Images of coronal and sagittal whole body sections were obtained from reformatting the transverse PET images. This study demonstrates that, the use of PET via ^{86}Y allows an individual in vivo quantification of activity uptake and radiation dose to both normal tissue and tumor, in pain treatment with ^{90}Y - labeled radiotherapeutics.

W. Krahwinkel et al ^[65] assessed the data of pharmacokinetic distribution of radiation dose from ^{201}Tl Chloride used in routine myocardial scintigraphy based on animal studies or on small groups of human not taking part in any sort of physical exercise. In order to obtain data under routine conditions pharmacokinetic of ^{201}Tl were measured in 15 individuals who had undergone diagnostic myocardial scintigraphy and were classified as normal. Ventral and dorsal whole body scans were acquired until 9 days after injection. Conjugate pixels were averaged geometrically. Percentage value of total administered dose were obtained for total body and 13 organs by using a calculation method that takes into account the differentiation of overlapping organs.

Richard J. Quinn and Grahame J. Elder ^[66] measured the poor uptake of technetium-99m-dimercaptosuccinic acid (DMSA) with near normal technetium-99m-diethylenetriaminepentacetic acid (DTPA) caused by tubulointerstitial renal disease. In general, the renal uptake of $^{99\text{m}}\text{Tc}$ -DMSA is a good measure of global renal function and correlates with the effective

renal plasma flow (ERPF), glomerular filtration rate (GFR) as measured by creatinine clearance and renal scanning with ^{99m}Tc -DTPA. They have represented a patient who had minimal uptake of ^{99m}Tc -DMSA on two occasions with only moderate GFR impairment as measured by creatinine clearance and a near normal renal scan with ^{99m}Tc -DTPA. They found from biochemical and biopsy studies that renal tubular damage was present. The lack of uptake of ^{99m}Tc -DMSA is most likely due to a discrete tubular defect and does not reflect overall renal impairment. They have also demonstrated the need to consider ^{99m}Tc -DMSA uptake an index of “functioning tubular mass” rather than “global renal function” and that in the face of predominant tubulointerstitial disease.

D. Groshar et al ^[67] observed the ability to evaluate kidney function in each kidney separately by quantitative SPECT using 20 patients with a single kidney and varying degrees of renal disease. ^{99m}Tc -dimercaptosuccinic acid (^{99m}Tc -DMSA) uptake was compared with renal function measured by creatinine clearance and serum creatinine. There was good correlation for both serum creatinine and creatinine clearance. The result indicate that SPECT quantification of ^{99m}Tc -DMSA uptake can be used as an indicator of the function of each kidney individually.

P. Shreve et al ^[68] evaluated the Carbon-11-acetate PET imaging in renal disease. 18 patients underwent dynamic PET imaging of kidneys after intravenous bolus injection of 10-20 mCi [^{11}C] acetate. Time-activity curves of renal parenchyma tracer activity were fitted to a two-compartment model using direct arterial blood sampling for the arterial input function. They found that, renal uptake of [^{11}C] acetate is prompt and high target-to-background ratios are achieved even in the presence of

markedly reduced renal function. [^{11}C] acetate is cleared from the renal parenchyma without any urinary excretion and the rate of clearance is comparable to myocardial clearance rate. So they conclude that carbon-11-acetate is a promising physiologic tracer for the study of renal disease.

J.V. Nally Jr. et al ^[69] studied the captopril renography in two kidney and one kidney goldblatH Hypertension in dogs in order to improve the technique of non-invasive detection of renal artery stenosis. The study suggests that the $^{99\text{m}}\text{Tc}$ -DTPA renal flow study coupled with captopril challenge may unmask intra-renal angiotensin II- dependent functional and hemodynamic changes of stenotic kidney and offer promise in the detection of renin-dependent hypertension.

Charles D. Russell et al ^[70] investigated the technical procedures for use of new kidney agent technetium- $^{99\text{m}}\text{MAG}_3$. The findings help to identify the benefits of imaging with MAG_3 , recognize the different properties of the agents DTPA, OIH and MAG_3 , utilize developed imaging technique and also to identify some abnormal conditions.

J. R. Buscombe et al ^[71] found that, volume rendered three-dimensional displays could improve the accuracy of reporting renal cortical scars in patients imaged with $^{99\text{m}}\text{Tc}$ -dimercaptosuccinic acid (DMSA). They compared volume rendered three dimensional displays of SPECT data for 20 patients, with a total of 37 kidneys, with SPECT data displayed as transaxial, coronal and sagittal slices as well as planer images. All patients were imaged 2-3 hr after administration of a standard dose of 2mCi (74MBq) of $^{99\text{m}}\text{Tc}$ -DMSA and the results were reported using two readings of the images 14 days apart. They found that, volume-rendered three

dimensional display of ^{99m}Tc -DMSA SPECT data increases the number of defects reported as renal cortical scars.

M.K.O'Connor et al ^[72] assessed the hepatic arterial and portal venous components of liver blood flow. 82 studies were performed in 56 patients with both normal and abnormal liver function. Using regions of interest analysis, time-activity curves were obtained for the lung, liver, spleen and left kidney. These curves were analyzed by four different methods. Two of those, based on measurement of slopes of uptake and washout curves from the liver and spleen. The other two methods employ deconvolution analysis to permit area measurement under the deconvoluted curves as an indication of blood flow. The deconvolution based method provided the most significant separation between normal and patients with various liver disorders and would appear to be the most suitable techniques for monitoring the effect of various drugs and surgical procedure and the relative arterial /portal contribution to hepatic blood flow.

F. Mut et al ^[73] determined optimum processing protocols for volume determination of the liver and spleen from SPECT imaging with technetium-99m-sulfur colloid. A method for volume determination using threshold algorithm was calibrated against phantoms applied to 60 patient studies. Good reproducibility was found using different projections and computing the volume on separate days. Variations of the measured volumes with threshold value, reconstruction filter cut-off frequency and attenuation corrections were investigated. Reconstruction parameters producing best image quality were also determined. It is concluded that optimal parameters must be determined for any processing protocol, and must then be adhered to in future applications to insure clinical accuracy,

especially those parameters demonstrating the most quantitative and qualitative sensitivity.

H. D. Fawcett and B.A Sayle [74] reviewed five hundred and three, planar and SPECT hepatic studies separately by two experienced observers looking for focal disease. An equivocal reading meant referral to ultrasound or computed tomography (US/CT). The increase in correct readings and decrease in US/CT referrals per 100 positive and per 100 negative SPECT readings were calculated, then the increase in correct readings and decrease in US/CT referrals for various positive rate of liver involvement is determined. It is found that the overall positive rate is $\approx 13\%$, yielding 1.1 and 0.83 more correct readings and 1.8 and 2.0 few US/CT referrals per 100 cases for each reader, respectively; a marginal benefit for SPECT over planer scintigraphy.

K. Wintch and A. Meyers [75] correlated positive liver SPECT images with normal or equivocal CT studies. Two patients were studied, both of them intravenously injected with ^{99m}Tc -Sulfur Colloid. The SPECT liver/spleen images were corrected with CT images. The SPECT scans detected abnormalities that were neither present nor differentiated from normal tissue on the CT images. This demonstrate that ^{99m}Tc -Sulfur Colloid SPECT correlated with CT can detect abnormalities that would be normal or equivocal when using CT alone.

CHAPTER 3

Experimental Details

Experimental Details

3.1 INTRODUCTION

Radiation is an outward flow of energy from some energy source. Radiation interacts with matter through the transfer of energy to its surroundings. These interactions are of great importance as these mechanisms are the means by which radiation is detected and measured. Interactions are also the means by which radiation dose is delivered to tissues. Generally the ionizing radiation interact with nuclei, electrons or with the total atom of the matter, with energy being transferred totally or in part in the following ways:

I. Photoelectric effect, **II.** Compton scattering **III.** Pair production (triplet production may also occur), **IV.** Photonuclear reaction (photodisintegration), **V.** Thomson scattering and **VI.** Rayleigh scattering. Among these, first three are most important as they play a significant role in interaction of ionizing radiation of low to moderate energies with either biological or inanimate matter^[13]. The radiation detecting devices are categorized in two different groups: **(a)** devices to detect and measure the level of radioactivity and **(b)** devices to measure the radiation dose rate or the accumulated dose. Various types of instruments have been developed for measuring the radioactivity and radiation dose. For the measurement of radioactivity, there are **(i)** gas-filled radiation detectors (which include ionization chamber, proportional counters, Geiger Muller counter etc.). **(ii)** Scintillation detectors (Solid and liquid; NaI(Tl), CsI(Tl), KI(Tl), LiI(Tl), ZnS(Ag), p-terphenyl, 2-phenyl-5-(4-biphenyl)-Ozazole(PBO), 2-phenyl-5-(4-biphenyl)-1,3,4-oxadiazole (PBD) etc), **(iii)** Semiconductor radiation detectors (Si-Li, Ge-Li,

Cd-Te, Cd-S, HPGe etc), and (iv) Cerenkov detector (high density glasses whose refractive index is 1.6 to 1.7 for sodium D-lines, and some liquids of high refractive index^[9]). For measuring radiation dose rate or accumulated dose over a certain time period, instruments like gas filled chamber which includes GM tube based survey meters, pocket dosimeter, thimble chamber, electret ionization chamber (EIC)^[76], ion current chamber^[9] are there. There are also instruments for the measurement of absorbed dose by measuring chemical change in certain radiation sensitive matter [FeSO_4 ^[77], alanine or a mixture of alanine and paraffin]^[78], measurement of absorbed dose by calorimeters^[79], measurement of absorbed dose by photographic technique (film badge), measurement of absorbed dose by autoradiographic technique (transparent detectors) radioluminescent detectors and thermoluminescent detectors (TLD) [LiF , $\text{Li}_2\text{B}_4\text{O}_7$: Mn, $\text{Li}_2\text{B}_4\text{O}_7$: Cu, LiF (Mg, Cu, P), BeO : Li, BeO : Na, NaCl : Ba(T), CaF_2 , CaF_2 :Dy, CaSO_4 :Mn, CaSO_4 :Dy, CaSO_4 :Tm etc]. Gamma-ray spectrometry is another very important non-destructive technique to perform qualitative as well as quantitative analysis of radionuclides. Moreover, to provide visual information on various body processes, nuclear medicine imaging procedures come forward. With the help of these imaging device and techniques it is now possible to assess the radionuclidic distribution in different parts of a given organ after in-vivo administration of a radiopharmaceutical to distinguish between the normal and abnormal tissues. Two major types of imaging systems are employed for the purpose, one is rectilinear scanner and the other is a scintillation camera.

Principle, working procedures, merits and demerits of some of the commonly used radiation detectors are briefly described as follows:

(i) *Gas-Filled Radiation Detectors:*

The basic approach of a gas filled detector is very simple: radiation is sensed by detecting the ionization of gas molecules produced by deposition of energy during radiation's passage through the gas-filled detector. In essence, a gas-filled detector is a container whose total volume is filled with gas with two electrodes on both sides, one positive (the anode) and one negative (the cathode) that are connected with a d.c. powersupply. Thus a potential difference is established between the two plates. A sensitive current measuring device is placed in the circuit. When ionizing radiation passes through the sensitive volume it interacts with the gas and produces ion pairs in the gas; the resulting free electrons are attracted to the anode, and the positively charged gas molecule ions are attracted to the cathode. This results in a flow of current that is sensed by detector. Since the negative ions are much lighter than the positive ions, they travel at a higher velocity and reach the positive electrode (anode) more quickly. Commonly used gases are helium, neon, argon, hydrogen and air. There are three types of gas-filled ionization detectors, which are classified by the voltage levels at which they operate. A plot of current flow versus applied voltage is shown in the following figure 3.1 to characterize the ionization chamber, proportional counter and Geiger Muller counter regions.

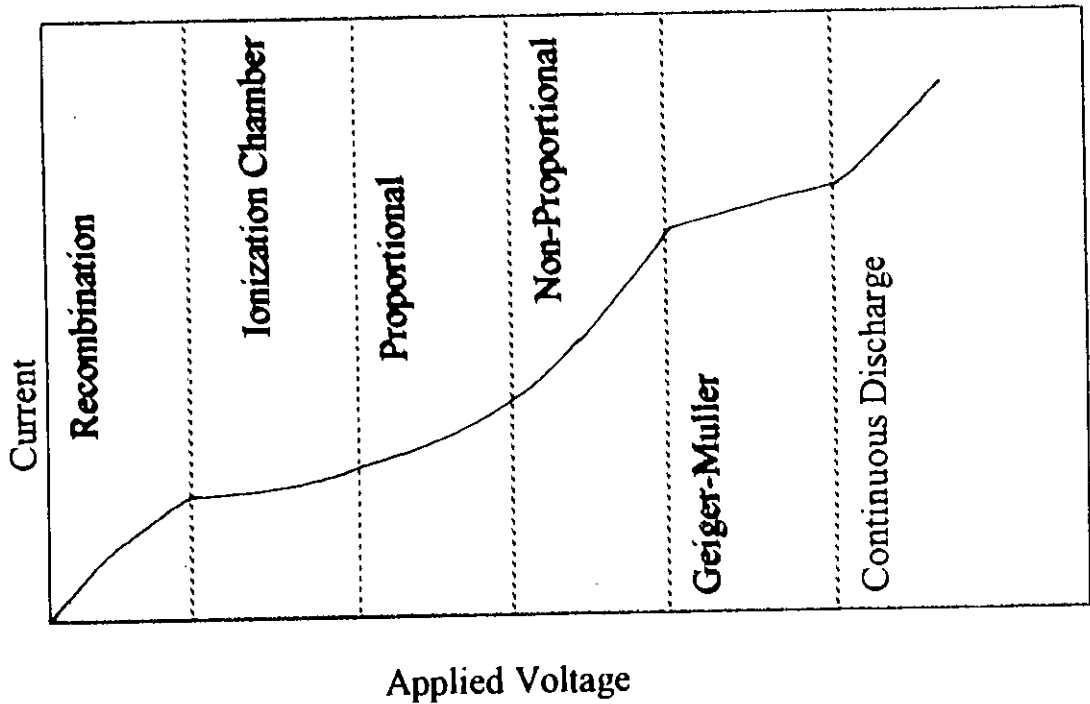


Figure 3.1 Measured Current Versus Applied Voltage For Ionization Detector

Ionization Chamber:

The first area located in the figure 3.1 is considered as the recombination region. The potential difference in this region between the two electrodes is not sufficient to clear all of the ions from the sensitive volume. Moreover some recombine again to form the electrically neutral atoms. With the increase of voltage, a plateau or saturation region is reached which defines the ionization chamber region.

In this portion of curve, the voltage is sufficient to clear all of the ions from the sensitive volume. But it is not sufficient to accelerate the ions to the point that they become ionizing radiation themselves. So the resulting current flow from the individual interaction is very small which is beyond measurement. For this reason, ionization chambers are used to measure total current induced in the sensitive volume, caused by a source of radiation such as an X-ray beam or a vial of a radiopharmaceutical.

Proportional Counter:

An increase in voltage past the ionization chamber region results in an increase in current flow and characterizes the proportional region. In this area voltage between the two electrodes is sufficient to produce secondary ionization by accelerating the primary ions to the point that they become ionizing radiation. Gas amplification factors of 10^3 to 10^6 are common with these instruments. As a result current flows for individual particle interactions are enough to be measured separately. Thus individual particles can be counted easily.

Geiger Müller Counter:

As the voltage continues to increase, the current flow in the ionization chamber becomes no longer directly related to energy deposited and the region of limited proportionality is reached. Gas amplification occurs by secondary ionization as was in proportional counter. The accelerating voltage between the electrodes provides a high degree of energy to the electrons. As a consequence of it, the electron produces ultraviolet radiation whenever they reach the positive electrode. This radiation travels to the negative electrode where additional electrons are freed and accelerated toward the positive electrode. The overall effect is an avalanche of ionization that spread throughout the sensitive volume and this process is terminated by another process known as quenching. A relatively large output pulse that is independent of the energy of the incident particle energy characterizes the Geiger Müller Counter. So it can not be used for counting procedures based on energy discrimination. Since it takes a significant amount of time to quench the detector the Geiger Müller counter has a dead time, that prevents it from being used as a measuring device for high intensity radiation fields.

The applications of ionization detectors in nuclear medicine are hindered by their low detection efficiency for electromagnetic radiation. Radiation survey meters, calibration devices, pocket dosimeter, the thimble chambers etc. are example of ionization chambers. These instruments are generally calibrated to read in units of exposure such as roentgens per hour and have wide applicability in nuclear medicine with a broad spectrum of range of exposure, e.g. from one milli-roentgen/hour to several hundred roentgen/hour. Proportional counters are relatively insensitive to electromagnetic radiation and are generally used only in counting alpha and beta radiation. The Geiger-Müller detectors are widely used in nuclear medicine as survey meters to locate sites of contamination, to evaluate the handling and disposal of radioactive materials and as a general room monitors. So it could be said that the ionizing detectors serves as detectors of α -and β -radiation and also have capabilities for detecting X-rays and γ -rays where their detection efficiency is not a problem.

(i) Solid -State Detectors:

There are certain crystalline substances, which are capable of exhibiting measurable effects when exposed to ionizing radiation. In these substances electrons exist in a definite energy band, separated by forbidden bands. Electrons normally exist in the valence band. When the ionizing radiation passes through such substances, the kinetic energy of the radiant particle is transferred into the valence electrons, which causes them to rise into excitation or conduction band [80] through the forbidden band or may be trapped within the forbidden band. The place left by the electron is known as hole. These effects are measured individually in different types of detectors viz. (a) scintillation detectors (b) semiconductor detectors and (c) thermoluminescence detectors.

(a) Scintillation Detector:

The penetrating radiations like γ - and X-rays, travel through the low density gas with a little interaction. So the gas detectors have a very low detection efficiency for these radiations. Therefore improvement was necessary. To improve counting efficiency for this radiation, solid and liquid scintillation detectors with high density came forward to be used. These detectors have the unique property of emitting scintillation or flashes of light photons which are converted to an electrical pulse by means of a photomultiplier (PM) tube. This pulse is then amplified by a linear amplifier and analysed by a pulse-height analyzer (PHA) and is then registered as a count. Solid or liquid type of detectors are being used for different types of radiation. For example Sodium Iodide crystals containing a trace of thallium (NaI (Tl)) are widely used for γ - and X-rays detection. This is a most commonly used scintillation crystal in nuclear medicine. Organic crystals like anthracene and plastic fluors are used for β -particle detection.

In liquid scintillation counting, a β^- -emitting radioactive sample and an organic scintillator are dissolved in the solvent. The β^- particles reacts with the molecules of the solvent and as a result of that, electrons are emitted. These electrons interact with the organic scintillators, whereby light photons are emitted which are then directed to two PM tubes coupled in coincidence. The PM tube produces a pulse which is registered as count. The organic scintillators are normally of a lower density and hence a lower counting efficiency than inorganic scintillators. But the decay time for light emission for organic scintillators is much shorter than that for inorganic scintillators. The decay time for NaI (Tl) is 0.25μ - sec whereas that for anthracene is 0.026μ - sec. The faster decay time permits the use of organic scintillators at higher count rates. The scintillation detector is most commonly used

detector in nuclear medicine. This detector is used generally to determine which radionuclides and in what amount of that are present in a mixed sample. Scintillation detector also helps to determine how much activity of a known radionuclide is present in a sample.

(b) *Semiconductor Detectors:*

Semiconductor detectors are made of germanium or silicon elements commonly doped with lithium. These detectors are designated as Ge (Li) or Si(Li) detectors of whom the former is commonly used for gamma-ray detection while the other one is for alpha ray detection. The basic principle of operation of these detectors involves ionization of the semiconductor atoms, as in gas detectors. The ionization produced in the detector by the radiation are collected as current and converted to voltage pulses through a resistor by applying a voltage. The pulses are then amplified and counted. The size of the pulse is proportional to the radiation energy absorbed in the detector. Since the semiconductors have higher density than that of gases, the semiconductor detectors show more efficiency in detecting X-ray and γ -ray than that of any gas detectors. Moreover in semiconductor detectors, each ionization requires only about 3eV compared to 35eV in gas detectors. Thus almost 10 times more ions are produced in semiconductor detectors than in gas detectors for a given γ -ray energy, thus yielding a better energy resolution of γ -ray photons of closer energies. These detectors are small in size (e.g. about 4 cm in diameter by 4cm in thickness for Ge (Li) detectors) and therefore, the detection efficiency for x-ray and γ -rays is much lower than that of NaI(Tl) detectors. Though the semiconductor detectors are most useful in differentiating among photon energy because of the high energy

resolution, particularly in detecting radionuclidic contamination, these are not in common use in nuclear medicine.

(c) Thermoluminescent Detector:

Thermoluminescence (TL) is the phenomenon of light emission caused by heating pre-irradiated TL materials. The TL property can be explained by the solid's energy band theory. Normally this process occurs in the crystals when the ionizing radiation passes through it by the process known as electron trapping. Traps are impurity atoms in the crystal structure which cause electrons to be caught in the forbidden band and may exist there at room temperature for a long time. If the irradiated crystal is subsequently heated at $\sim 200^{\circ}\text{C}$, the trapped electrons first jump to the excitation band and then returns into the valance band with the emission of light photon. The detector or dosimeter operated in this mode is known as thermoluminescence dosimeter (TLD). TLD offers several advantages. This can be used perfectly as a personnel monitoring device because of it's wide spectrum of dose measurement, linearity in dose response, more or less no angular dependence, negligible fading and smaller physical structure.

Photographic Film Dosimeter:

A strip of photographic film emulsion sandwiched between sets of absorbers or filters are used to estimate both the radiation level and the nature of the radiation, such as penetrating γ -radiation versus non-penetrating beta radiation or high energy γ - radiation versus low energy γ -radiation .The combination of this film strip with it's holder, constitutes the film monitor and often referred to as "film badge". The holder has two standard features: (i) an open window that permits exposure of the film to most types of radiation and (ii) a series of plastic and metal filters. The film

badges are used to record personnel doses as low as 10 milli-rem and as high as several hundred rem. They can be employed to record estimates of whole body doses, skin doses, hand and finger doses, eye doses and so forth, depending on where the badge is worn. The photographic film is very energy dependent when used as a radiation detector. However the use of filter system results in differing the film densities when the film is developed. This allows the type and energy of radiation to which the film is exposed to be estimated with a reasonable degree of confidence. The film badge has a number of advantages such as (i) economical, especially for institutions where hundreds of people work (ii) keeps permanent records for several years as a developed film for the purpose of re-examination and re-evaluation in cases of litigation (iii) helps in estimating of whether the film was exposed to a single exposure or to a series of exposures and also helps in case of on acute exposure, to estimate the angle of incidence of the radiation on the body.

Imaging Device:

Radionuclide imaging is one of the most important applications of radioactivity in medicine. The purpose of radionuclide imaging is to obtain a picture of the distribution of a radioactively labeled substance within the body after it has been administered intravenously to a patient. This is accomplished by recording the emissions from the radioactivity, with external radiation detectors placed at different locations outside the patient. The preferred emissions for this application are gamma rays of energy approximately within the range of 80-500 keV or for annihilation photons 511 keV. Gamma rays of these energy range are sufficient enough to penetrate the body tissues of deep seated organs but can also be shielded properly with a reasonable thick lead sheet. Alpha particles, β - particles,

Auger and Conversion electrons are of little use because of their less penetrating ability. Therefore these rays can not get out of the body and reach the detector except from very superficial tissues. However the Bremsstrahlung generated by electron emissions is more penetrating, but the intensity of this radiation is generally very weak. The imaging system detectors must have good detection efficiency for γ -rays. These detectors are also capable of discriminating the energy so that gamma rays that have lost energy by Compton Scattering within the body can be rejected. Sodium Iodide provides both these features at a reasonable cost. For this reason it is currently the detector material of choice for imaging system. A variety of imaging devices are used routinely in nuclear medicine. These include the rectilinear scanner, the scintillation camera and emission tomography devices.

Rectilinear Scanners:

The rectilinear scanner was the first device in nuclear medicine to portray the distribution of radioactivity within patient as an image (Figure 3.2). This device was first introduced in the decade of 1950 by Benedict Cassen^[81]. A rectilinear scanner is a moving detector imaging system that utilizes either a single or a dual probe. A rectilinear scanner consists of a scintillation probe detector, focusing collimator, mechanical detector motion system, spectrometer and an image recording system. The probe has a Sodium Iodide crystal 3 to 5 inches in diameter and 2 to 3 inches thick. This thick crystal gives the scanner excellent detection efficiency with high-energy gamma rays. Rectilinear scanners use multihole focusing collimators that limits the field of view of the detector to a geometrically defined spatial location. The distinguishing characteristic of a focusing collimator is that all the holes aim at the same point in space in front of the collimator called the

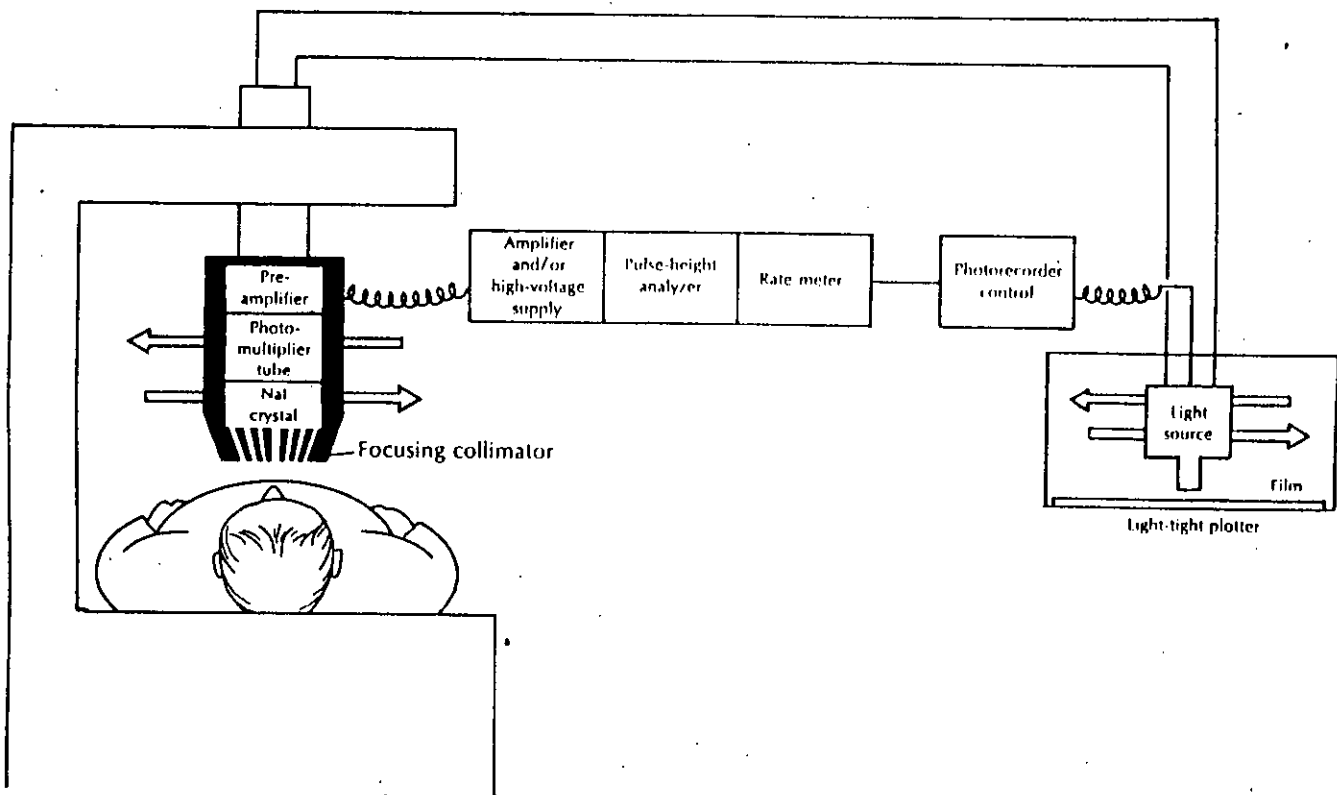


Figure 3.2 Single Probe Rectilinear Scanner Illustrating The Component Parts Of Typical System

focal point. Collimators are typically made from lead to minimize the likelihood of photons passing through the material separating individual holes. The photons that successfully traverse the channels of the collimator interact with NaI(Tl) crystal which serves as the detector of the scanner. When the photons interact with the crystal, they lose their energy by photoelectric effect or Compton interactions or by the combination of both. The crystals absorb the total energy and convert it into light photons. The photosensitive layer of photomultiplier tube (photo-cathode) which is optically coupled to NaI (Tl) crystal then absorbs these photons. As a result of this photoelectric process, electrons are released. The original number of electrons is then augmented by the dynodes of the PMT by a factor of approximately 1 million to produce an output pulse, the magnitude of which is directly proportional to the total energy absorbed by the crystal. The output pulse is then passed through pre-amplifier system. The system converts the pulse into one having enough amplitude and proper shape to drive the pulse height analyzer elements of the counting system. The pulse height analyzer allows the pulses of pre-selected amplitude range to the data-recording portion of the scanning system. The selected pulses are directed to output devices such as paper tapper, photo recorder or oscilloscope. A number of nuclear medicine clinics are still using the rectilinear scanner for thyroid, bone and ^{67}Ga imaging, but with the introduction of whole body imaging device like scintillation cameras the rectilinear scanner has lost some of its importance. For this reason, the rectilinear scanners have been almost phased out in nuclear medicine whereas scintillation cameras are the equipment of choice for routine use in nuclear medicine imaging.

The present study has been carried out by employing a **dose calibrator, a scintillation gamma camera, $^{99\text{m}}\text{Tc}$ - as radioactive agents for imaging**. The experiment involved studying about the **human kidney** and

liver. A brief description regarding instrumentation and organs portray are given as follows:

3.2 Equipment Setup

Dose Calibrator

96112
Dose calibrator is one of the most essential devices in nuclear medicine to measure the activity of radiopharmaceutical administered to the patient. Normally the dose calibrator is used to determine the radioactivity in a test tube, vial or syringe. The calibrator is cylindrical in shape, with a geometry of 4π radius. It's detector is a sealed chamber with a central well, which is filled with argon and traces of halogen at high pressure ($\approx 25-30$ atmospheres). The calibrator usually operates at a voltage of about 150V. The chamber is sealed to avoid variations in response with ambient temperature and atmospheric pressure. Whenever radioactive material is placed in the specified position of the well, the activity is measured in terms of the ionization current produced by the interaction of radiation (β & γ) emitted by the sample with the filled inert gases. The ionization current is converted into voltage signal, then amplified and processed and finally the activity is displayed in units of Becquerels (Bq) or Curies (Ci) for a fixed geometry. The response of the ionization chamber to various types of radiation varies with the kind of energy ranges and abundance of the radiation. Necessary corrections are performed as per requirements.

For the on going experiment setup an **Atom Lab 100 Dose calibrator** (model no.086-250) Biodex Medical systems Inc, was used. Atomlab Dose calibrator has a display unit, a detector unit, a detector cable, power card, vial syringe dipper, well liner, Moly Shield, Rs-232 Cable (optional) Rs-232 equipped (optional) and syringe Moly Assay shield (optional) as its component. This Biodex Medical systems Atomlab 100

dose calibrator is designed to perform accurate radioisotope measurements easily and quickly. The detailed specification of Atom Lob 100 Dose calibrator (model no. 086-250) is given in the Appendix.

Anger Scintillation Camera:

The Scintillation Camera is the most commonly employed imaging device in nuclear medicine today. The camera performance is being improved, keeping in line with constant technical development. The introduction of accessory equipments has allowed the versatility of the scintillation camera to be continuously expanded. The complete gamma camera/system usually consists of several components: a detector, a collimator, PM tubes, a preamplifier, an amplifier, a Pulse height analyser (PHA), a Positioning Logic Network and a display or recording device (Figure: 3.3).

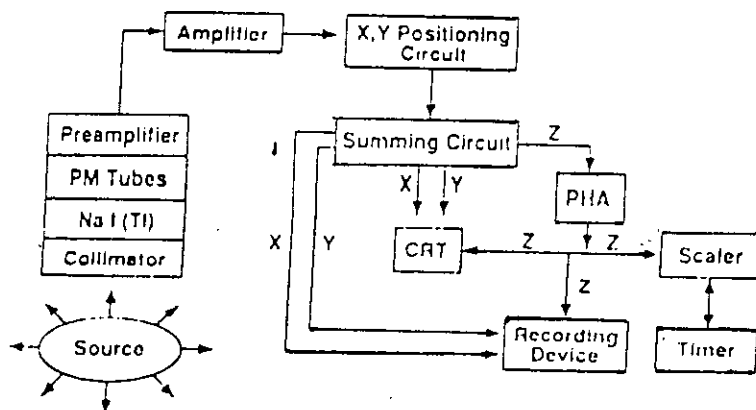


Figure 3.3 A Schematic Electronic Diagram of A Gamma Camera.
 CRT-Cathode Ray Tube, PHA- Pulse-Height Analyzer, PM -
 Photomultiplier Tube

The detector, PM tubes and amplifiers are encased in a unit termed as "detector head" which is mounted on a stand. This head can be made to move up or down and rotate with electrical switches to position it in the field of view on the patient. The X-, Y- positioning logic circuits, PHA and some recording devices are mounted on a console. Only a few days back the cameras were being operated by switches and dials on the console. But now a days, the total operation of the camera is performed by a computer built in it (Figure: 3.4). This computer is run by an appropriate software packages in conjunction with a keyboard and a video monitor. High voltage, intensity, window and photopeaks are all set by the operator's choice of parameters in the computer. Normally the acquisition of data and processing of that data, at a time is carried out by computer but it varies also, depending on the choice of manufacturer.

Detector:

Typically circular NaI (Tl) detectors are used in gamma cameras. The detector have a diameter of 25-50cm and 0.64-1.27cm of thickness. Normally 0.64 cm of thickness of the detectors are widely used for ^{201}Tl , $^{99\text{m}}\text{Tc}$ and ^{123}I radionuclides. Larger crystals (>40cm in diameter) are used in larger field of view (LFOV) cameras. Increase in thickness of the detector increases the probability of complete absorption of γ -rays and hence the sensitivity of the detector. But using thicker detector also increases the probability of multiple Compton scattering; as a result the X; Y coordinates of the point of γ -ray interaction can be obscured. This leads the way of obtaining poor resolution of the image of area of interest. For this reason, inspite of having decreased sensitivity, a thin NaI (Tl) detector is used in gamma camera.

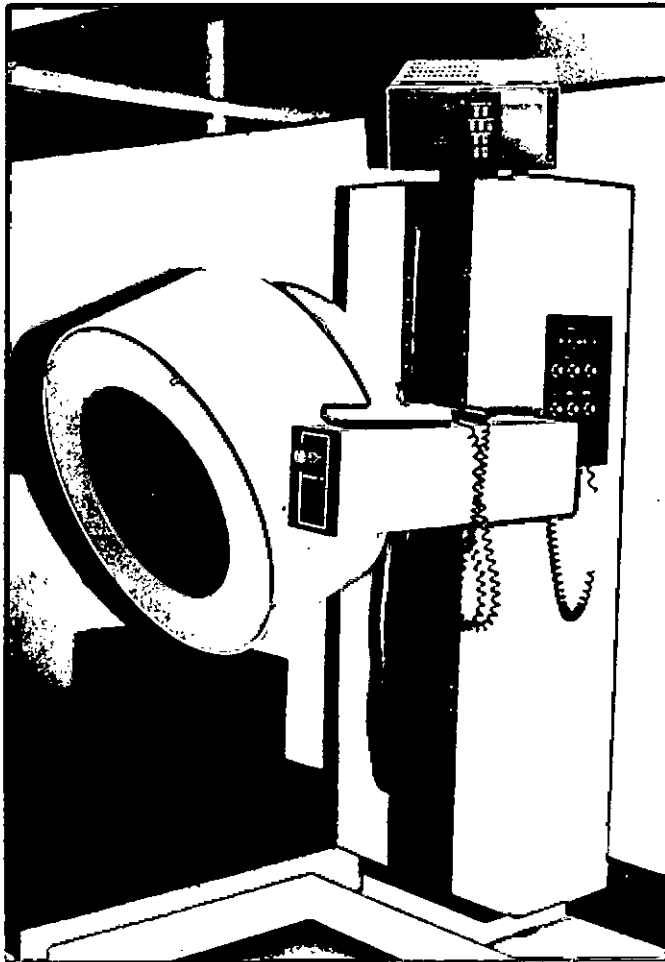
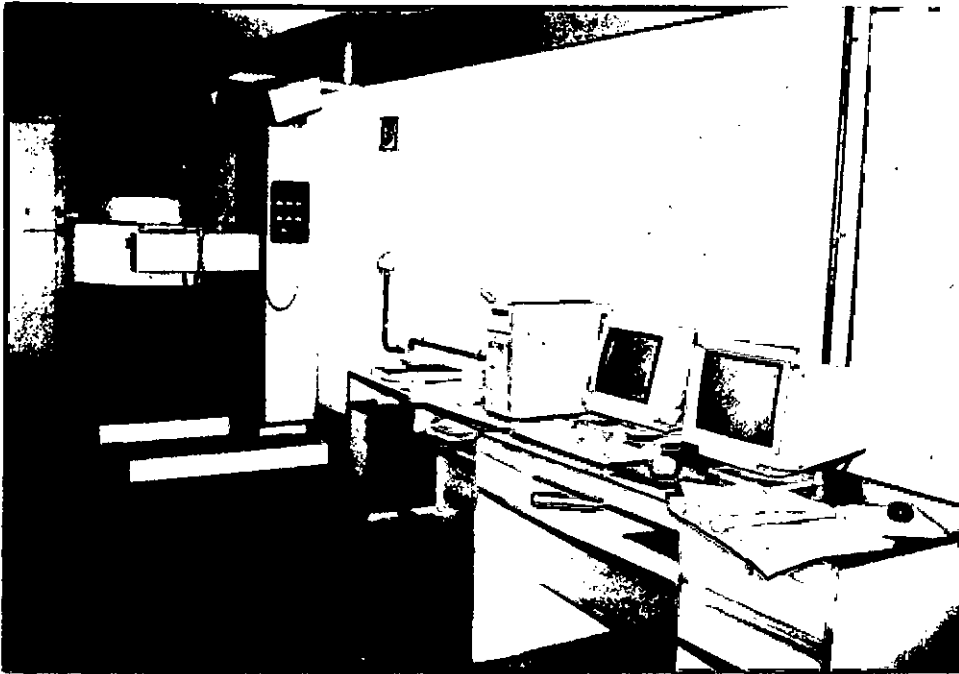


Figure 3.4 A Typical Gamma Camera.(Courtesy of Medx Inc. Ltd, USA)

Collimator:

A collimator of gamma camera is attached to the face of NaI(Tl) detector to limit the field of view by preventing the γ -radiation of the outside field of view from the detector. Collimators are made of material with high atomic number such as tungsten, lead and platinum. Among all, lead is widely used as a material of collimator in nuclear medicine because of economic choice. These collimators are designed in different sizes and shapes containing one or multiple holes to view the area of interest (Figure 3.5).

COLLIMATOR DESIGNS

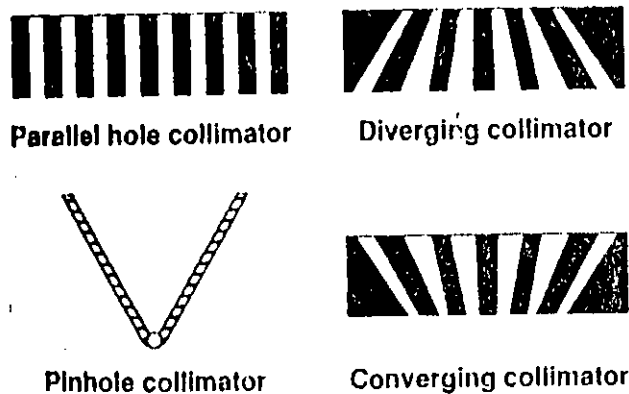


Figure 3.5 Different Designs of Collimators

The collimators with a single hole are known as **pinhole collimator**. Depending on the various design of the collimator the parallel hole collimators have holes of 4000 to 46000. Depending on the type of focusing and on the septal thickness of the hole, the collimators are classified as **parallel hole, pinhole, converging and diverging hole** types (Figure 3.6).

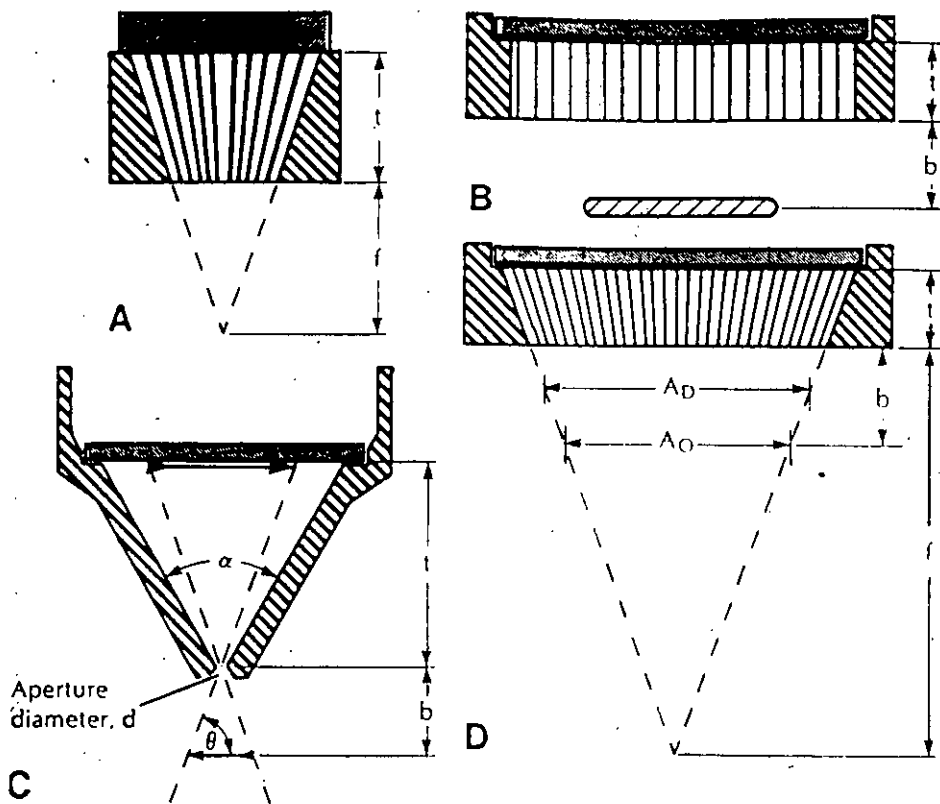


Figure 3.6 Schematic Illustration of Four Typical Collimator types Used in Nuclear Medicine: (A) Focusing Collimator (B) Parallel-hole Collimator (C) Pinhole Collimator (D) Converging Collimator For Each Collimator: t = Collimator thickness; b = Collimator-to-object distance; f = Collimator focal length. For the pinhole Collimator α and θ are geometrical angles that define the magnification property of the Collimator. For the Converging Collimator A_D and A_O illustrate the diameters of the field- of - view at two different Collimator-to-object distances.

Pinhole collimators are conical in shape with a single hole. These are used to image the small organs like thyroid glands to provide magnified images. Converging collimators have holes, converging to an outside point and are employed to provide magnified images when the organ of interest is smaller than the size of detector (e.g. Fan beam collimators, used for brain imaging). Diverging collimators are constructed with holes that are divergent from the detector face and are used in imaging organs like lungs that are larger in size than the detector. These collimators reduce the images of the organ. Parallel-hole collimators have holes parallel to each other and perpendicular to the detector face. These collimators are commonly used in nuclear medicine and furnish an one to one projected image.

Photomultiplier Tube:

PM tubes play the vital role in converting the light photons in the NaI(Tl) detector to an electrical pulse (Figure 3.7). PM tubes are mounted in an array of hexagonal fashion, to the back of the detector with optical grease, or in some cases, using lucite light pipes between the detector and the PM tubes. Square or hexagonal PM tubes are also used for better packing. The output of the PM tube defines the X, Y coordinate of the point of interaction of the γ -ray in the detector by using the X, Y positioning circuit and also is summed up by a summing circuit to form a pulse known as the Z pulse. This Z pulse is then subjected to pulse height analysis and is accepted, if it falls within the range of selected energies.

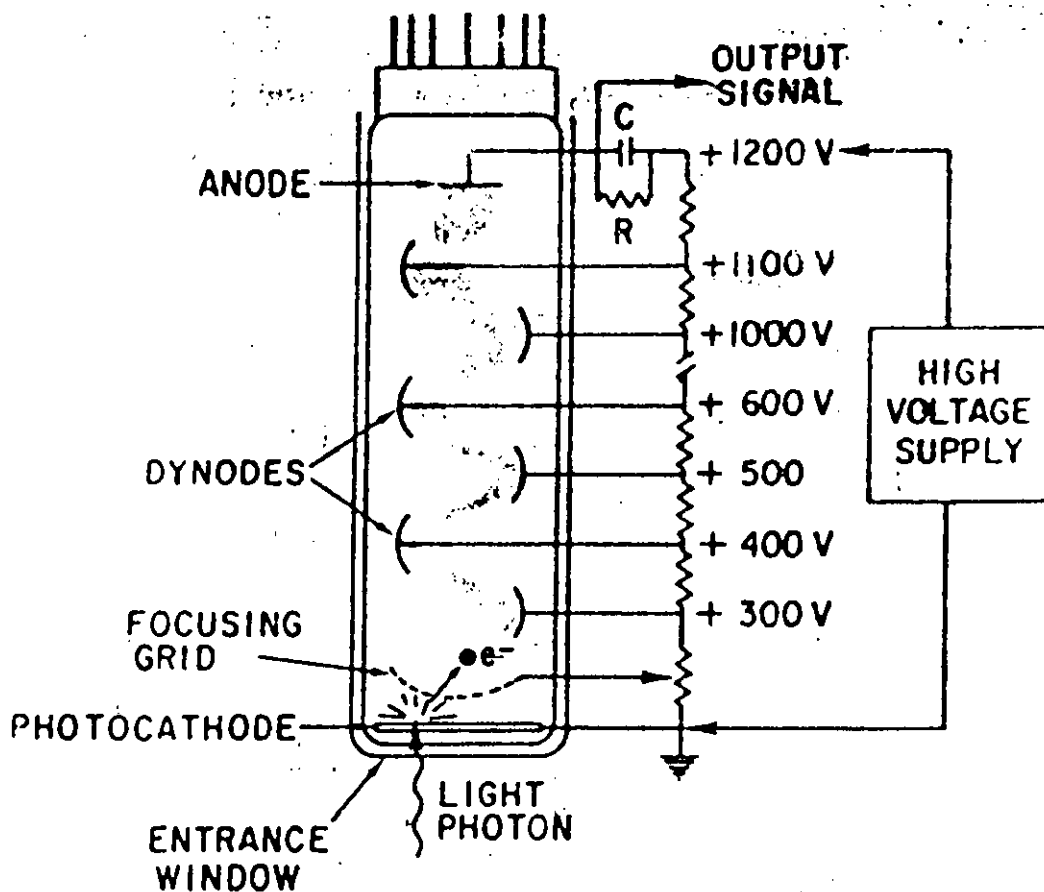


Figure 3.7 Basic Principle of Photomultiplier (PM) Tube.

X, Y Positioning Circuit:

Each pulse arising from the interaction of γ -ray interaction in the NaI(Tl) detector is projected at an X, Y location on the image corresponding to the X, Y location of the point of interaction of the x-ray. This is performed by an X, Y positioning circuit in conjunction with the PM tubes and a summing circuit (Figure 3.8). In the Fig.3.8 the principles of X, Y positioning of pulses, arising from γ -ray interactions in the detector, employing seven PM tubes is shown.

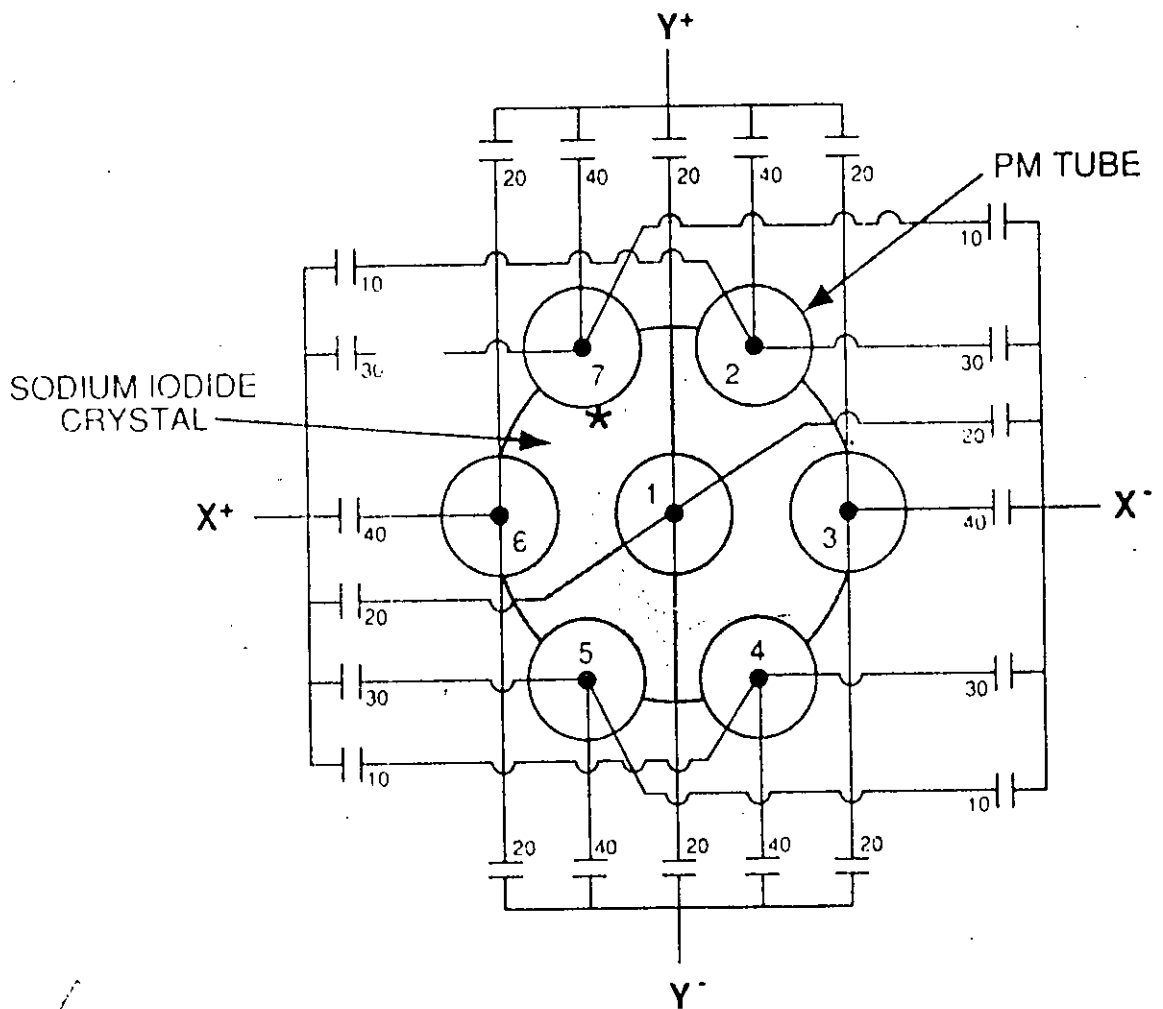


Figure 3.8 Arrangement of Seven Photomultiplier (PM) Tubes To Produce X and Y Pulses for the X,Y, Location of the γ -Ray Interaction in the Detector , X^+ , X^- , Y^+ and Y^- Pulses are Obtained by the Outputs of All PM Tubes Weighted by Capacitors for The Location of Each PM Tube in Relation to The Site of γ -Ray Interaction.(Adapted from Anger HO. Scintillation Camera, Rev Sci Instr. 1958;29:27)

All PM tubes are connected through capacitors to four output leads representing four directional signals X^+ , X^- , Y^+ and Y^- . The capacitance values are directly proportional to the location of the PM tube relative to the four signals. If a γ -ray interaction occurs at a location closer to tube 7 (indicated by a *), then this tube will receive the largest amount of light.

The other tubes will receive light in proportion to their distances from the point of interaction. The output signal of PM tubes are weighted by the appropriate choice of capacitor and the values are then summed to from each of the X^+ , X^- , Y^+ and Y^- signals individually. For the better accuracy of the X, Y, locations of all the pulses on the image, a large number of PM is needed.

Pulse-Height Analyser:

γ - rays of different energy spectrum can arise from a source of same or different radionuclides or can be due to scattering of γ -rays in the source and detector. Thus the output pulses of the amplifier may differ in magnitude .A PHA is a device that selects the pulses for counting within the pre-selected voltage intervals or “channels” and rejects the remaining. This selection of pulses are performed by energy discriminator knobs known as the lower level or upper level or the baseline and window; provided on the PHA and are ultimately delivered to the recording devices like scaler computer films and so on. The resultant Z pulses from the summing circuit, are analyzed by the PHA .The PHA analyses the amplitude of the pulses and select only those of desired energies by using appropriate peak and window setting.

Display and Recording System:

The output pulses from the PHA and X, Y - positioning circuit are projected in a persistence oscilloscope to see the instantaneous images of the distribution of activity in a source. Data are either collected for a preset time or for a preset total counts. Using scaler-timer, images can be obtained on photographic films or can be stored for future display in the video monitors of the digital computer.

Emission Tomography Systems:

The scintillation camera system has an inherent limitation of providing images of three-dimensional distribution in two-dimensional

displays. The structural information in the third dimension, depth, is obscured by superimposition of all data along this direction. Although information on depth is obtained by complementary views at different angles, the difficulty in this technique lies in the fact that, many times underlying or overlying activity prevents an imaging device from obtaining an accurate representation of plane of interest. To overcome these problems, emission systems have been constructed which attempt to provide sectional maps of activity distributions within the body. All these systems permit the imaging of organs by providing either longitudinal or transverse sectional maps of distribution of radioactivity.

There are many requirements for emission tomography systems:

(i) the detector system must have uniform resolution and sensitivity versus depth. Variation in detector response with depth result in unacceptable distortion of image. (ii) The photon attenuation must be accurately corrected, so that activity concentrations at different depths can be compared. (iii) Adequate discrimination against scattered radiation is important in all radioisotopes imaging procedures but essential to emission tomography applications to preserve the image contrast. (iv) The detector positioning and sampling plays an important role in tomographic technique. Besides all this requirements, the spatial resolution of the system is needed to be high so that the distribution under study can be reconstructed as accurately as possible. The detector is expected to have a high sensitivity so that adequate statistics are provided for reconstruction algorithms. Finally because of the complexities of the technique and large amount of data processing, a computer is generally required for emission tomography. The data collection, data storing, reconstruction of plane of interest is controlled by the computer. The reconstruction algorithms are used to provide images to compare quantitatively with the actual distributions. According to the type of radiation

emitted by the radioisotope the emission tomography systems are categorized into two groups:

(i) The Single Photon Counting (SPC) System or Single Photon Emission Computed Tomography (SPECT) Systems:

The systems are normally designed to collect data from a solid angle about the patient that is as large as possible either through the use of large position sensitive detector or by utilizing detectors at multiple angles or by combinations of the two. The routine gamma emitters like ^{99m}Tc , ^{131}I , ^{123}I , ^{67}Ga etc are used for SPECT system (Figure: 3.9).

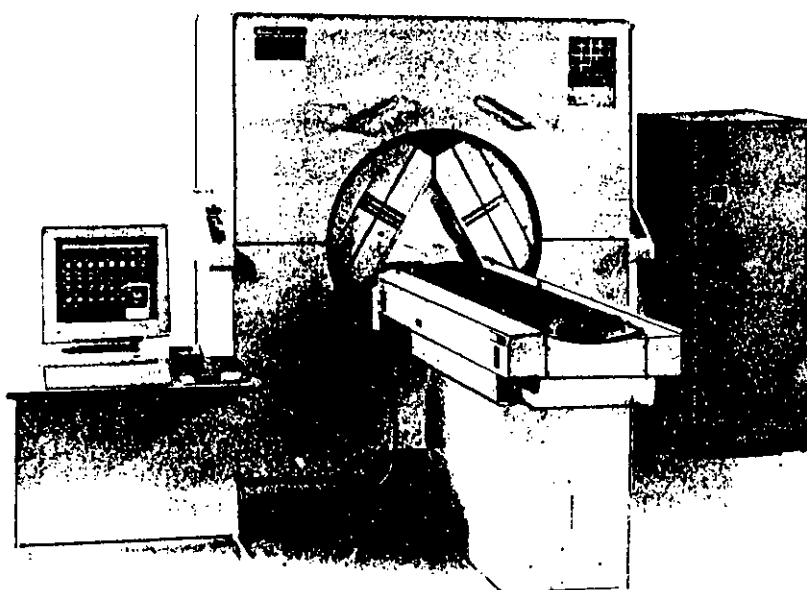


Figure 3.9 A Three head Single Photon Emission Computed Tomography Camera, TRIAD Model (Courtesy of Trionix Research Laboratory, Inc., Twinsburg, Ohio)

(ii) The Annihilation Coincidence Detection (ACD) Systems or Positron Emission Tomography (PET) Systems:

The systems are used to detect the 511 keV annihilation radiation from the positron emitters, such as ^{11}C , ^{13}N , ^{15}O , ^{18}F , ^{68}Ga etc.

The present study was carried out by applying Single Photon Emission computed Tomography [SPECT]. The principle of the technique is described in brief as follows:

The Principle of The SPECT System:

The SPECT system consists of a typical gamma camera with one to three NaI(Tl) detector heads mounted on a gantry, an on-line computer for data acquisition and processing and display system. It allows the user to choose the display grid and reconstruction filter.

The detector head rotates around the long axis of the patient at small angle increments (3° - 10°) for 180° or 360° angular sampling. The collected data at each angular position are stored in a 64×64 or 128×128 matrix in a computer for the reconstruction of images of plane of interest afterwards. The collected data helps in generating transverse (short axis) sagittal (vertical long axis) and coronal (horizontal long axis) images.

Principle of Reconstruction of Images from Projection:

The tomographic reconstruction of transaxial slice images from the collected data is performed using the principle of filtered back projection. The essence of the reconstruction is the smearing back (back projection) into the reconstruction space of each projection, maintaining the correct angular offset. The technique is described in short as follows:

According to the diagram of Figure: 3.10 (A, B, C) three projection views are obtained by the gamma camera at three equidistant angles around

the object with two hot spots .In two dimensional data acquisition technique, each single count in an image profile is the sum of all counts along a single line through the depth of the object ,whereas in back projection [Figure: 3.10 (A)] technique each count is projected back along the line of collection perpendicular to the face of the detector whereby individual back projected profiles superimpose to form an image. Whenever a large number of projection views are superimposed, a final image is [Figure: 3.10 (B)] obtained.

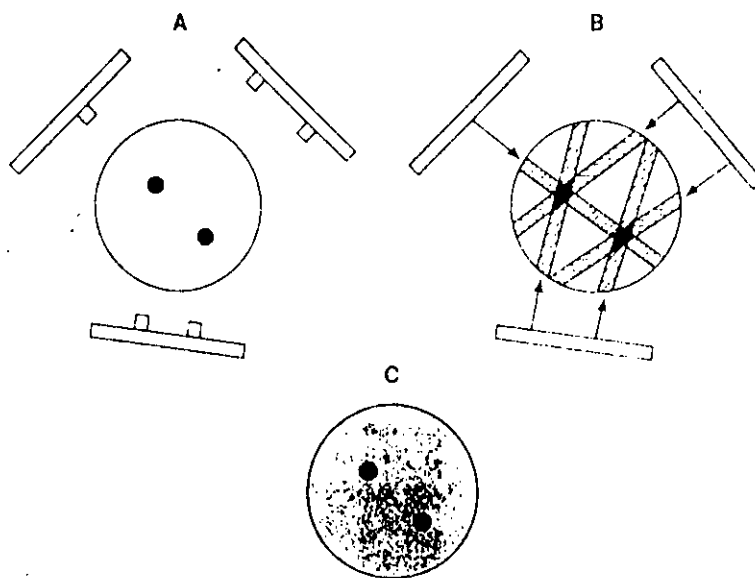


Figure 3.10 Basic Principle of Reconstruction of An Image by The Backprojection Technique. (A) An Object With Two "Hot" Spots (Solid Spheres) is Viewed At Three Projections (At 120 Angles), (B) Collected Data Are Used to Reconstruct the Images by Backprojection, (C) When Many Views are Obtained, The Reconstructed Images Represents The Activity Distribution With "Hot" Spots.

This back projection can be better explained in terms of data acquisition in the computer matrix. Suppose the data are collected in a 4x4-acquisition matrix [Figure: 3.11 (A)]. In this matrix, each row represents a slice of a certain thickness and is back projected individually. Each row consists of four pixels. The first row has pixel A₁, B₁, C₁ and D₁. Data in each pixel is considered to be the sum of all counts along the depth of view. In the back projection technique, a new reconstruction matrix of the same size (i.e. 4x4) is designed so that counts in pixel A₁ of the acquisition matrix are added to each pixel of the first column of the reconstruction matrix [Figure: 3.11 (B)]. Similarly, counts from pixel B₁, C₁ and D₁ are added to each pixel of the second, third and fourth column of the reconstruction matrix respectively. Next, suppose a lateral view (90°) of the same object is taken, and the data are again sorted in a 4x4 acquisition matrix. The first row of the pixel (A₂, B₂, C₂ and D₂) in the 90° acquisition matrix is shown in [Figure: 3.11 (B)]. Counts from pixel A₂ are added to each pixel of the first row of the same acquisition matrix, counts from pixel B₂ to the second row, counts from pixel C₂ to the third row, and so on. If more projection views are taken at angles between 0° and 90°, or any other angle greater than 90° and stored in 4x4 acquisition matrices, then counts from each pixels of the first row of every acquisition matrix can be added to each pixel of the corresponding diagonal row of the reconstruction matrix. This type of back projection results in superimposition of data in each pixel, thereby forming the final transverse image with areas of increased or decreased activity [Figure: 3.10 (C)]. Using the 4x4 matrix, four transverse cross-sectional images (slices) can be produced.

A

A_1	B_1	C_1	D_1	←First row
				←Second row
				←Third row
				←Fourth row

Acquisition Matrix at 0^0

First row at 0^0

B

A_1	B_1	C_1	D_1	
↓	↓	↓	↓	
				=
A_1	B_1	C_1	D_1	
A_1	B_1	C_1	D_1	
A_1	B_1	C_1	D_1	
A_1	B_1	C_1	D_1	

Reconstruction Matrix

C

A_1	B_1	C_1	D_1	←	A_2	=	A_1+A_2	B_1+A_2	C_1+A_2	D_1+A_2
A_1	B_1	C_1	D_1	←	B_2		A_1+B_2	B_1+B_2	C_1+B_2	D_1+B_2
A_1	B_1	C_1	D_1	←	C_2		A_1+C_2	B_1+C_2	C_1+C_2	D_1+C_2
A_1	B_1	C_1	D_1	←	D_2		A_1+D_2	B_1+D_2	C_1+D_2	D_1+D_2

Fig. 3.11 An Illustration of The Back projection Technique Using The Data From An Acquisition Matrix into a Reconstruction Matrix

Similarly, using 64×64 matrices for both acquisition and reconstruction, 64 transverse slices can be generated. From all transverse slices, appropriate pixels are sorted out along the horizontal and vertical axes and used to form coronal and sagittal images. It is a common practice to lump several slices together to increase the count density on the individual slices for better contrast. A camera with a circular field of view (FOV) completely samples a spherically shaped volume in one complete rotation around the patient, whereas a rectangular FOV results in complete sampling of a cylindrical volume. Both type of camera head shapes are used for SPECT. Most system permits the user to define the limits of reconstruction within the sampled volume, i.e. the number of slices and spatial extent of the reconstructed volume.

The back projection technique has a problem of "Star Effect" artifacts caused by "shining through" radiation from adjacent areas of increased radioactivity (Figure: 3.10). The correction is done by applying a filter to each individual row or column of the acquisition matrix. The filtered profiles are back projected on the reconstruction matrix, which leads the way to produce a sharper image without the star effect. Various types of filters are commercially available in the form of software package, most of which use the ramp filters. The ramp filter suppresses the "star effect" of the back projection method. Other than back projection technique, the image reconstruction method can be performed from the acquired data by applying the analytic technique using Fourier transform. The Fourier transformation of any function is essentially a change of coordinates, in which the function $f(x, y)$ is described not in terms of its amplitude at individual spatial coordinates (x, y) but as a summation of sine and cosine functions of different spatial frequencies, v_x and v_y in the x and y directions. The Fourier transform $F(v_x, v_y)$ of a function $f(x, y)$ represents the function in

“frequency space” as opposed to “real space”. It is obtained by integrating the product of the original function with sine and cosine function, which involve a rigorous mathematical treatment. The entire reconstruction process including the filtering process is known as “linear superposition of filtered back projections” (LSFBP). The LSFBP and the Fourier filtering techniques are now- a-days being commonly used reconstruction methods for SPECT.

The present study is carried out using “Siemens SPECT Patient Handling system With Carbon Fiber Pallet”. The system is used for acquiring circular ECT study with Model 3219 Digital Operator’s Terminal (DOT) with Digitrac[®] and with an “OrbitarTM” Gamma Camera. Detector rotation and view parameters are set on ECT Control page displayed on the DOT screen. The computer system used to interface to the ORBITER is the Siemens ICON Workstation. The ICON workstation is a simple straightforward nuclear medicine computer associated with software that is powerful and easy to use. DIGITRAC is a type of Microprocessor-controlled circuits, which adjusts the gain of each individual photomultiplier tube to compensate for normal drift to keep the gamma ray photopeak precisely aligned throughout the camera’s field of view. The ICON Workstation is designed with Macintosh[®] user interface; the ICON workstation adapts to the way the user works.

General Information for the following components of Siemens Gammasonics Unit are given below:

1. The SPECT patient handling system with carbon Fibre pallet:

Powered Extended –Reach Table [Model No.820-826276 (#44 49 278)]
Head rest [Model No.12 45 864] and Body Wrap Accessory [Model No.570-018384 (#44 49 609)].

The SPECT scanning accessory provides the circular orbiting motions required for single photon emission computed tomography (SPECT). It is field convertible to also provide noncircular orbiting motions. The patient positioning table secures in position to floor sockets which align the central longitudinal axis of the pallet transversely to the rotational axis of the detector. Powered vertical adjustment of its pallet simplifies patient transfer and allows alignment of the patient's longitudinal midpoint to the rotational axis. The table can also be used for oblique and lateral views in conventional nuclear medicine procedures while secured, or it can be moved away from the detector stand. The detailed specification of SPECT patient handling system with carbon fibre pallet is enclosed in the Appendix.

2. General Information DOT with Digitrac®

The Dot is a control /imaging terminal for ZLC™ Series of scintillation camera systems. It provides control over photo-peak levels and window widths for three analyser, the starting and the terminating parameters of a study, annotation of patient/study parameters and of text, image exposure to film, and DIGITRAC camera calibration functions. Additional optional functions can control image manipulations, gating of acquisition on the cardiac R-wave peaks, anatomical marking and motion correction. In addition to standard image display, an emulated persistence (P-Scope) image can be displayed for patient positioning and previewing. DIGITRAC is a digital means of adjusting the gain of each photomultiplier tube (PMT) and the high voltage applied to those tubes in a ZLC scintillation camera detector to precisely align the gamma ray photopeaks throughout the camera's entire field of view. These adjustments are made under microprocessor control during the clinical studies and routine quality assurance (QA) testing procedures whenever suitable gamma rays are

detected, regardless of their scatter characteristics. In addition, this method of digital control permits the user to select a camera dead-time at which the "high count-rate" mode will begin and to offset an analyzer's window from photo-peak center by selecting the amount of offset directly as a percentage of the analyzer's energy level setting. An integral diagnostic program allows the operation of DIGITRAC functions to be tested as a routine quality assurance (QA) procedure. The camera can also be manually re-calibrated using a scatter-free point source of ^{57}Co or $^{99\text{m}}\text{Tc}$.

The detailed *Specification of DOT with Digitrac®* is enclosed in the Appendix.

3. The detailed *Specification of ECAM gamma camera* which is the latest version of "ORBITER" gamma camera is enclosed in the Appendix.

3.3 Radiopharmaceuticals

For performing the ongoing study, besides the instrumentation, a number of factors contribute to form the required image. The important factors are:

1. Characteristics of the radiopharmaceutical that is used as imaging agent.
2. Administered doses.
3. Patient

Radiopharmaceuticals or radioactive drugs are radioactive elements or labeled compounds whose physical, chemical and biologic properties render them both safe and useful for administration to humans. Most of the radiopharmaceuticals are used for diagnostic purpose. These imaging agents imply that, the amount of administered drug to provide useful imaging information does not produce any effect from chemical toxicity and also the resultant dose is always maintained much smaller than the levels producing demonstrable somatic radiation damage. In therapeutic application, the

quantities of radioactivity of the radiopharmaceutical required to produce a desired result, produce secondary radiation effects from which the body recovers.

The agents of value for external imaging constitute only a small segment of a large group of radioactive factors employed in medical diagnosis and biologic research. The physical and biological characteristics of this special group of agents are significantly different from those of the non-radioactive drugs. The fundamental physical properties of any radioactive nuclide, to be used in any external imaging device are:

1. The radioactive nuclide must emit a gamma or X-ray with an energy between 20 and 600 keV, and
2. The Radioactive agent must possess a physical half-life normally between approximately 1 hour and 1 year.

The ideal gamma-emitting nuclide decays by isomeric transition or electron capture without internal conversion. For the use in gamma camera or in any scanning device the radiopharmaceutical is expected to be a mono-energetic gamma emitter of approximately 150 keV.

Table 3.1 Characteristics of Commonly Used Radionuclide

Nuclide	Physical Half-life	Mode of Decay (%)	γ -Ray Energy	γ -Ray Abundance (%)	Common Production Method
^3_1H	12.3 Years	β^- (100)	-	-	$^6\text{Li}(n,\alpha)^3\text{H}$
$^{11}_6\text{C}$	20.4 Minutes	β^+ (100)	0.511 (annihilation)	200	$^{10}\text{B}(d,n)^{11}\text{C}$ $^{14}\text{N}(p,\alpha)^{11}\text{C}$
$^{13}_7\text{N}$	10 Minutes	β^+ (100)	0.511 (annihilation)	200	$^{12}\text{C}(d,n)^{13}\text{N}$ $^{16}\text{O}(p,\alpha)^{13}\text{N}$ $^{13}\text{C}(p,n)^{13}\text{N}$
$^{14}_6\text{C}$	5730 Years	β^- (100)	-	-	$^{14}\text{N}(n,p)^{14}\text{C}$
$^{15}_8\text{O}$	2 Minutes	β^+ (100)	0.511 (annihilation)	200	$^{14}\text{N}(d,n)^{15}\text{O}$ $^{15}\text{N}(p,n)^{15}\text{O}$
$^{18}_9\text{F}$	110 Minutes	β^+ (97) EC (3)	0.511 (annihilation)	194	$^{18}\text{O}(p,n)^{18}\text{F}$
$^{32}_{15}\text{P}$	4.3 Days	β^- (100)	-	-	$^{32}\text{S}(p,n)^{32}\text{P}$
$^{57}_{27}\text{Co}$	271 Days	EC (100)	0.014 0.122 0.136	9 86 11	$^{56}\text{Fe}(d,n)^{57}\text{Co}$
$^{67}_{33}\text{Ga}$	78 Hours	EC (100)	0.093 0.184 0.300 0.393	40 20 17 5	$^{68}\text{Zn}(p,2n)^{67}\text{Ga}$
$^{68}_{31}\text{Ga}$	68 Minutes	β^+ (89) EC (11)	0.511 (annihilation)	178	$^{68}\text{Zn}(p,n)^{68}\text{Ga}$
$^{99}_{42}\text{Mo}$	67 Hours	β^- (100)	0.181 0.740 0.780	6 12 4	$^{98}\text{Mo}(p,\gamma)^{99}\text{Mo}$ $^{235}\text{U}(n,f)^{99}\text{Mo}$

Contd..

Nuclide	Physical Half-life	Mode of Decay (%)	γ -Ray Energy	γ -Ray Abundance (%)	Common Production Method
$^{99m}_{43}\text{Tc}$	6.0 Hours	IT (100)	0.140	90	$^{99}\text{Mo} \xrightarrow{\beta^-, 67\text{h}} ^{99m}\text{Tc}$
$^{111}_{49}\text{In}$	2.8 Days	EC (100)	0.171 0.245	90 94	$^{111}\text{Cd} (\text{p}, \text{n}) ^{111}\text{In}$
$^{123}_{53}\text{I}$	13.2 Hours	EC (100)	0.159	83	$^{121}\text{Sb} (\alpha, 2\text{n}) ^{123}\text{I}$ $^{127}\text{I} (\text{p}, 5\text{n}) ^{123}\text{Xe}$ $\downarrow 2.1\text{hr}$ ^{123}I $^{124}\text{Xe} (\text{p}, 2\text{n}) ^{123}\text{Cs}$ $\downarrow 5.9\text{min}$ ^{123}Xe $\downarrow 2.1\text{hr}$ ^{123}I
$^{125}_{53}\text{I}$	60 Days	EC (100)	0.035 X-ray (0.027-0.032)	7 140	$^{124}\text{Xe} (\text{n}, \gamma) ^{125}\text{Xe}$ $^{125}\text{Xe} \xrightarrow{\text{EC}, 67\text{h}} ^{99m}\text{Tc}$
$^{131}_{53}\text{I}$	8.0 Days	β^- (100)	0.284 0.364 0.637	6 81 7	$^{130}\text{Te} (\text{n}, \gamma) ^{131}\text{Te}$ $^{235}\text{U} (\text{n}, \text{f}) ^{131}\text{Te}$ $^{131}\text{Te} \xrightarrow{\beta^-, 25\text{min}} ^{131}\text{I}$
$^{133}_{54}\text{Xe}$	5.3 Days	β^- (100)	0.081	37	$^{235}\text{U} (\text{n}, \text{f}) ^{133}\text{Xe}$
$^{137}_{55}\text{Cs}$	30.0 Years	β^- (100)	0.662	85	$^{235}\text{U} (\text{n}, \text{f}) ^{137}\text{Cs}$
$^{201}_{81}\text{Tl}$	73 Hours	EC (100)	0.167 X-ray (0.069-0.083)	9.4 93	$^{203}\text{Tl} (\text{p}, 3\text{n}) ^{201}\text{Pb}$ $^{201}\text{Pb} \xrightarrow{\text{EC}, 9.3\text{h}} ^{201}\text{Tl}$

The fundamental property of a radioactive agent used for imaging:

Some radionuclides have the propensity to concentrate selectively in the targeted organ or structure which are to be visualized. A measurable fractional amount of injected radioactivity must localize in the structure of interest; the smaller and deeper the structure, the higher concentration is needed to obtain the visualization. The radioactive isotopes are attached to a substance to enable the distribution or location of the substance to be determined following its administration by labeling process. The label or tagged component is incorporated into the molecular structure of the compound. The labeled compound must have chemical structure identical to that of the unlabeled compound. The factors influencing the biologic localization of radioactive drugs or compounds are very complicated. Most of the radiopharmaceuticals, which are injected intravenously, leave the vascular compartment to enter various organs and tissues normally through the capillaries. The localization of drugs, is highly influenced by certain characteristics of the body organs, these are: (i) fraction of the total cardiac output delivered to the organs. (ii) types of capillary (iii) capillaries per cubic millimeter of tissue (iv) receptor sites having a specific biochemical affinity for extraction and concentration of a drug. Normally, the organ like kidneys and livers with a high blood flow, have a tendency of extracting a larger fraction of radioactivity than the structures with a low blood flow like tendons, fats or cartilage. In reality, no agent is fully ideal under all mentioned conditions. Generally the agents are chosen with best possible compromise of factors mentioned above. The radioactive agent of choice for the demonstration of the particular organs of the present study, is:

99m-Techneium:

^{99m}Techneium is the most important short-lived radionuclide in nuclear medicine (Figure: 3.12).

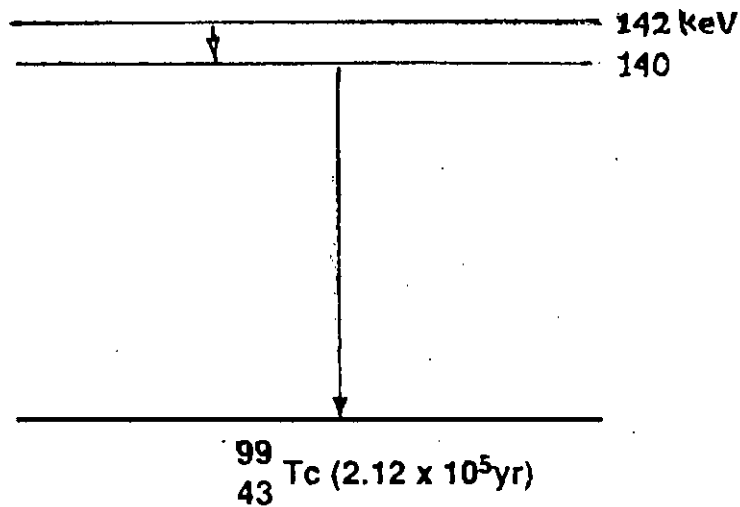


Figure 3.12(a) Isomeric Transition of ${}^{99m}\text{Tc}$. Ten Percent of Decay Follows Internal Conversion

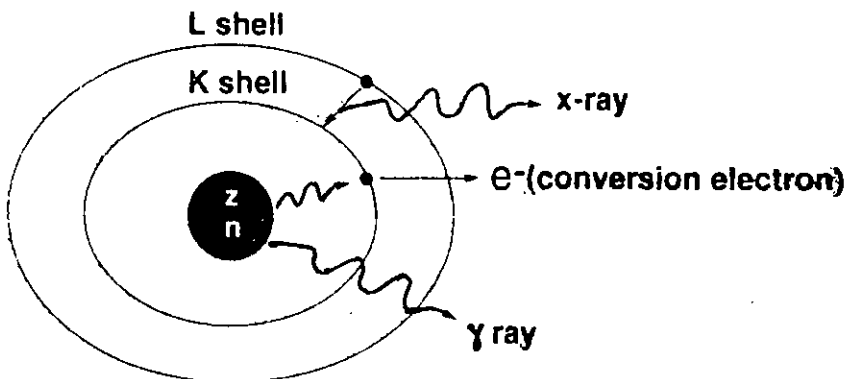


Figure 3. 12(b) Internal Conversion Process .The Excitation Energy of The Nucleus is Transferred to a K-Shell Electron, Which is Then Ejected , And The K-Shell Vacancy is Filled by An Electron From the L-Shell. The Energy Difference Between The L-Shell And The K-Shell Apperars As the Characteristics K x-Ray

The Technetium and its various radionuclides were first produced in the year 1937 by deuteron bombardment of naturally occurring molybdenum. It was introduced in nuclear medicine in 1957. The physical characteristics of ^{99m}Tc are almost ideal for external detection procedure which led the way of widespread acceptance of it. It has got a physical half-life of only 6 hours; no beta emission and a gamma emission of 140 keV.

Table 3.2 Radionuclide Generators Used in Nuclear Medicine

Daughter*	Decay Mode	T _{1/2}	Parent	T _{1/2}
^{68}Ga	β^+ , EC	68 Minutes	^{68}Ga	275 Days
^{82}Rb	β^+ , EC	1.3 Minutes	^{82}Sr	25 Days
^{87m}Sr	IT	2.8 Hours	^{87}Y	80 Hours
^{99m}Tc	IT	6.0 Hours	^{99}Mo	66 Hours
^{113m}In	IT	100 Minutes	^{113}Sn	120 Days

♣ Generator Product

It is conveniently available by the elution of a generator containing its parent ^{99}Mo whose physical half-life is 67 hours.

Because of all these physical properties, ^{99m}Tc have become a choice for a variety of nuclear medicine procedures. Technetium is obtained from a generator. A radionuclide generator consists of a parent-daughter radionuclide pair contained in an apparatus that permits separation and extraction of the daughter from the parent. The daughter product activity is replenished continuously by the decay of the parent and may be extracted repeatedly. The ^{99}Mo - ^{99m}Tc system is one of the most important generator, because of the widespread use of ^{99m}Tc for radionuclide imaging. Technetium-99m delivers a relatively low radiation dose per emitted gamma ray. A ^{99}Mo - ^{99m}Tc generator is shown in Figure: 3.13.

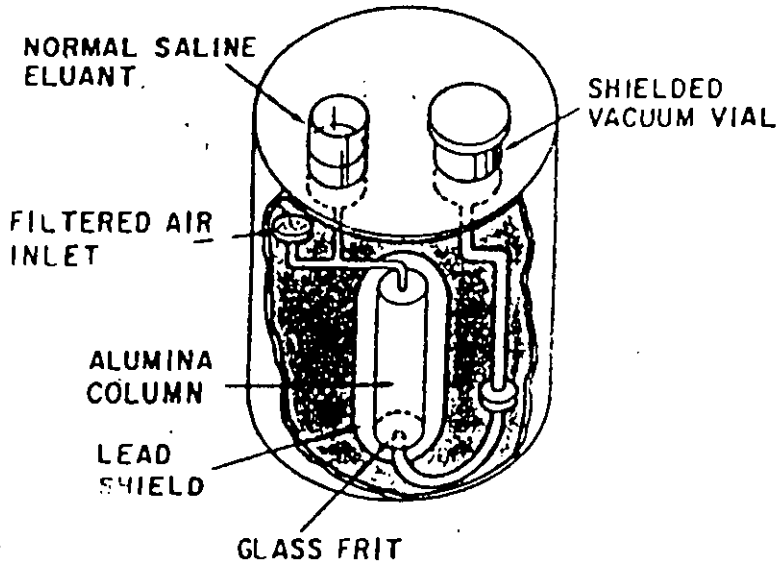


Figure 3.13 Cross- Sectional Drawing of A ^{99}Mo - $^{99\text{m}}\text{Tc}$ Generator. (Courtesy of The Society of Nuclear Medicine and Thomas R. Gnau)

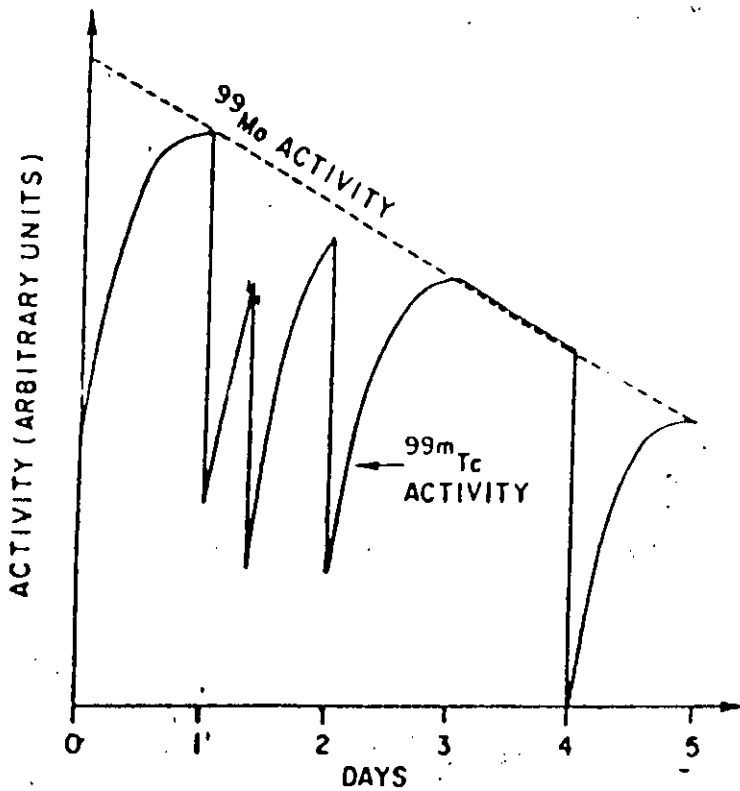


Figure 3.14 Build-up and Decay of $^{99\text{m}}\text{Tc}$ Generator Eluted on Days 0, 1, 4, 2, and 4.

The ^{99}Mo activity in the form of molybdate ion, MoO_4 is bound to an alumina (Al_2O_3) column. The Technetium-99m activity, being chemically different, is not bound to the alumina and is eluted from the column with 5-25 ml of normal saline. Typically, 75%-85% of the Technetium-99m activity is extracted in a single elution. Technetium-99m activity builds up again after an elution as a result of transient equilibrium between ^{99}Mo - $^{99\text{m}}\text{Tc}$ (Figure:3.14) and maximum activity is available about 24 hours later; however, usable quantities of Technetium-99m can be extracted 3-4 hours later. Commercially prepared generators are sterilized, well shielded, and largely automated in operation. Typically they are used for about one week and then discarded because of natural decay of the ^{99}Mo parent. Molybdenum-99 activity is obtained by (n, γ) activation of stable Molybdenum (23.8% Molybdenum) or by separation from the reactor fission fragments. The later sometimes called "fission moly", has significantly higher specific activity. The volume of alumina required for ^{99}Mo - $^{99\text{m}}\text{Tc}$ generator is determined essentially by the amount of stable Mo-carrier that is present. Therefore "fission moly" generators requires much smaller volumes of alumina per unit of ^{99}Mo activity. they can be eluted with very small volumes of normal saline ($\leq 5\text{ml}$), which is useful in some imaging techniques requiring bolus injection of very small volumes of high activity (740 MBq) of $^{99\text{m}}\text{Tc}$.

Technetium-99m is eluted from the generator in physiologic saline (Sodium Chloride) as $^{99\text{m}}\text{Pertechnetate}$ ion. This $^{99\text{m}}\text{Pertechnetate}$ ion is a singly charged anion with oxygen at the corners of tetrahedrons. It concentrates primarily in the thyroid and salivary glands, gastric mucosa, and choroid plexus. It is primarily excreted via the gastrointestinal tract and the kidneys; and it is also used in brain and thyroid imaging and first-pass radionuclide angiocardiology applications. Technetium is a transition metal most closely resembling rhenium chemically and a variety of valances (oxidation

states) are possible from -1 to +7^[82,83]. To prolong the intravascular biologic half-life of Technetium, it can be attached to carriers that have a reasonably long life in plasma. Most biomedical products are labeled with Technetium by a reducing agent in an acid medium. The changing process in oxidation state in the labeling reactions have always been a topic of research and controversy. The chemistry of labeling process with carrier free ^{99m}Tc has proven to be a very difficult task as the conventional method of chemical analyses that can not help in defining the molecular configurations of the labeled complexes. Many methods have been developed for labeling radiopharmaceuticals with ^{99m}Tc. This can be accomplished using a variety of reducing agents- Stannous Chloride, Ferric ion, and Ascorbate and Electrolytic methods. But in most, the commercial radiopharmaceutical kits for “instant labeling” with ^{99m}Tc, stannous ion is the reducing agent in acidic media. The effects of stannous ion reducing agent on ^{99m}Tc - pertechnetate is not limited to an in-vitro reaction. Alternation in the tissue distribution of ^{99m}Tc -pertechnetate has also been observed which shows that the tin prolonged the disappearance of ^{99m}Tc from the blood. This is an evidence of increased blood pool activity on brain scans as well as bone scans. The altered distribution is most likely attributable to chemical reduction and fixation of ^{99m}Tc -pertechnetate to red blood cell.

In the present study **Technetium-99m DTPA**, a chelate, which is a complex of diethylene-triamine-pentaacetic acid (DTPA) and reduced ^{99m}Tc is used as renal imaging agent [Chelate- Ligands that has two or more potential bonding sites. Ligand –(i) Molecules attached to a central atom using coordinate covalent bonds; (ii) in radioimmunoassay an antigen or small molecule that binds to a native carrier protein].The chelating agents are substances which form complexes with stable or radioactive metals (Table 3.3).

Table 3.3 Renal Radiopharmaceutical

Radiopharmaceutical	T _{1/2}	Principal Gamma Energy(keV)	Administered Dose	Radiation Dose(rad)*	
				Kidney	Whole Body
²⁰³ Hg-chlormerodrin*	46.6d	279	100-150μCi	20.00- 30.00	0.030-0.040
³⁹⁷ Hg-chlormerodrin*	2.7d	77	100-150μCi	1.20-1.80	0.010-0.020
¹⁹⁷ Hg-bichloride ⁺⁺	2.7d	77	100-150μCi	20.00- 25.00	-
¹³¹ I-Hippuran*	8.1d	364	100-400μCi	0.10-0.40	0.020-0.080
^{99m} Tc-pertechnetate	6h	140	10 mCi	0.05-0.10	0.100-0.200
^{99m} Tc-DTPA*	6h	140	10-15 mCi	0.9	0.160-0.240
^{99m} Tc-iron ascorbate	6h	140	10 mCi	2.7	0.08
^{99m} Tc-glucoheptonate*	6h	140	10-15 mCi	1.70-2.40	0.014-0.021
^{99m} Tc- dimercaptosuccinate*	6h	140	1-5 mCi	1.40-7.0	0.016-0.080
¹²³ I-Hippuran	13.3h	160	1-2 mCi	0.025- 0.050	0.010-0.020

*Dosimetry from multiple reference sources.

* Historical interest only

⁺⁺ Not used in USA

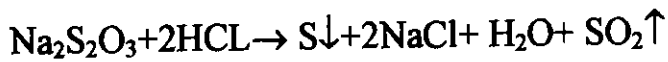
* Commonly used

The Technetium-99m-DTPA, meet most closely the criteria that are the basic requirement for the renal imaging. Moreover it provides the necessary abundance of photons for the detection with the scintillation camera. Because of its rapid clearance it is not an ideal agent for demonstrating lesions within the kidney. However, it is an excellent radionuclide for demonstrating obstruction of the collecting system. It is injected for obtaining the imaging sequence in conjunction with a diuretic drug such as furosemide (Lasix). ^{99m}Tc -DTPA is injected intravenously in doses of 10 to 20 mCi and distributed throughout the extra-cellular space. It is rapidly cleared from the body by glomerular filtration (GFR).

For the on going study of renal imaging, the “Amerscan™ Pentetate II Technetium Agent for kidney/brain scintigraphy” by Nycomed Amersham plc, Amersham, UK was used. The agent comprises pre-dispensed, freeze-dried, sterile ingredients which, when reconstituted with Pertechnetate solution from a sterile Technetium generator, provides a sterile solution for intravenous injection. It's content are: (a) 10ml vials containing a freeze-dried mixture of calcium- trisodium-diethylene-triamine-pentaacetate, Stannous Chloride and stabilizer (b) labels for reconstituted injection and (c) Swabs (70% isopropylalcohol). After intravenous injection of ^{99m}Tc -DTPA, it rapidly penetrates the capillary walls entering extracellular fluid in 3.8 minutes. DTPA does not enter cells because of lipid insolubility and negative charges. It disappears from the plasma into three components with a half -life time of 10,90 and 600 minutes respectively; by two hours less than 10% injected dose remains in blood.

For studying liver, the ^{99m}Tc -Sulfur Colloid is used. ^{99m}Tc -Sulfur Colloid is the most widely used agent for hepatic, splenic and bone-marrow imaging. An intravenous dose of 5mCi of ^{99m}Tc -Sulfur Colloid visualizes the liver and spleen well on camera images. In normal human body, it is

assumed that about 85% of the administered activity localize in the liver, 7% in the spleen and 5% in the red marrow ^[84]. Earlier ^{99m}Tc-Sulfur Colloid was prepared from a colloid of ^{99m}Tc by bubbling hydrogen sulfide gas into a solution of pertechnetate with gelatin as stabilizing agent ^[85]. For removing the unreacted hydrogen sulfide, nitrogen gas was used. In a later method ^[86] sodium thiosulfate is reduced in sulfuric or hydrochloric acid solution and heated according to the following reaction:



This method is still used in commercial sterile kits. The acid solution is usually 0.5N; 40% of the mass of sodium thiosulfate is converted to free sulfur particles and in a typical preparation around 1 mg of sulfur is injected which is considered pharmacologically safe. The commercial preparation of ^{99m}Tc-Sulfur Colloid have a mean particle size of approximately 0.3 μ and around 80% of the particle are in between the ranges of 0.1 μ -1 μ . Several other colloidal preparations labeled with ^{99m}Tc have been proposed as a substitute for ^{99m}Tc-Sulfur Colloid. These include preformed particles of antimony sulfide, microaggregated albumin, small albumin microspheres, and stannous oxide colloid. Technetium dioxide colloid (TcO₂) is prepared by the reduction of pertechnetate in 0.5N HCl or in 0.5N sodium borohydride without any stabilizing agent and without heating. Sodium borate is formed in the reaction and serves as buffer, and free hydrogen gas is liberated. Although the particle sizes have not been well defined, they are probably about 1 μ in diameter. The reduced Tc in a valence state of intravenous is oxidized by the liver back to pertechnetate. Hence the radioactivity disappears from the liver with a biologic half-time of about 32 hours.

Small albumin microspheres 0.3 to 1 μ m in size were prepared as an albumin-oil homogenate in a hot cottonseed-oil bath, extracted, and washed with diethylether. They were labeled with ^{99m}Tc by an iron-ascorbic acid method with a boiling step. The particle size was more uniform than for other short-lived colloids but about 1 hour was required for labeling and separation of unbound technetium before clinical use. Stannous oxide colloid has been employed on a limited basis as a liver imaging agent because it is quickly prepared without heating, human serum albumin or gelatin may be used as stabilizing agents. The particles formed are often smaller than 1 μ in diameter. In rats, the initial radioactivity in the liver and spleen decreases, with an initial half-life of 55 hours. At least part of the injected technetium, therefore, is not retained permanently. This colloidal preparations not readily affected by aluminum ions in the generator elute as is ^{99m}Tc -sulfur colloid.

In the present study the liver imaging is performed by using "AmerscanTM Hepatate IITM Agent" which is the "kit for the preparation of Technetium-99m, colloidal tin injection". Each of the vial of the AmerscanTM Hepatate IITM Agent contains stannous fluoride (0.125mg) sodium fluoride (1.0mg) and poloxamer 188 (0.5mg) as a freeze-dried mixture sealed under nitrogen. The powder for injection, following reconstitution with 3-9 ml of sterile Sodium Pertechnetate [^{99m}Tc] Injection Ph.Eur. at a radioactive concentration of 0.41-1.23 GBq/ml to a maximum total activity of 3.7 GBq. The pH of the injection is 4.0-6.0. This yields technetium [^{99m}Tc] colloidal tin injection, a diagnostic radiopharmaceutical imaging agents for multi-dose use.

Nuclear medicine studies of the gastrointestinal tract and the genitourinary (GU) system are recognized as reliable noninvasive means to

evaluate the anatomy and function of its components. This is performed without the danger of algebraic reactions, unpleasant side effects or excessive radiation dose to the organs involved. A clear conception of physiology of gastrointestinal tracts and the GU tracts is necessary to optimize the technique and understand the obtained result. Radionuclide techniques represent a major contribution to the evaluation of this field in both health and disease.

3.4 Anatomical Portray of the Organs Understudy

The Kidney:

The kidneys are paired organs, which are lying in the retroperitoneal space. Each of the kidney is of 150 to 160 gm weight in an adult. The main artery vein and the renal pelvis are situated at the medial portion. On sectional view, each kidney is made up of a cortex and medulla. The extended portions of medulla from just below the outer cortex, down towards the renal pelvis, are the pyramids (Figure: 3.15).

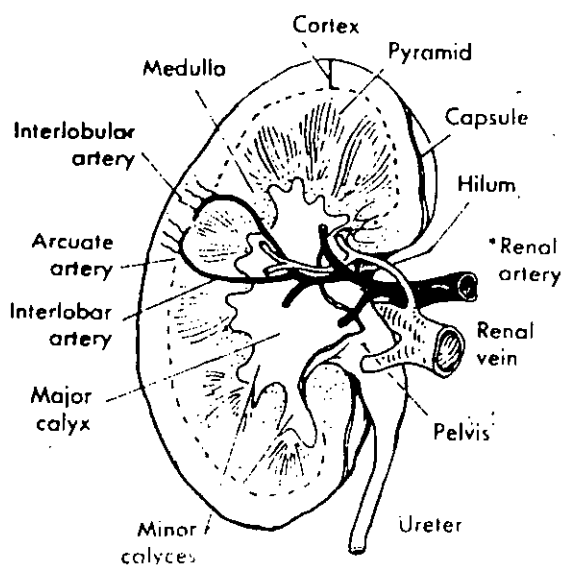


Figure 3.15 Diagram of Coronal Section of Right Kidney. Vascular Distribution of Renal Artery (black) is Magnified for Clarity.

Cortical projections between the pyramids are known as the columns of Bertin. The glomeruli are in the cortex, as are a large number of proximal and distal convoluted segments of the tubules. Each kidney receives the blood through a main renal artery rarely duplicated, which divides into anterior and posterior branches. The upper, middle and lower renal segment get the supplied blood from the branches of the anterior limb. The posterior limb divides into branches to the apical and posterior segments. Each segmental vessel extends to the cortical medullary junction where the arcuate branches originate; these in turn branches into the interlobar arteries that run straight tapering course into the peripheral portions of the renal cortex. These interlobar vessels are the origin of afferent arterioles, which supplies the glomeruli.

The Liver:

The liver is a lobulated organ located in the right upper quadrant of abdomen, beneath the right side of the diaphragm (Figure: 3.16). The liver weighs about 1500-1800 gms in an adult. It is the largest of all organs. It is divided into two lobes, the right lobe and the left lobe, separated by falciform ligament. The inferior quadrate and the posterior caudate lobes are associated with the right lobe. The configuration of the normal liver widely varies, but usually the right lobe is bigger than the left. The liver is composed of two major cell populations, the reticuloendothelial cells (Kupffer cells) and hepatocytes. The liver possesses a dual blood supply; arterial oxygenated blood is received from the hepatic artery, which is the branch of abdominal aorta; venous blood draining from the intestines is carried through the hepatic portal vein in to liver.

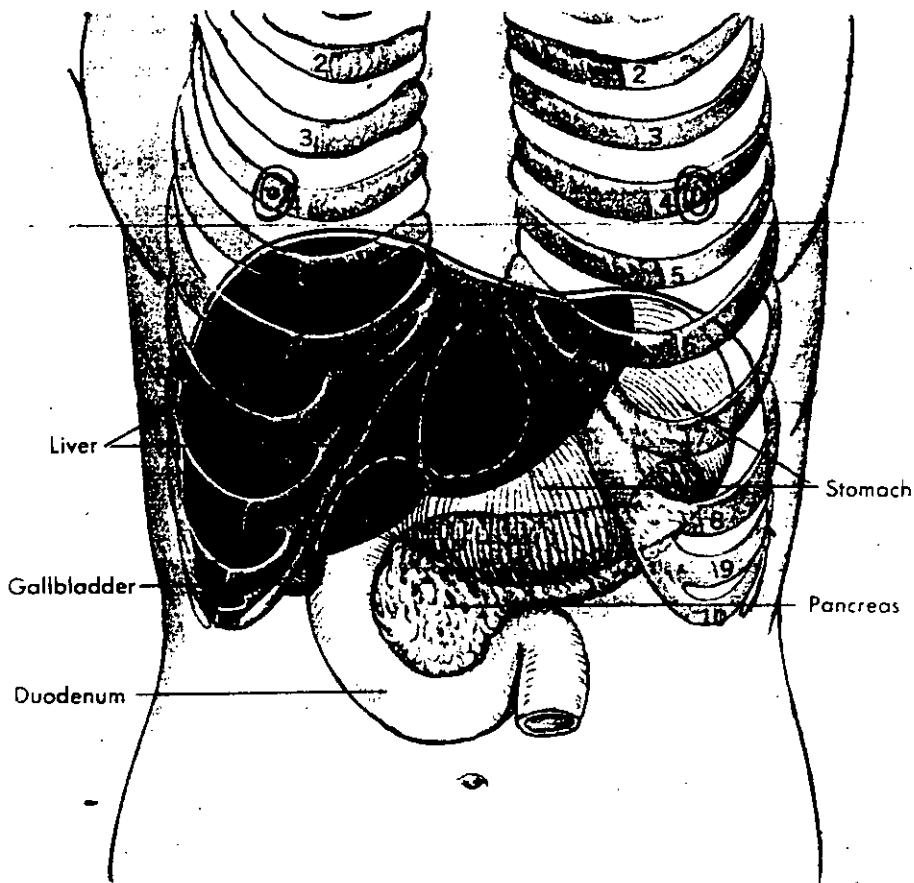


Figure 3.16 Liver in Normal Position Relative to Rib Cage, Diaphragm, Stomach, and Pancreas. (From Anthony, C.P. and Thibodeau, G.A.: Text Book of Anatomy and Physiology, ed.10, St.Louis,1979,The C.V. Mosby Co.)

3.5 Methodology of the Proposed Topic

Internal Radiation Dosimetry

To assess the radiation effects on an organ the amount of radiation energy deposited in that organ have to be sought out. The internal radiation dosimetry deals with this calculation of radiation energy deposition by internally deposited radionuclides. The absorbed fraction method is the versatile and accurate technique to perform the calculation. The radiation dose delivered to the target organ from the source organ, which contains the radioactivity, can easily be calculated by the absorbed fraction dosimetry method. The source and target organ can be the same, when the target organ also plays the role of the source organ by containing the radioactivity within itself (Figure: 3.17).

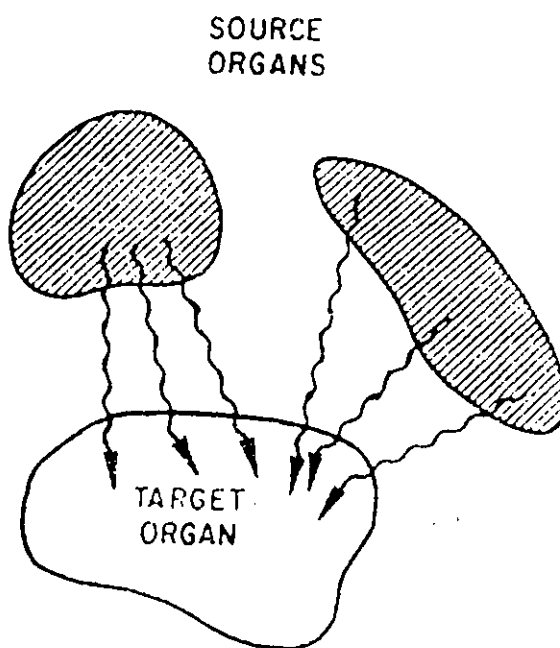


Figure 3.17 Absorbed Dose delivered to Target Organ From One or More Source Organs Containing radioactivity is Calculated by Absorbed Fraction Dosimetry Method.

Usually the organs other than the target organ, that contain concentration of radioactivity exceeding the average concentration in the body, are considered to be the source organs. For calculating the radiation dose to a target organ from radioactivity in a source organ, the amount of activity and its duration of stay within the source organ have to be determined. The greater the activity and the longer the duration time within the organ, the greater amount of radiation doses are delivered by it. Also the total amount of radiation energy emitted by the radioactivity in source organ is needed to be calculated, though it depends on the radionuclides emissions and their frequencies of emission. The fraction of energy emitted by the source organ that is being absorbed by the target organ is the core point of determination. But this determination of fraction of energy emitted by the source organ is highly dependent on the type and energy of the emissions and on the anatomic relationships between source and target organs. All this above-mentioned procedures are accompanied with various types of difficulties.

Moreover there are variations in metabolism and distribution of radionuclides among human subjects. Also the radioactive distribution within an organ may be inhomogeneous which leads further uncertainties in the dose specification for that organ. Due to these sort of complications and variables, radiation dose calculation are performed for anatomic models that incorporate "average" anatomic sizes and shapes. All values regarding absorbed fraction is calculated for humanoid models incorporating organs and anatomic structures of average size and shape. Following is the representation of an "average man" used for MIRD dose calculation and tables, which is used for the present study (Table 3.4 and Figure: 3.18).

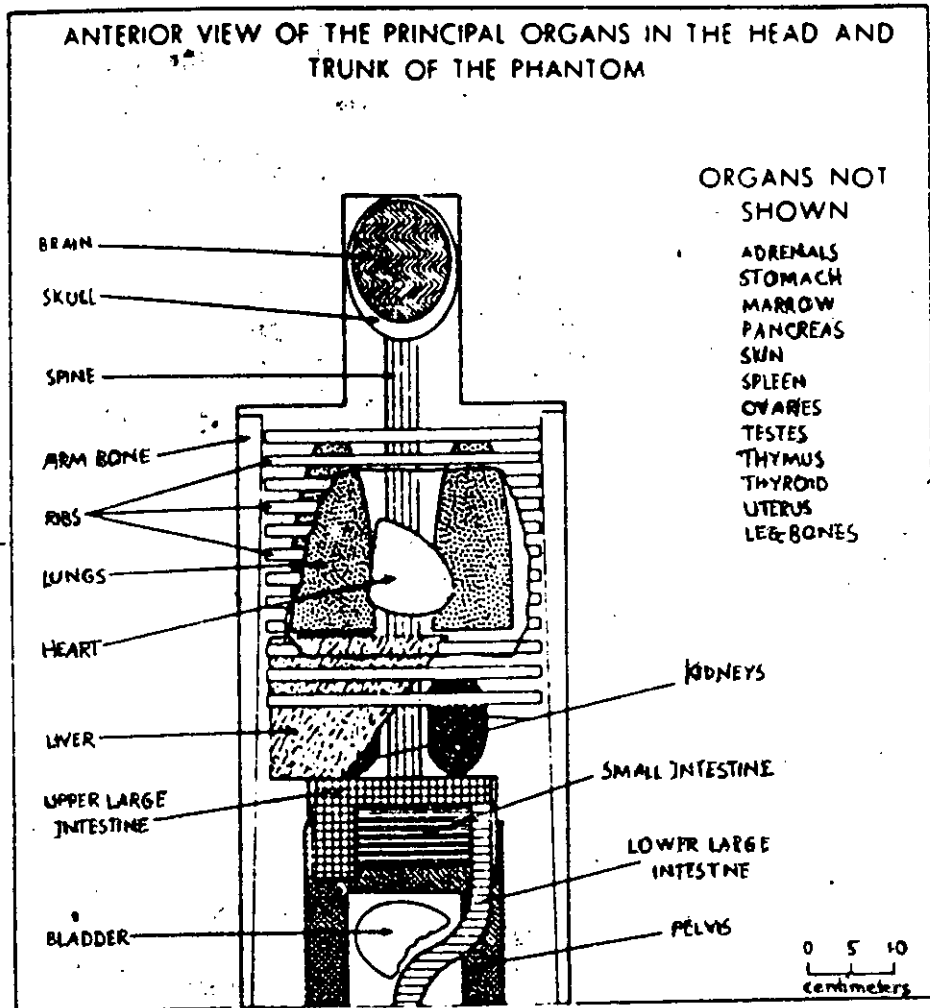


Figure 3.18 Representation of An "Average Man" Used For MIRD Dose Calculations and Tables.[From ref. Snyder WS, Ford MR, Warner GG, et al: Estimates of Absorbed Fractions For Monoenergetic Photon Sources Uniformly Distributed in Various Organs of A Heterogeneous Phantom. J.Nucl. Med., pp9, 1969, With Permission of The Society of Nuclear Medicine]

Cumulated Activity Calculation “ \bar{A} ”

The amounts of radioactivity existing within the source organ and the length of persisting time of the activity plays a vital role in delivering the radiation dose to a target organ. These two factors determine the cumulated activity “ \bar{A} ” in the source organ. The cumulated activity is the measure of total number of radioactive disintegration occurring during the time that radioactivity is present in the source organ. The radiation dose that is delivered by the radioactivity in a source organ is directly proportional to its cumulated activity. This amount of activity within an organ changes with time, depending on the different physical decay of the radionuclide and biologic uptake and excretion processes. The cumulated activity can easily be obtained by measuring the area of the time activity curve (Figure: 3.19).

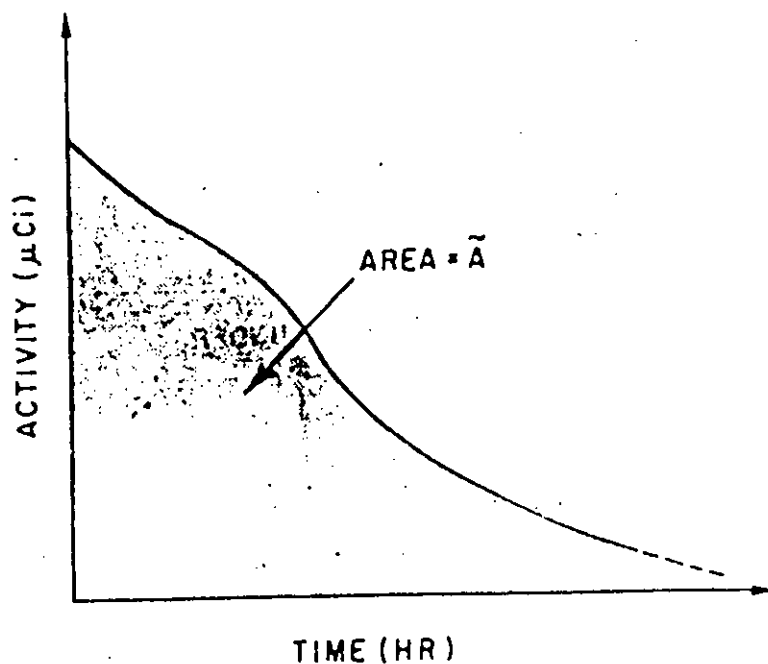


Figure 3.19 Hypothetical Time-Activity Curve For Radioactivity in A Source Organ. Cumulative Activity \bar{A} in μ Ci-hrs is The Area Under Curve.

This time-activity curve can be described mathematically as follows by the function A (t):

$$A = \int_0^{\infty} A(t) dt \dots \dots \dots (i)$$

It is assumed in equation (i) that, the activity administered to the patient at time t=0 and it is measured after the complete disappearance from the organ at time t= ∞. The activity 'A' administered to the patient is usually directly proportional to the number of radioactive atoms 'N'. With the passage of time, the no. 'N' of radioactive atoms in a sample decreases, leading to a decrease in the activity A of the sample. Thus both the activity and the number of radioactive atoms remaining in the sample decrease continuously with time and gradually approaches zero. Mathematically it can be expressed as follows:

$$A(t) = A(0) e^{-\lambda t} \dots \dots \dots (ii)$$

That is, A (t) is the activity at time t, is equal to A (0) the activity at time t=0, multiplied by the factor e^{-λt}. This factor e^{-λt} is known as decay factor. It is a number equal to e, the base of natural logarithm (2.718.....)-- raised to power -λt. λ is the decay constant for the radionuclide. It has a characteristic value for each radionuclide. It is the fraction of the atoms in a sample of that radionuclide undergoing radioactive decay per unit of time, during a time period that is so short that only a small fraction decay during that interval. The radioactive decay is characterized by the disappearance of a constant fraction of the activity present in the sample during a given time interval. The Half-life (T_{1/2}) of a radionuclide is the time required for it to decay to 50% of its initial activity level. Half-life can be expressed in terms of decay

constant of a radionuclide as follows:

$$\frac{A(t)}{A(0)} = \frac{1}{2} = e^{-\lambda T_{1/2}}$$

$$\Rightarrow 2 = e^{-\lambda T_{1/2}}$$

$$\Rightarrow \ln 2 = \lambda T_{1/2}$$

$$\Rightarrow T_{1/2} = \frac{\ln 2}{\lambda} = \frac{0.693}{\lambda} \dots\dots\dots (iii)$$

Since the natural logarithm of 2 has a value of approximately 0.693,

$$\lambda = \frac{0.693}{T_{1/2}} \dots\dots\dots (iv)$$

So, the decay factor can be rewritten as:

$$DF = e^{-\lambda T_{1/2}} \dots\dots\dots (v)$$

The life- time of radioactive atoms varies from very short to very long. The concept of average life- time is of great importance in radiation dosimetry calculation. The average life time “ τ ” of a radioactive atom in a sample has a value that is characterized by the nuclide itself and is expressed in terms of decay constant :

$$\tau = \frac{1}{\lambda} \dots\dots\dots (vi)$$

Combining equation (iv) & (vi)

$$\tau = 1.44 T_{1/2} \dots\dots\dots (vii)$$

Thus, it is seen that the average lifetime for the atoms of radionuclide is somewhat longer than its half-life.

Considering all these concepts, it becomes a complicated job to draw a time-activity curve and it is obviously difficult to analyze the related equations. For this reason, certain assumption was made to simplify the calculations. Suppose, when the uptake of the administered dose by organ is instantaneous i.e. it is very fast with respect to the half-life of radionuclide; the biologic excretion do not take place in such cases, then the time-activity curve can be described by the ordinary radioactive decay equation (2) in reference with equation (iii) & (v):

$$A(t) = A_0 e^{\frac{-0.693t}{T_p}} \quad \text{dt} \dots \dots \dots \text{(viii)}$$

Where T_p is the physical half-life of the radionuclide and A_0 is the activity initially present in the organ.. Thus equation (i) can be rewritten as:

$$\bar{A} = A_0 \int_0^{\infty} e^{\frac{-0.693t}{T_p}} dt \quad \dots \dots \dots \text{(ix)}$$

$$\text{or, } \bar{A} = \frac{(T_p A_0)}{0.693} \quad \dots \dots \dots \text{(x)}$$

$$\text{or, } \bar{A} = 1.44 T_p A_0 \quad \dots \dots \dots \text{(xi)}$$

The quantity $1.44T_p$ is the average life- time of the radionuclide. So the cumulated activity in a source organ, when eliminated by physical decay

only, is the same as if the activity were present at a constant level A_0 for a time equal to the average lifetime of the radionuclide. Again there are situations, when the uptake is instantaneous but the clearance is by biologic excretion only. That means that, there is no physical decay or the half-life of the radionuclide is very long in comparison to biologic excretion. In such situation, the biologic excretion is analyzed with caution. It is usually described by a set of exponential excretion components, with a fraction f_1 of the initial activity A_0 being excreted with a biologic half-life T_{b1} , a fraction f_2 with a half-life T_{b2} and so on. Hence the cumulated activity can be expressed as:

$$\bar{A} = A_0 \int_0^{\infty} f_1 e^{-\frac{0.693t}{T_{b1}}} dt + A_0 \int_0^{\infty} f_2 e^{-\frac{0.693t}{T_{b2}}} dt \dots \dots \dots (xii)$$

$$\Rightarrow \bar{A} = 1.44 T_{b1} f_1 A_0 + 1.44 T_{b2} f_2 A_0 \dots \dots \dots (xiii)$$

It may also happen that, the uptake is instantaneous but clearance is by both physical decay and biologic excretion. The biologic excretion is described here by the single-component exponential curve with the biologic half-life T_b and the physical half-life T_p . Hence the total clearance curve is expressed by the single-component exponential curve with an effective half-life T_e as follows:

$$\frac{1}{T_e} = \frac{1}{T_p} + \frac{1}{T_b} \dots \dots \dots (xiv)$$

$$\Rightarrow T_e = \frac{T_p T_b}{T_p + T_b} \dots \dots \dots (xv)$$

Therefore the cumulated activity:

$$A = 1.44 T_e \bar{A}_0 \dots\dots\dots (xvi)$$

One point of consideration that lies here is that, if there is more than one component to the biologic excretion curve then each of the component [in equation (xiii)] will possess an individual half-life for each of them, which can be obtained by the equation (xv). If the physical decay is very slow in comparison to the biologic excretion i.e. $T_p \gg T_b$, then $T_e \approx T_b$ and if it is reverse case, i.e. $T_b \gg T_p$, then $T_e \approx T_p$. But the interesting point is that, the effective half-life T_e is shorter than either the physical or the biologic half-life. In all above mentioned cases, the uptake was instantaneous. But if situation occurs when the uptake is not instantaneous, than already developed equation discussed above will overestimate the radiation dose when uptake by the source organ is not rapid in comparison to physical decay. This occurs with the radionuclides that have slow pattern of uptake in comparison to their physical half-life. Uptake in such cases is described by a form of exponential equation :

$$A(t) = A_0 \left(1 - e^{-\frac{0.693}{T_u} t} \right) \dots\dots\dots (xvii)$$

where T_u is the biologic uptake half-life.

So cumulated activity:

$$\bar{A} = 1.44 T_e \left(\frac{T_{ue}}{T_u} \right) \dots\dots\dots (xviii)$$

where T_e is the effective half-life and T_{ue} is the effective uptake half-life:

$$T_{ue} = \frac{T_u T_p}{T_u + T_p} \dots\dots\dots (xix)$$

Dose Calculation:

The final step is to determine the fraction of energy emitted by the source organ that is absorbed by the target organ. This radiation dose calculations for penetrating radiation is quite tedious, especially where multiple radiation emission is being considered. Introducing the mean dose per unit cumulated activity, “S” helps in trying to solve this problem in a simplified way. This quantity “S” is calculated for different source- target organ pair for a number of radionuclides of interest. This factor can be expressed as:

$$S(r_k \leftarrow r_h) = \frac{1}{m_k} \sum_i \Delta_i \phi_i (r_k \leftarrow r_h)$$

or, $S(r_k \leftarrow r_h) = \sum_i \Delta_i \Phi_i (r_k \leftarrow r_h) \dots\dots\dots (xx)$

The notation $\phi_i (r_k \leftarrow r_h)$ is used to indicate absorbed fraction ϕ for energy delivered from a source organ or region, r_h to a target organ, r_k for the “i”th emission of the radionuclide. The summations \sum_i include values of ϕ_i and Δ_i

for all the emissions of the radionuclide and values of $\phi_i (r_k \leftarrow r_h)$ for appropriate source -target pair. The specific absorbed fraction is given as $\Phi = \phi/m_k$ where m_k is the mass of the target organ. The quantity S, has units rad / μ Ci-hr. Obtaining the value of S and value for cumulated activity \bar{A} , the average dose to an organ is calculated as:

$$\bar{D}(r_k \leftarrow r_h) = [\bar{A}(r_k \leftarrow r_h)] \times S \text{ -value } \mu\text{rad} \dots \dots \dots (\text{cx1})$$

3.6 Experimental Procedure

Patients:

A total of forty patients (twenty for each group) were studied for studies on kidney and liver. The age of all these patients lie between 20 and 48 years. The patients are dehydrated from condition of full bladder which can simulate upper tract obstruction on the scan.

Isotope:

^{99m}Tc was obtained from $^{99}\text{Mo} - ^{99m}\text{Tc}$ generator. For both kidney and liver imaging, almost in all cases around 5 mCi of dose was administered through intravenous injection in almost all cases.

Imaging:

Images were obtained for 30 minutes of post administration for both dynamic study on a large field of view gamma camera that is equipped with a medium energy collimator with a 20% window centered over the 140 keV photo peak of ^{99m}Tc . The camera is interfaced with a digital computer. Digital data was stored in a 128×128-word matrix for subsequent analysis. Regions of interest were assigned manually for kidney and livers as well as for other organs too. Total counts, counts of regions of interests, background counts along the pixel measurements were determined from multiple areas. All these are necessary in determining the bio-distribution and internal dosimetry, while for pharmacokinetic study of kidney, the radioactivity counts were taken from the static images. Their related counts shows the time-activity decay curve i.e, the pharmacokinetics of the used radiopharmaceuticals.

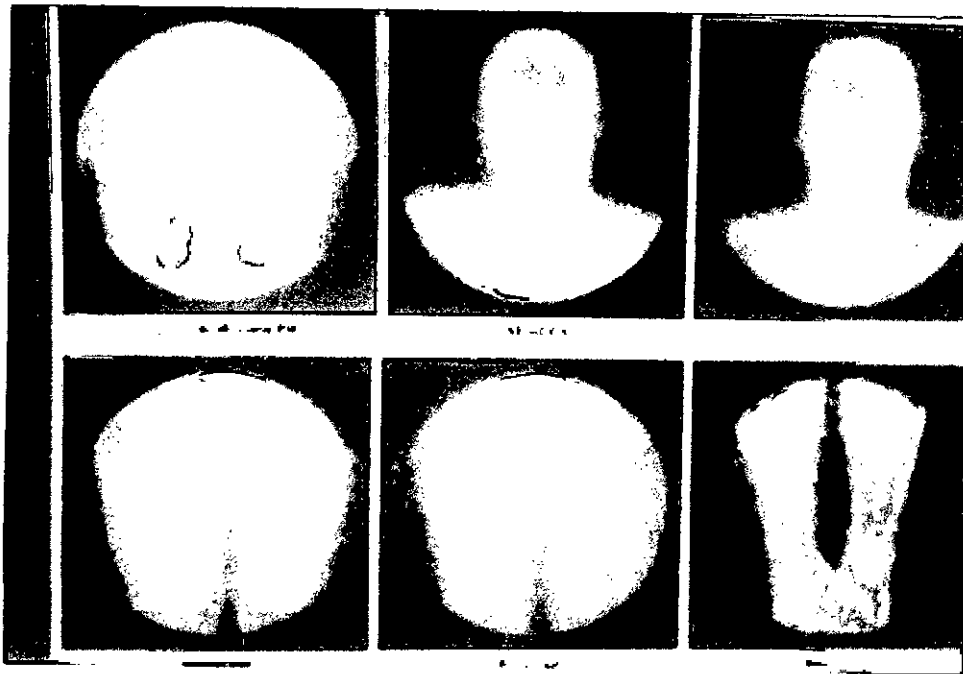
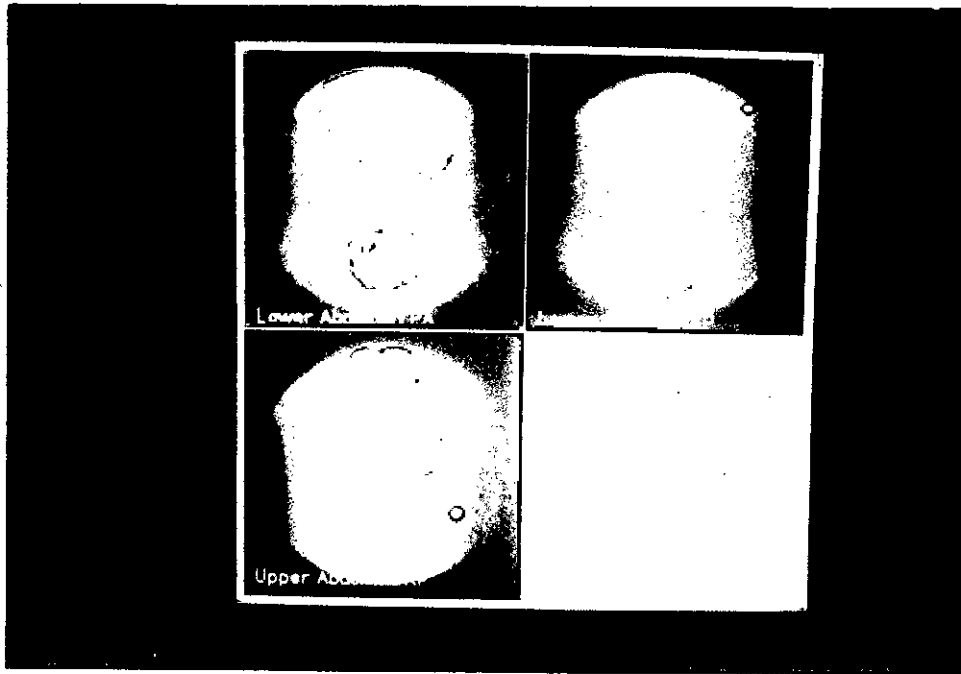


Figure : 3.20 (a, b) Photograph of The Distribution of ^{99m}Tc - DTPA in Different Organs in Static Study of Kidney

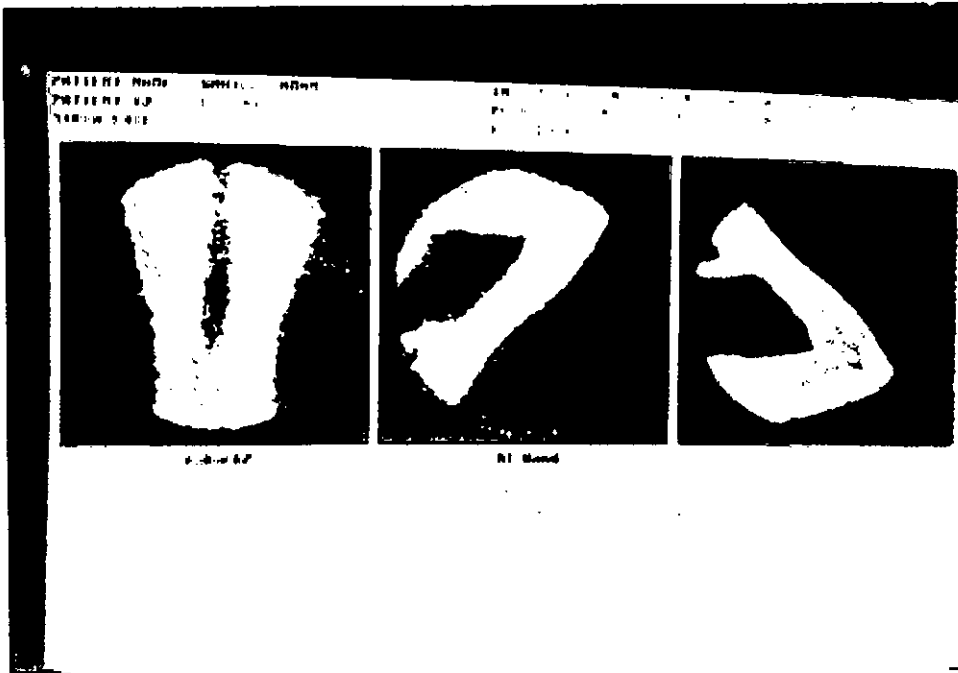


Figure : 3.20 (c) Photograph of The Distribution of ^{99m}Tc - DTPA in Different Organs in Static Study of Kidney

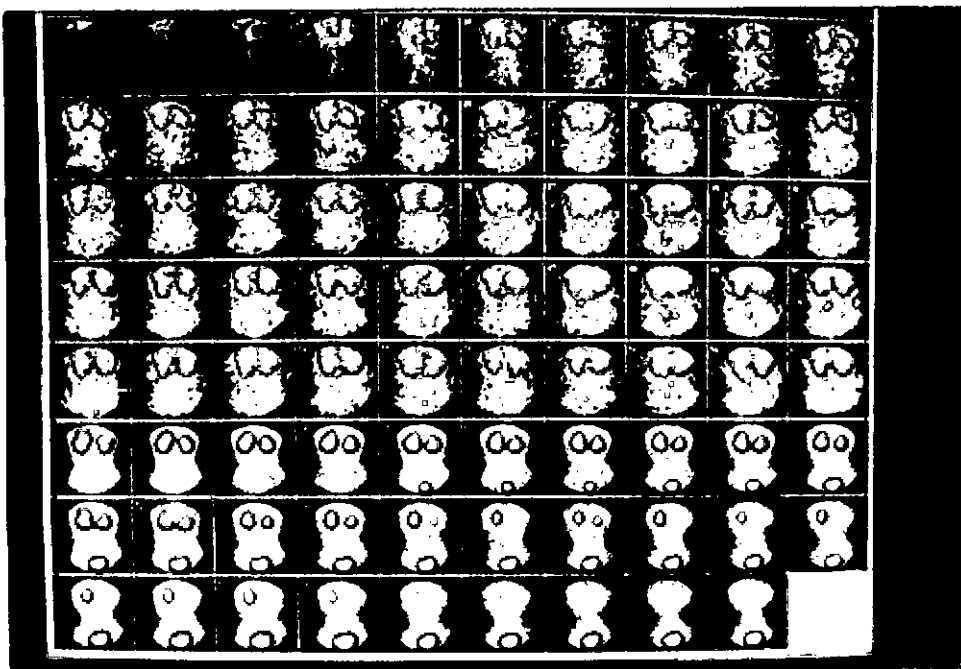


Figure : 3.20 (d) Photograph of Dynamic Study of Kidney

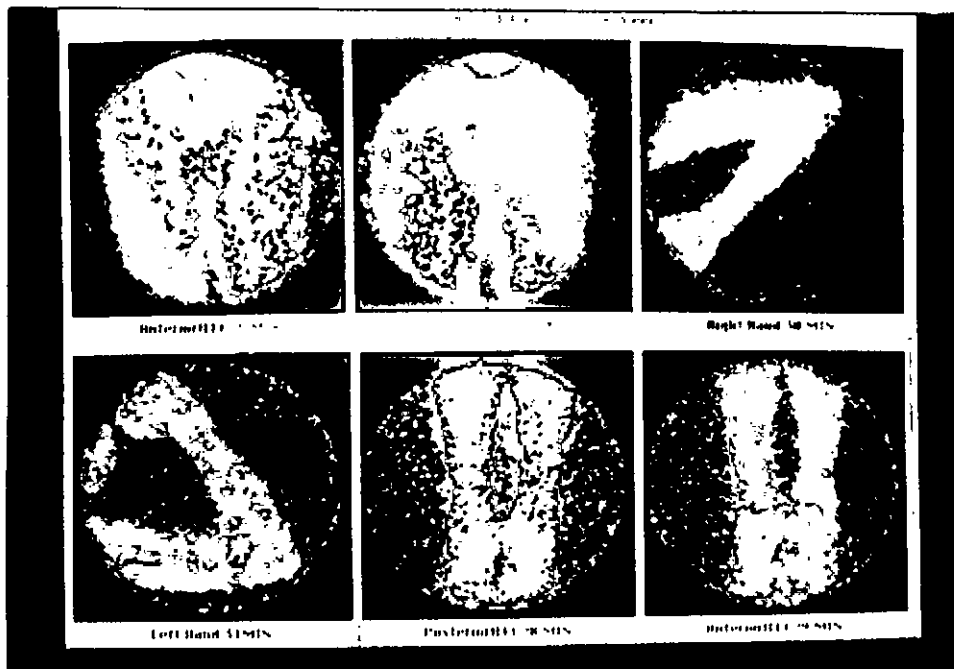
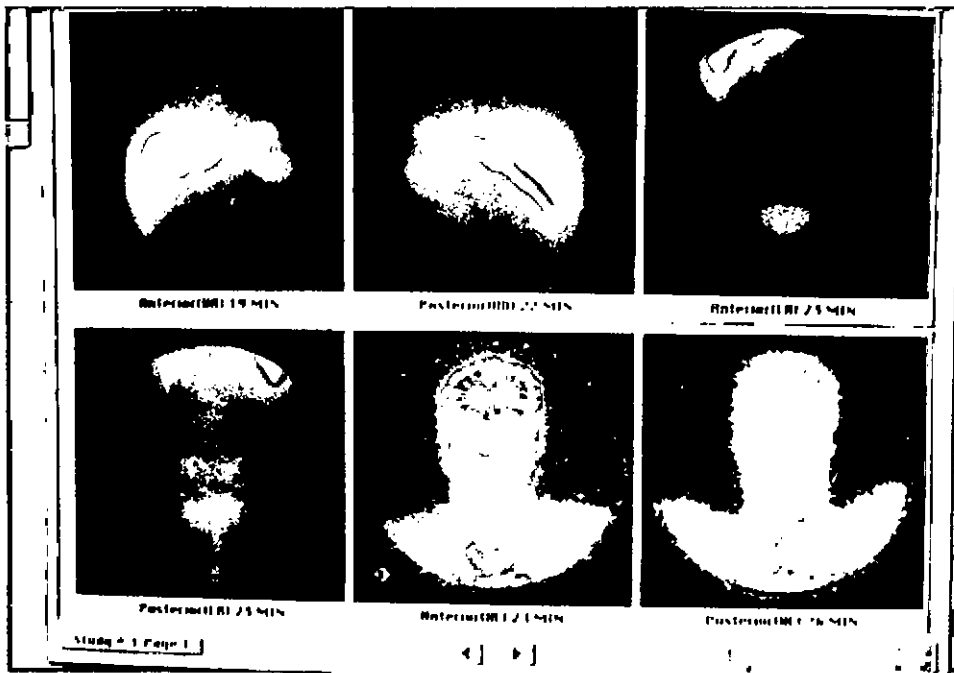


Figure : 3.20 (e, f) Photograph of The Distribution of ^{99m}Tc - Tin Sulfur Colloid in Different Organs in Static Study of Liver

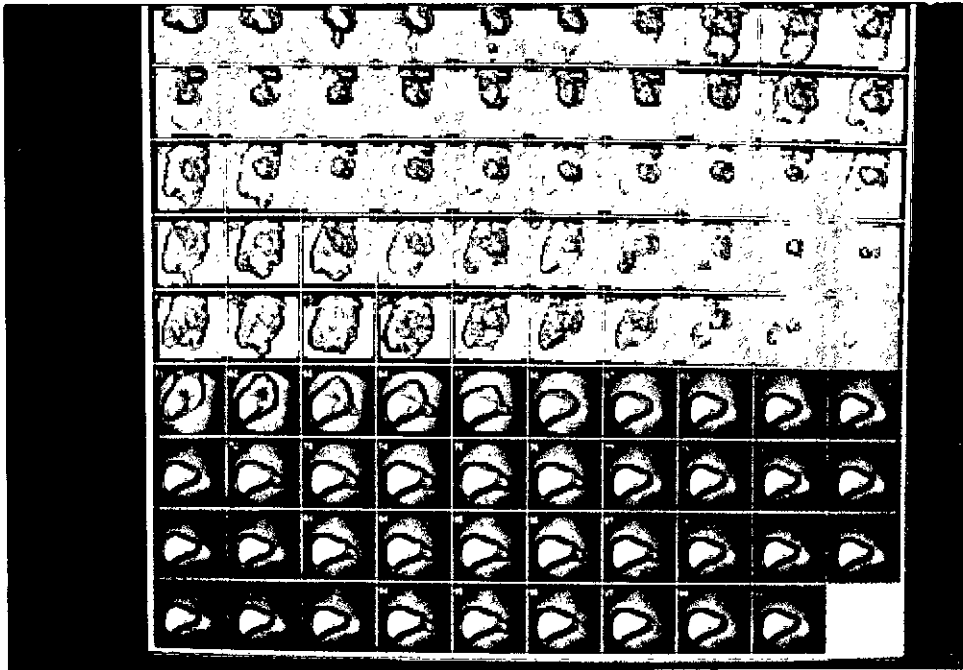


Figure : 3.20 (g) Photograph of Dynamic Study of Liver

CHAPTER 4

Results

And

Discussion

Results And Discussion

4.1 Introduction

The present work was carried out in the Nuclear Medicine Institute of the Bangladesh Atomic Energy Commission (BAEC) located in the campus of Bangabandhu Sheikh Mujib Medical University. Forty patients, twenty each, for kidney and liver were included in the study and were categorized in three different age groups. ^{99m}Tc -DTPA for target organ kidney and ^{99m}Tc -Tin Colloid for target organ liver were the injected radiopharmaceuticals, measured on all these patients. The target organs were sources of radioactivity in the total body from where the distribution of the radiopharmaceutical in different organs within the body can be measured. For studying kidney, taking itself as the target organ, the dose is measured in kidney, bladder, upper large intestine (ULI), lower large intestine (LLI), small intestine (SI), lungs, liver, stomach, thyroid, testis, bones and in other tissues of the remaining body. While for studying liver, taking itself as the target organ, the dose is measured in liver, kidney, spleen, bone marrow, upper large intestine (ULI), lower large intestine (LLI), small intestine (SI), bladder and in other tissues of the remaining body. The cumulative activity of the radiopharmaceuticals in different organs help in determining the absorbed dose in them. Finally these lead the way of obtaining the radiation absorbed dose from internally administered radiopharmaceutical in adults. All these are described briefly in the following paragraphs.

4.2 Results of Target Organ of Kidney

Biodistribution of ^{99m}Tc -DTPA Within Different Organs

The detailed results of biodistribution of ^{99m}Tc -DTPA within different organs when the target organ is kidney, is presented in the table: 4.1. The biodistribution was highest in lungs followed by kidneys. In kidney of 20 patients, biodistribution ranged from 5.68% to 10.28%, the average value being 7.89%. In lungs it varied from 9.31% to 13.26%, the average being 11.05%. Most of the radiopharmaceutical remained concentrated in other tissues of the body ranging from 52.30 to 63.08%. It is observed from the data that, biodistribution in different organs did not vary significantly among the twenty patients. The lowest biodistribution was recorded in bones of the body which indicated that the radiopharmaceutical did not move sufficiently through the more solid part of the body. These were true in case of biodistribution of radiopharmaceutical for all the organs studied.

Cumulative Activity of ^{99m}Tc -DTPA in Different Organs

The detailed result of cumulative activity ^{99m}Tc -DTPA within the different organs of the 20 patients taking kidney as target are shown in Table: 4.2. Although the highest cumulative activity was observed in the tissue but individually it was highest in lungs .The lowest was recorded in bones of the human body. The mean value of cumulative activity of the radiopharmaceutical in lungs was 4817.02 $\mu\text{Ci-hrs}$, which ranged from 4021.92 to 5408.64 $\mu\text{Ci-hr}$. No significant variation among the twenty patients was observed. The cumulative activity value in other tissues of the body was much greater in all the twenty patients, the mean value being 25219.57 $\mu\text{Ci- hr}$.

Table 4.1: Biodistribution of The Radiopharmaceutical in Different Organs (Target Organ : Kidney)

Patient	Percentage Uptake											
	Kidney	Bladder	ULI	LLI	SI	Lung	Stomach	Liver	Thyroid	Testis	Bones	Other Tissue
1	7.02	5.30	4.79	2.71	4.70	13.00	2.94	3.32	1.09	0.77	0.80	53.56
2	7.55	4.10	3.26	2.68	3.11	11.36	2.84	3.55	1.00	0.78	0.63	59.14
3	7.94	4.06	3.18	2.56	2.79	10.99	2.61	3.38	0.96	0.73	0.62	60.18
4	8.03	4.42	3.47	2.62	3.98	11.08	2.70	2.99	1.00	0.59	0.59	58.53
5	10.26	4.16	3.68	3.33	3.15	14.06	3.14	3.37	1.00	0.72	0.83	52.30
6	8.57	4.73	3.57	2.83	4.30	13.26	3.31	3.44	1.04	0.75	0.62	53.62
7	10.28	4.08	3.67	3.29	3.71	9.31	2.61	3.13	1.00	0.58	0.46	57.88
8	8.50	2.58	2.93	2.33	2.86	9.98	3.05	3.60	0.79	0.76	0.53	62.09
9	7.56	3.89	3.08	2.53	2.94	10.09	2.75	3.34	0.91	0.70	0.58	61.63
10	6.95	5.02	4.80	2.53	4.53	12.50	3.03	3.18	1.04	0.71	0.78	54.93
11	7.19	3.10	4.72	2.70	3.94	10.75	2.54	2.60	0.94	0.67	0.69	60.16
12	5.68	2.66	4.15	2.27	2.87	10.86	2.72	3.19	1.01	0.77	0.74	63.08
13	8.06	2.85	3.89	3.29	3.55	9.58	2.79	3.29	0.94	0.71	0.59	60.35
14	7.71	4.26	5.22	2.98	4.46	11.77	3.16	3.32	1.03	0.71	0.83	54.55
15	7.48	3.83	4.64	3.44	2.95	10.23	2.46	2.57	0.84	0.85	0.75	62.09
16	8.78	4.12	4.26	2.21	4.63	10.16	2.22	3.42	1.07	0.80	0.73	57.60
17	7.84	3.96	3.73	2.77	4.61	10.87	2.59	3.64	0.96	0.77	0.84	57.42
18	6.99	5.04	5.03	3.39	2.99	9.62	3.11	3.36	0.87	0.72	0.77	58.11
19	8.05	4.09	3.44	3.46	3.59	11.06	2.91	2.84	1.00	0.69	0.72	58.15
20	7.42	3.68	3.29	2.64	3.88	10.46	2.85	3.58	1.02	0.72	0.68	59.78
Mean	7.893	3.996	3.94	2.828	3.677	11.05	2.816	3.256	0.976	0.725	0.689	58.258

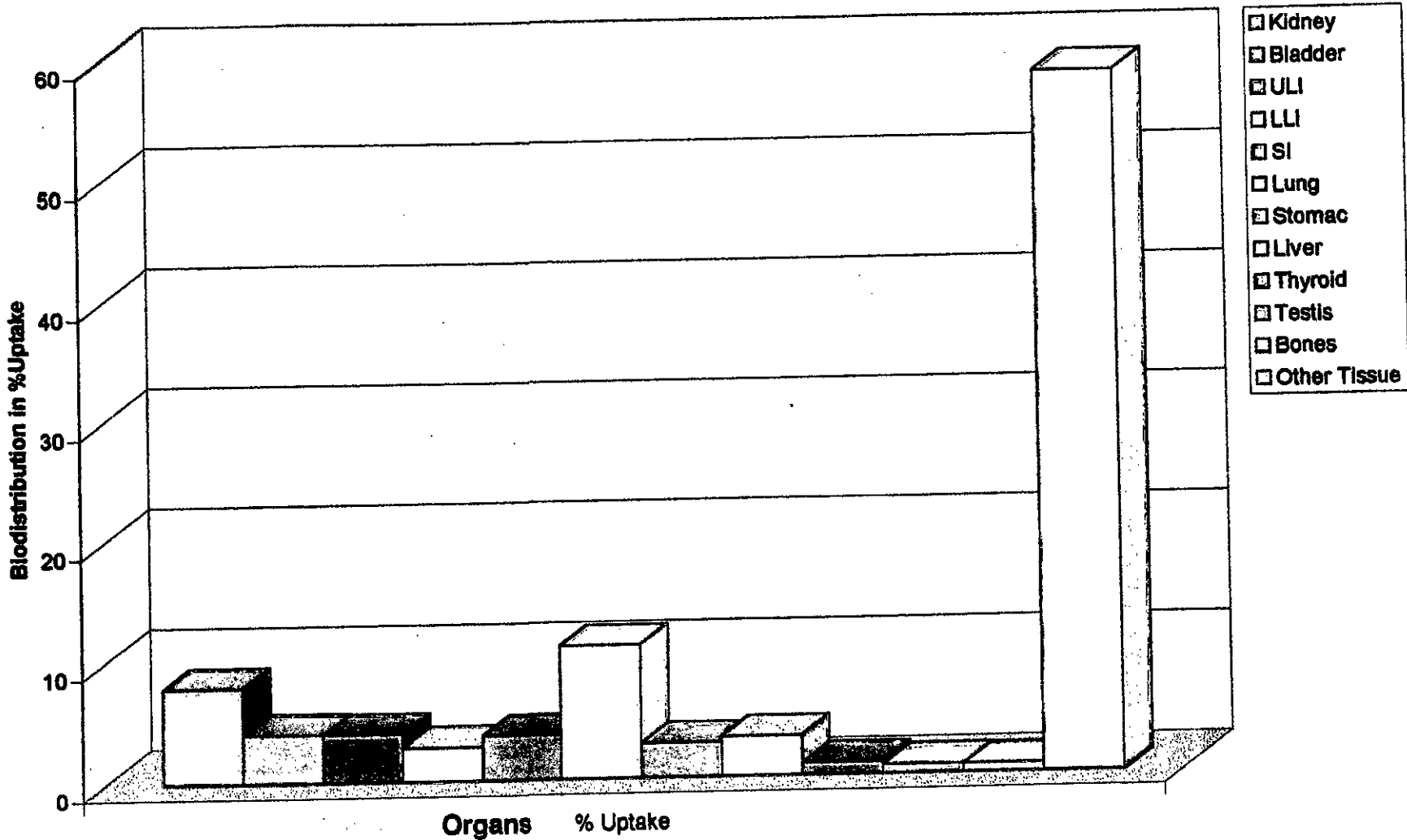


Figure : 4.1 Biodistribution of The Radiopharmaceutical in Different Organs (Target Organ:Kidney)

**Table 4.2 : Cumulative Activity of The Radiopharmaceutical in Different Organs
(target organ : kidney)**

Patient	In $\mu\text{Ci-hrs}$					
	Kidney	Bladder	ULI	LLI	SI	Lung
1	859.25	2289.60	2069.30	1170.70	2030.40	5616.00
2	924.12	1771.20	1408.32	1157.76	1343.52	4907.52
3	971.86	1753.92	1373.76	1105.92	1205.28	4747.68
4	942.87	1909.44	1499.04	1131.84	1719.36	4786.56
5	1542.24	1797.12	1589.76	1438.56	1360.80	6073.92
6	1048.96	2043.36	1542.24	1222.56	1857.60	5728.32
7	1258.27	1762.56	1585.44	1421.28	1602.72	4021.92
8	1040.40	1114.56	1265.79	1006.56	1235.52	4311.36
9	925.34	1680.48	1330.56	1092.96	1270.08	4358.88
10	850.68	2172.96	2077.92	1097.28	1961.28	5408.64
11	880.05	1339.20	2039.04	1166.40	1702.08	4644.00
12	695.23	1149.12	1792.80	980.64	1239.84	4691.52
13	986.54	1231.20	1728.00	1421.28	1533.60	4138.56
14	943.70	1840.32	2255.04	1287.36	1926.72	5084.64
15	793.14	1425.60	1745.28	1486.08	1274.40	4419.36
16	865.26	1744.11	1819.42	1233.5	1415.33	4214.15
17	889.65	1821.2	2026.31	1195.3	1297.10	4325.66
18	1021.44	1954.57	2178.50	1263.8	1941.22	5226.67
19	911.17	1710.98	1866.43	1145.2	1504.32	5061.47
20	844.57	1785.81	1910.06	1168.9	1642.46	4573.54
Mean	959.74	1714.87	1755.15	1209.70	1553.18	4817.02

Contd.....

Patient	In $\mu\text{Ci-hrs}$					
	Liver	Stomach	Thyroid	Testis	Bones	Other Tissue
1	1434.24	1270.08	470.90	332.64	345.60	23137.920
2	1533.60	1226.80	432.00	336.96	272.16	25548.480
3	1127.52	1460.16	414.72	315.36	267.84	25997.760
4	1291.68	1166.40	432.00	254.88	254.88	25284.960
5	1455.84	1356.48	432.00	311.04	358.56	22593.600
6	1486.04	1429.92	449.28	324.00	267.84	23163.840
7	1352.16	1127.52	432.00	250.56	198.72	25004.160
8	1555.20	1317.60	341.28	328.32	228.96	26822.880
9	1442.88	1188.00	393.12	302.40	250.56	26624.160
10	1378.08	1313.28	449.28	306.72	336.96	23690.880
11	1123.20	1097.28	406.08	289.44	298.08	25989.120
12	1378.08	1175.04	436.32	332.64	319.68	27250.560
13	1421.28	1205.28	406.08	306.72	254.88	26071.200
14	1434.24	1365.12	444.26	306.72	358.56	23565.600
15	1110.24	1062.72	362.88	367.20	324.00	26822.880
16	1142.32	1121.88	355.12	351.42	289.55	23159.740
17	1507.14	1210.31	426.00	286.90	361.52	24567.210
18	1362.84	1189.74	486.37	311.56	346.82	26753.150
19	1178.35	1356.33	389.41	379.48	278.49	26846.940
20	1442.31	1149.35	438.57	376.25	342.76	25496.340
Mean	1357.86	1239.46	419.88	318.56	297.82	25219.57

Absorbed dose of ^{99m}Tc-DTPA in Different Organs

The absorbed dose ^{99m}Tc-DTPA in different organs of 20 patients are presented in Table: 4.2. The highest amount of ^{99m}Tc-DTPA was absorbed in the target organ kidney itself followed by other tissues. Lowest absorption was recorded in thyroid. This indicated that, the movement of the radiopharmaceutical varied according to the position of the organ from the source organ. Absorbed dose in different organs of twenty patients did not vary significantly among themselves. In kidney, the absorbed dose ranged from 0.132 to 0.293 rads, the average value being 0.182 rad.

Radiation Absorbed dose of ^{99m}Tc-DTPA in Kidney

The radiation absorbed dose in the kidney of twenty patients ranged from 0.0383 to 0.06952 rad/mCi (Table: 4.4). The mean value was 0.048 rad/mCi. Some variations were observed in radiation absorbed dose but these variations are not very significant. The variation may be due to the difference in age group of patients. This would be evident from Figure: 4.2 and Figure: 4.3. The 20 patients were grouped into three categories, 5 being in the 21-30 yrs age group, 8 in the 31-40 yrs age group and 7 in the 41-50 yrs age group. The radiation absorbed dose is higher in patients of lower age group of 21-30 yrs, followed by mid age group 31-40 yrs. The lowest absorbed dose was observed in older age group of 41-50 yrs. The Pie chart (Pie chart) in Figure: 4.3 shows that 38% of the patients belonging to the 21-30 age group showed highest radiation absorption followed by mid age group of 31-40 yrs which is 34%. The older group of 41-50 yrs includes only 28%. This indicates that the radiation absorption was higher in younger patients.

**Table 4.3 : Absorbed Dose of The Radiopharmaceutical in Different Organs
(Target organ: kidney)**

Patient	In per 5mCi of Injected Dose in rads					
	Kidney	Bladder	ULI	LLI	SI	Lung
1	0.1600	5.95E-04	5.79E-03	1.01E-03	6.49E-03	4.72E-03
2	0.1760	4.61E-04	3.94E-03	9.96E-04	4.30E-03	4.12E-03
3	0.1840	4.56E-04	3.85E-03	9.51E-04	3.86E-03	3.99E-03
4	0.1860	4.96E-04	4.19E-03	9.73E-04	5.50E-03	4.02E-03
5	0.2930	4.67E-04	4.45E-03	1.24E-04	4.35E-03	5.10E-03
6	0.1993	5.31E-04	4.32E-03	1.05E-03	5.94E-03	4.81E-03
7	0.2391	4.58E-04	4.44E-03	1.22E-03	5.12E-03	3.38E-03
8	0.1977	2.89E-04	3.54E-03	8.65E-04	3.95E-03	3.62E-03
9	0.1758	4.36E-04	3.72E-03	9.40E-04	4.06E-03	3.66E-03
10	0.1619	5.65E-04	5.81E-03	9.43E-04	6.27E-03	4.54E-03
11	0.1672	3.48E-04	5.71E-03	1.00E-03	5.44E-03	3.90E-03
12	0.1321	2.98E-04	5.02E-03	8.43E-04	3.96E-03	3.94E-03
13	0.1874	3.20E-04	4.83E-03	1.22E-03	4.91E-03	3.47E-03
14	0.1793	4.78E-04	6.31E-03	1.11E-03	6.16E-03	4.27E-03
15	0.1507	3.70E-04	4.89E-03	1.28E-03	4.08E-03	3.71E-03
16	0.1663	4.32E-04	5.06E-03	1.09E-03	3.89E-03	3.64E-03
17	0.1629	3.95E-04	4.46E-03	9.11E-04	4.57E-03	3.86E-03
18	0.1875	4.52E-04	4.32E-03	6.53E-04	6.04E-03	4.14E-03
19	0.1728	5.59E-04	3.99E-03	1.15E-03	4.28E-03	3.97E-03
20	0.1640	4.47E-04	4.76E-03	1.10E-03	4.73E-03	4.60E-03
Mean	0.1822	4.43E-04	4.67E-03	9.54E-04	4.89E-03	4.07E-03

Contd....

Patient	In per 5mCi of Injected Dose in rads					
	Liver	Stomach	Thyroid	Testis	Bones	Other Tissue
1	5.59E-03	4.45E-03	1.06E-05	1.33E-05	2.8E-04	0.03000
2	5.98E-03	4.29E-03	1.47E-05	1.35E-05	2.2E-04	0.03300
3	4.40E-03	5.11E-03	1.41E-05	1.26E-05	2.2E-04	0.03400
4	5.03E-03	4.08E-03	1.46E-05	1.02E-05	2.1E-04	0.03280
5	5.67E-03	4.75E-03	1.47E-05	1.24E-05	2.9E-04	0.02937
6	5.79E-03	5.00E-03	1.52E-05	1.29E-05	2.2E-04	0.03011
7	5.27E-03	3.94E-03	1.47E-05	1.00E-05	1.6E-04	0.03251
8	6.06E-03	4.61E-03	1.16E-05	1.31E-05	1.9E-04	0.03487
9	5.63E-03	4.16E-03	1.34E-05	1.21E-05	2.1E-04	0.03461
10	5.37E-03	4.59E-03	1.53E-05	1.23E-05	2.8E-04	0.03080
11	4.38E-03	3.84E-03	1.38E-05	1.15E-05	2.4E-04	0.03379
12	5.37E-03	4.11E-03	1.48E-05	1.33E-05	2.6E-04	0.03543
13	5.54E-03	4.22E-03	1.38E-05	1.22E-05	2.1E-04	0.03389
14	5.59E-03	4.78E-03	1.51E-05	1.22E-05	2.9E-04	0.03064
15	4.33E-03	3.72E-03	1.23E-05	1.46E-05	2.7E-04	0.03487
16	5.29E-03	3.54E-03	1.27E-05	1.31E-05	2.2E-04	0.03257
17	5.51E-03	3.79E-03	1.40E-05	1.17E-05	2.5E-04	0.02986
18	4.88E-03	4.29E-03	1.39E-05	1.28E-05	1.7E-04	0.02849
19	4.27E-03	4.11E-03	1.43E-05	1.34E-05	2.5E-04	0.03764
20	5.72E-03	5.24E-03	1.49E-05	1.19E-05	2.3E-04	0.03657
Mean	5.28E-03	4.33E-03	1.39E-05	1.25E-05	2.3E-04	0.03279

**Table 4.4 : Radiation Absorbed Dose of The Radiopharmaceutical in Patients
(Target organ: kidney)**

Patient	In per mCi of Injected Dose in rads	
	Age Group	Absorbed Dose
1	41-50	0.043790660
2	31-40	0.046669154
3	31-40	0.048172660
4	31-40	0.048804500
5	21-30	0.069520420
6	21-30	0.051419620
7	21-30	0.059124900
8	21-30	0.051143140
9	31-40	0.046649300
10	41-50	0.044218000
11	31-40	0.045175460
12	40-50	0.038272200
13	31-40	0.049207000
14	31-40	0.047783860
15	41-50	0.041648380
16	21-30	0.055107000
17	31-40	0.049278000
18	41-50	0.039471000
19	41-50	0.040974000
20	41-50	0.043728000
Mean		0.048007863

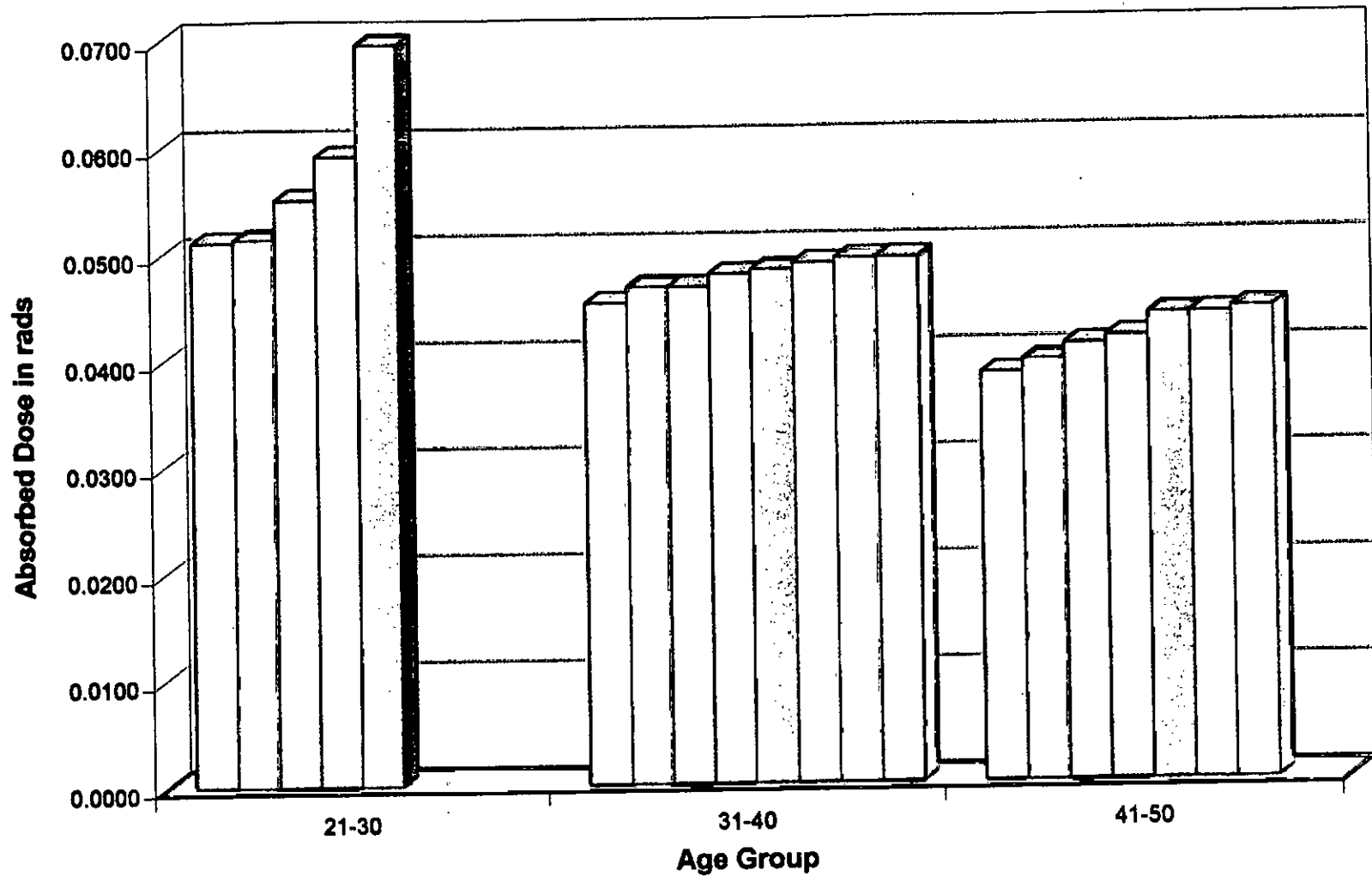


Figure: 4.2 Radiation Absorbed Dose of The Radiopharmaceutical in Patient According to Different Age Group (target Organ: Kidney)

128

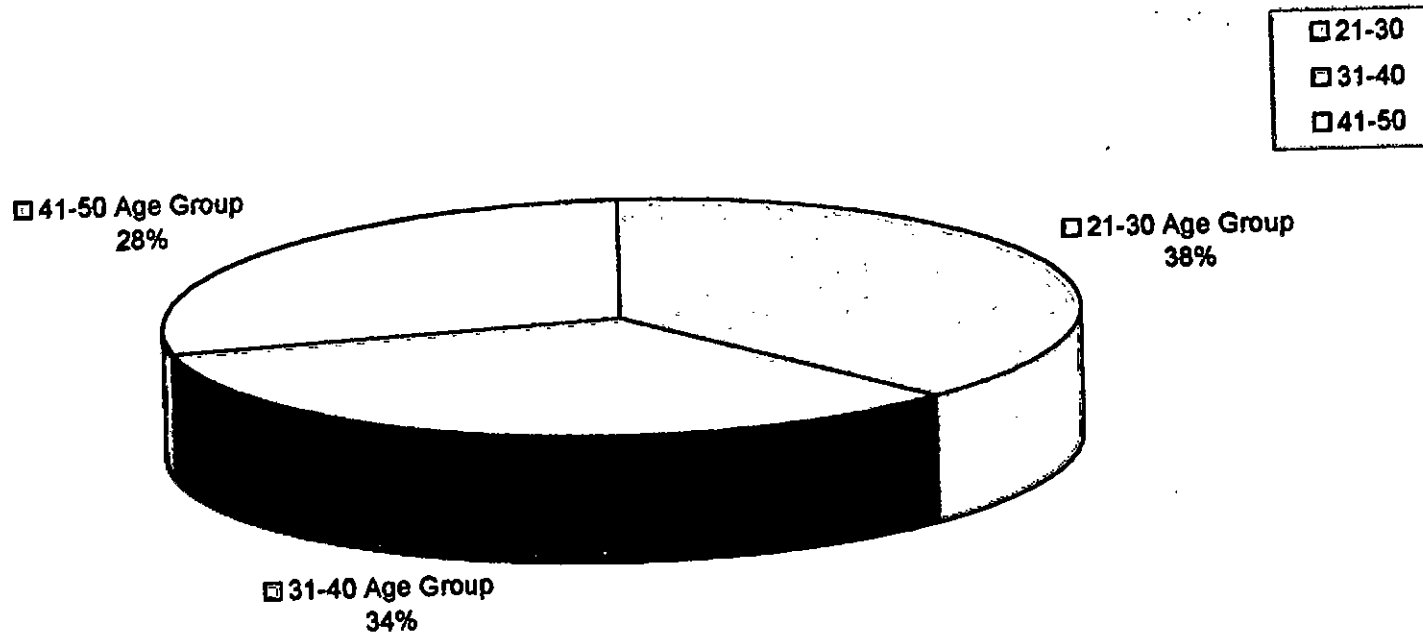


Figure: 4.3 Radiation Absorbed Dose of The Radiopharmaceutical in Patient According to Different Age Group (target Organ: Kidney)

Comparison Between Biodistribution of ^{99m}Tc -DTPA and Radiation Dose Absorbed by Kidney

Figure 4.4 shows the biodistribution of ^{99m}Tc -DTPA and dose absorbed in kidney alone/5mCi of the injected dose. It is evident from the figure that there is similarity in the trend of biodistribution and dose absorbed by kidney. The patient who showed higher biodistribution, had higher dose absorption in kidney. Similar trend was observed in case of lower biodistribution in the patient with lower radiation absorption, with an exception of one or two patient.

Pharmacokinetic of ^{99m}Tc -DTPA

^{99m}Tc -DTPA has a physical half-life of six hours only. The radiopharmaceuticals are expected not to remain within the body of the patients. Therefore a study was undertaken to observe the radioactivity remaining in the body and its clearance with time. This was done by taking dynamic images of the patients from the gamma camera after infusion. The regular thirty minute dynamic images of the patient was first collected from the camera. Then it was prolonged upto 630 minute and related radioactivity counts were collected from the static images by way of selecting the organs using ROI(region of interest). The radioactivity counts were plotted against the time presenting the time-activity concentration of ^{99m}Tc -DTPA within the kidney (Figure: 4.5,4.6 and Table:4.6,4.7). It is evident from the detailed result that the three effective half-lives of the radiopharmaceutical was observed at 9,90 and 600 min in case of both the kidneys. This indicates that the remaining activity of the radiopharmaceutical becomes negligible after 10 hrs of infusion and thereafter the activity is gradually cleared. So the patients become free of any hazardous effect of the radiopharmaceuticals.

Table 4.5 : Radiation Absorbed Dose by Kidney Vs Biodistribution of Kidney

Patient	In per 5mCi of Injected Dose in rads	In Percentage Uptake
	Dose Absorbed	Biodistribution
1	0.1600	7.02%
2	0.1760	7.55%
3	0.1840	7.94%
4	0.1860	8.03%
5	0.2930	10.26%
6	0.1993	8.57%
7	0.2391	10.28%
8	0.1977	8.50%
9	0.1758	7.56%
10	0.1619	6.95%
11	0.1672	7.19%
12	0.1321	5.68%
13	0.1874	8.06%
14	0.1793	7.71%
15	0.1507	7.48%
16	0.1663	8.78%
17	0.1629	7.84%
18	0.1875	6.99%
19	0.1728	8.05%
20	0.164	7.42%
Mean	0.1822	7.89%

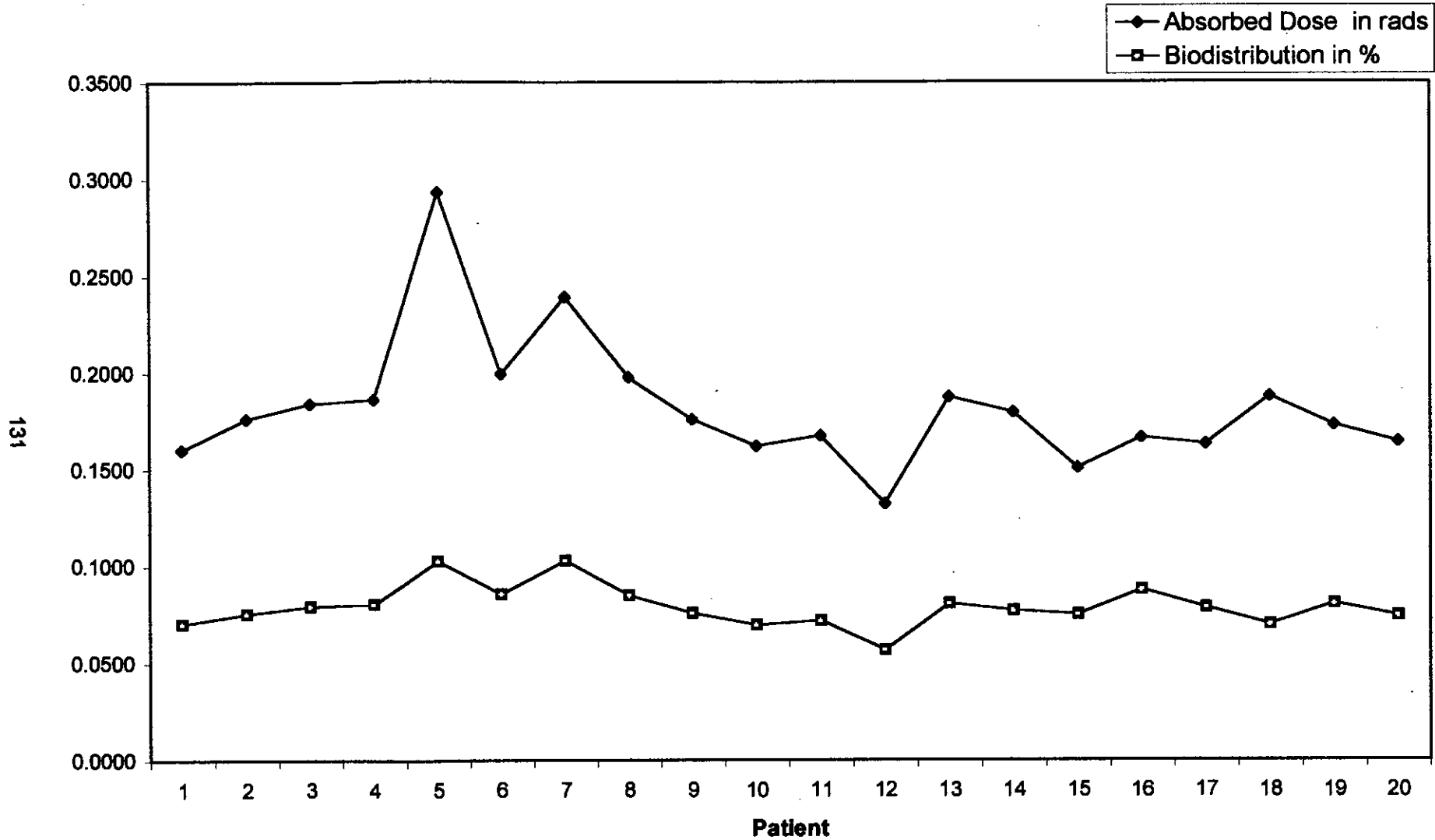


**Figure: 4.4 Radiation Dose Absorbed by Kidney
Vs
Biodistribution of Kidney**

Table 4.6 : Pharmacokinetic Study of Tc-99m DTPA in Left Kidney

Time in Min.	Radioactivity Counts	Time in Min.	Radioactivity Counts	Time in Min.	Radioactivity Counts	Time in Min.	Radioactivity Counts
Injection given	0	125th	10874	330th.	8817	540th.	7402
1st	38588	130th.	10697	335th	8801	545th	7362
2nd	36645	135th	10479	340th	8799	550th.	7124
3rd	48657	140th.	10346	345th	8782	555th	7111
4th	47652	145th	10115	350th.	8776	560th.	6730
5th	43555	150th.	9946	355th	8753	565th	6345
6th	40144	155th.	9975	360th.	8746	570th.	6311
7th	37721	160th.	9952	365th	8741	580th.	6278
8th.	28531	165th.	9910	370th.	8734	585th	6223
❖ 9th	24329	170th.	9888	380th.	8729	590th.	6187
10th	24285	175th.	9886	385th	8711	595th	6156
11th	24198	180th.	9881	390th.	8687	❖ 600th.	6088
12th.	23915	185th	9874	395th	8658	605th	5569
13th	23789	190th.	9808	400th.	8644	610th.	5238
14th.	23456	195th.	9693	405th	8638	615th	4987
15th	23173	200th.	9621	410th.	8623	620th.	4825
16th.	22741	205th.	9587	415th	8603	625th	4765
17th	22512	210th.	9547	420th.	8592	630th	4694
18th.	21857	215th.	9543	425th	8581		
19th	21416	220th.	9521	430th.	8576		
20th.	20971	225th.	9501	435th	8543		
25th.	20643	230th.	9488	440th.	8526		
30th.	19872	235th.	9468	445th	8488		
35th.	19451	240th.	9395	450th.	8471		
40th	18857	245th.	9377	455th	8465		
45h.	18045	250th.	9351	460th.	8432		
50th.	17764	255th.	9326	465th	8418		
55th.	16943	260th.	9313	470th.	8396		
60th.	15648	265th.	9279	475th	8381		
65th.	14798	270th.	9268	480th.	8377		
70th.	13564	275th.	9244	485th	8364		
75th.	13222	280th.	9191	490th.	8359		
80th.	12890	285th.	9164	495th	8338		
85th.	12475	290th.	9142	500th.	8310		
❖ 90th.	12167	295th.	9133	505th	8289		
95th.	11915	300th.	9121	510th.	8231		
100th.	11650	305th	9104	515th	8000		
105th.	11331	310th.	8887	520th.	7885		
110th.	11198	315th	8859	525th	7633		
115th.	11111	320th.	8846	530th.	7700		
120th.	11100	325th	8835	535th	7486		

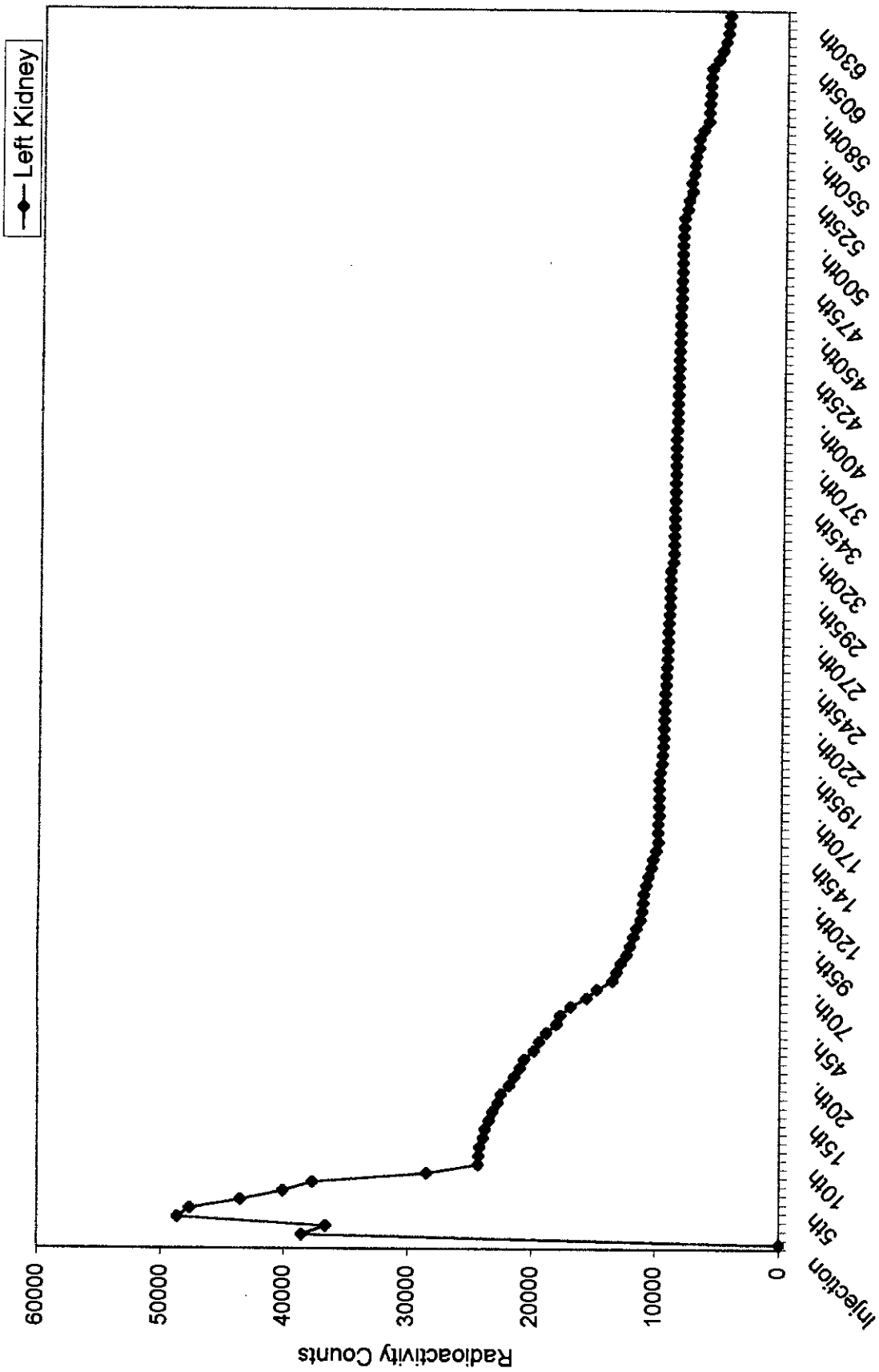


Figure: 4.5 Pharmacokinetic Study of Tc-99m DTPA in Left Kidney

Table 4.7 : Pharmacokinetic Study of Tc-99m DTPA in Right Kidney

Time in Min.	Radioactivity Counts	Time in Min.	Radioactivity Counts	Time in Min.	Radioactivity Counts	Time in Min.	Radioactivity Counts
Injection given	0	125th	10269	330th.	8411	540th.	6899
1st	48751	130th.	10461	335th	8291	545th	6881
2nd	42972	135th	10218	340th	8272	550th.	6869
3rd	52876	140th.	9745	345th	8251	555th	6844
4th	51875	145th	9721	350th.	8215	560th.	6821
5th	47597	150th.	9687	355th	8164	565th	6789
6th	44517	155th.	9756	360th.	8119	570th.	6769
7th	39300	160th.	9734	365th	7974	580th.	6736
8th.	28114	165th.	9722	370th.	7948	585th	6711
❖ 9th	26438	170th.	9651	380th.	7881	590th.	6697
10th	26338	175th.	9489	385th	7859	595th	6685
11th	25984	180th.	9475	390th.	7832	❖ 600th.	6610
12th.	25512	185th	9432	395th	7797	605th	6452
13th	24838	190th.	9410	400th.	7759	610th.	6421
14th.	24697	195th.	9287	405th	7734	615th	6214
15th	24117	200th.	9261	410th.	7679	620th.	6189
16th.	23897	205th.	9224	415th	7656	625th	5985
17th	23763	210th.	9213	420th.	7635	630th	5755
18th.	22921	215th.	9198	425th	7583		
19th	22598	220th.	9175	430th.	7548		
20th.	21784	225th.	9167	435th	7526		
25th.	21689	230th.	9143	440th.	7487		
30th.	20856	235th.	9121	445th	7451		
35th.	20642	240th.	9101	450th.	7437		
40th	20102	245th.	8948	455th	7423		
45h.	19794	250th.	8932	460th.	7395		
50th.	18672	255th.	8768	465th	7356		
55th.	17583	260th.	8732	470th.	7321		
60th.	16387	265th.	8500	475th	7258		
65th.	15692	270th.	8651	480th.	7231		
70th.	15283	275th.	8733	485th	7203		
75th.	14785	280th.	8720	490th.	7188		
80th.	13694	285th.	8588	495th	7158		
85th.	13494	290th.	8551	500th.	7149		
90th.	13219	295th.	8549	505th	7114		
95th.	12575	300th.	8539	510th.	6996		
100th.	12435	305th	8521	515th	6977		
105th.	11985	310th.	8509	520th.	6953		
110th.	11761	315th	8859	525th	6938		
115th.	11239	320th.	8486	530th.	6929		
120th.	10841	325th	8459	535th	6918		

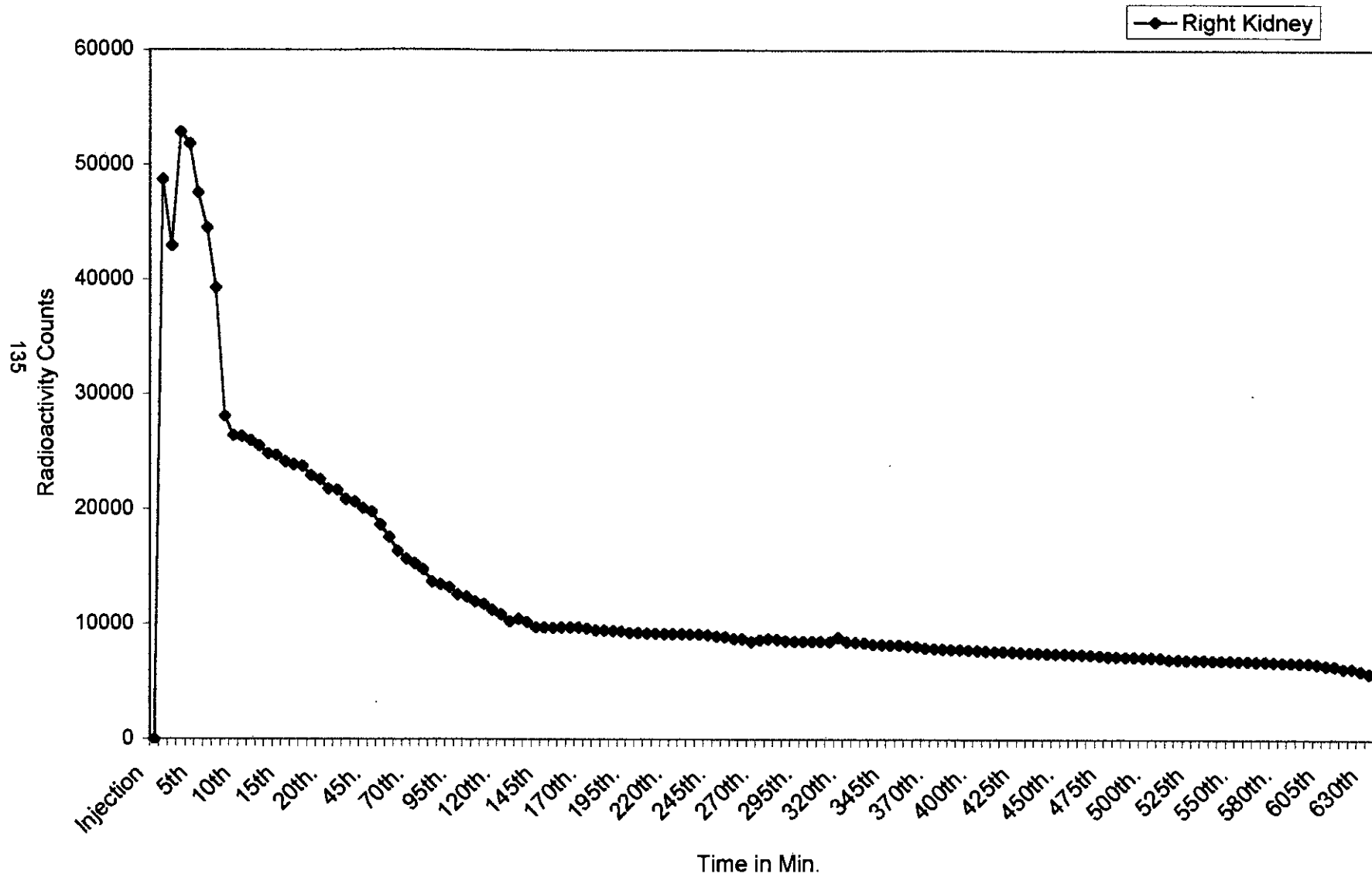


Figure: 4.6 Pharmacokinetic Study of Tc-99m DTPA in Right Kidney

Table 4.8: Comparative Pharmacokinetic Study of Tc-99m DTPA in Both Kidneys

Time in Min.	Left Kidney	Right Kidney	Time in Min.	Left Kidney	Right Kidney	Time in Min.	Left Kidney	Right Kidney	Time in Min.	Left Kidney	Right Kidney
Injection	0	0	130th.	10697	10461	340th	8799	8272	555th	7111	6844
1st	38588	48751	135th	10479	10218	345th	8782	8251	560th.	6730	6821
2nd	36645	42972	140th.	10346	9745	350th.	8776	8215	565th	6345	6789
3rd	48657	52876	145th	10115	9721	355th	8753	8164	570th.	6311	6769
4th	47652	51875	150th.	9946	9687	360th.	8746	8119	580th.	6278	6736
5th	43555	47597	155th.	9975	9756	365th	8741	7974	585th	6223	6711
6th	40144	44517	160th.	9952	9734	370th.	8734	7948	590th.	6187	6697
7th	37721	39300	165th.	9910	9722	380th.	8729	7881	595th	6156	6685
8th.	28531	28114	170th.	9888	9651	385th	8711	7859	600th.	6088	6610
9th	24329	26438	175th.	9886	9489	390th.	8687	7832	605th	5569	6452
10th	24285	26338	180th.	9881	9475	395th	8658	7797	610th.	5238	6421
11th	24198	25984	185th	9874	9432	400th.	8644	7759	615th	4987	6214
12th.	23915	25512	190th.	9808	9410	405th	8638	7734	620th.	4825	6189
13th	23789	24838	195th.	9693	9287	410th.	8623	7679	625th	4765	5985
14th.	23456	24697	200th.	9621	9261	415th	8603	7656	630th	4694	5755
15th	23173	24117	205th.	9587	9224	420th.	8592	7635			
16th.	22741	23897	210th.	9547	9213	425th	8581	7583			
17th	22512	23763	215th.	9543	9198	430th.	8576	7548			
18th.	21857	22921	220th.	9521	9175	435th	8543	7526			
19th	21416	22598	225th.	9501	9167	440th.	8526	7487			
20th.	20971	21784	230th.	9488	9143	445th	8488	7451			
25th.	20643	21689	235th.	9468	9121	450th.	8471	7437			
30th.	19872	20856	240th.	9395	9101	455th	8465	7423			
35th.	19451	20642	245th.	9377	8948	460th.	8432	7395			
40th	18857	20102	250th.	9351	8932	465th	8418	7356			
45th.	18045	19794	255th.	9326	8768	470th.	8396	7321			
50th.	17764	18672	260th.	9313	8732	475th	8381	7258			
55th.	16943	17583	265th.	9279	9712	480th.	8377	7231			
60th.	15648	16387	270th.	9268	8651	485th	8364	7203			
65th.	14798	15692	275th.	9244	8733	490th.	8359	7188			
70th.	13564	15283	280th.	9191	8720	495th	8338	7158			
75th.	13222	14785	285th.	9164	8588	500th.	8310	7149			
80th.	12890	13694	290th.	9142	8551	505th	8289	7114			
85th.	12475	13494	295th.	9133	8549	510th.	8231	6996			
90th.	12167	13219	300th.	9121	8539	515th	8000	6977			
95th.	11915	12575	305th	9104	8521	520th.	7885	6953			
100th.	11650	12435	310th.	8887	8509	525th	7633	6938			
105th.	11331	11985	315th	8859	8859	530th.	7700	6929			
110th.	11198	11761	320th.	8846	8486	535th	7486	6918			
115th.	11111	11239	325th	8835	8459	540th.	7402	6899			
120th.	11100	10841	330th.	8817	8411	545th	7362	6881			
125th	10874	10269	335th	8801	8291	550th.	7124	6869			

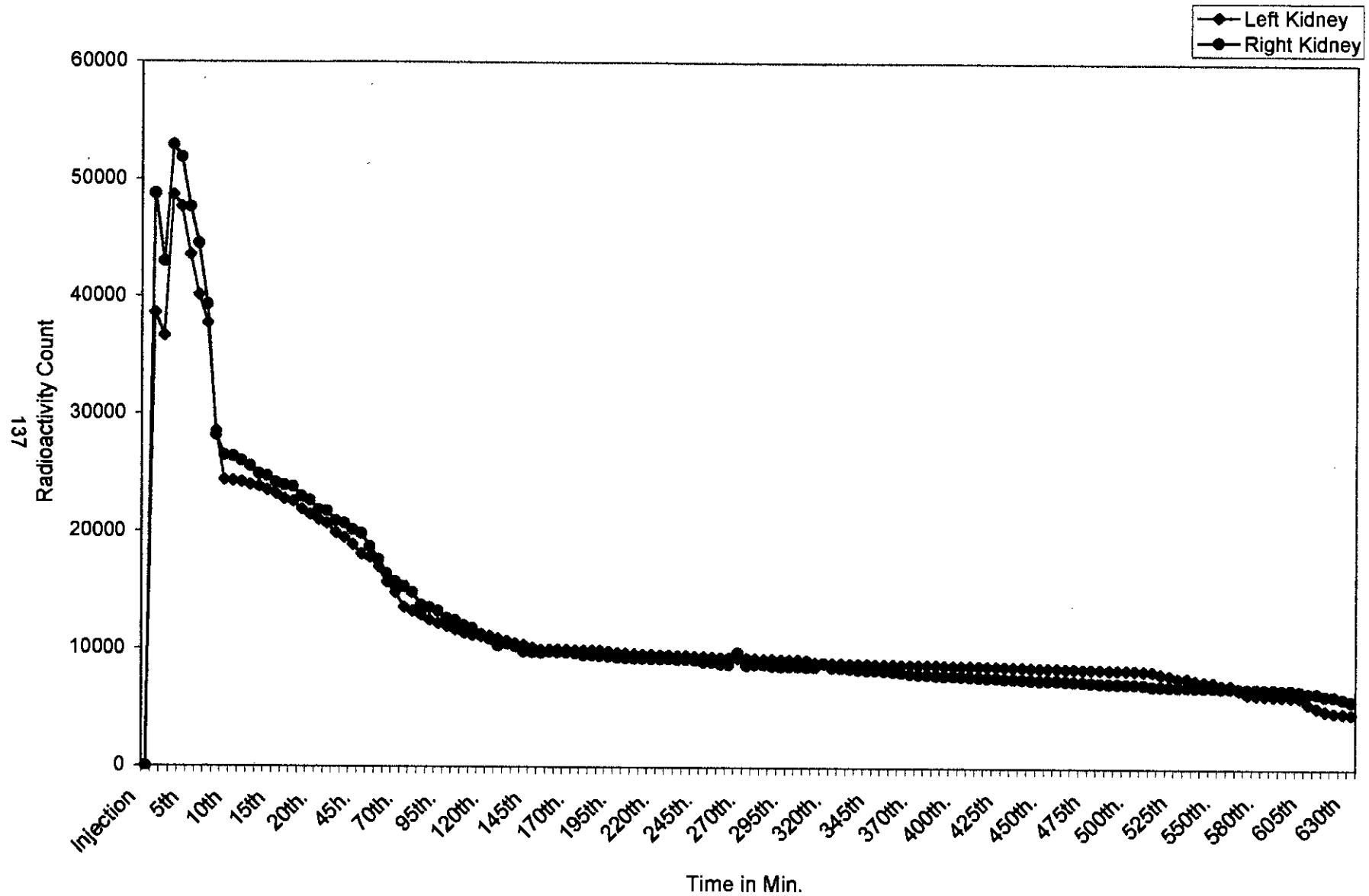


Figure :4.7 Comparative Phramacokinetic Study of Tc-99m DTPA in Left and Right Kidney

Table 4.9 : Pharmacokinetic Study of Tc-99m DTPA in Average in Both Kidney

Time in Min.	Average	Time in Min.	Average	Time in Min.	Average	Time in Min.	Average
<i>Injection given</i>	0	<i>130th.</i>	10579	<i>340th</i>	8535.5	<i>555th</i>	6977.5
<i>1st</i>	43669.5	<i>135th</i>	10348.5	<i>345th</i>	8516.5	<i>560th.</i>	6775.5
<i>2nd</i>	39808.5	<i>140th.</i>	10045.5	<i>350th.</i>	8495.5	<i>565th</i>	6567
<i>3rd</i>	50766.5	<i>145th</i>	9918	<i>355th</i>	8458.5	<i>570th.</i>	6540
<i>4th</i>	49763.5	<i>150th.</i>	9816.5	<i>360th.</i>	8432.5	<i>580th.</i>	6507
<i>5th</i>	45576	<i>155th.</i>	9865.5	<i>365th</i>	8357.5	<i>585th</i>	6467
<i>6th</i>	42330.5	<i>160th.</i>	9843	<i>370th.</i>	8341	<i>590th.</i>	6442
<i>7th</i>	38510.5	<i>165th.</i>	9816	<i>380th.</i>	8305	<i>595th</i>	6420.5
<i>8th.</i>	28322.5	<i>170th.</i>	9769.5	<i>385th</i>	8285	<i>600th.</i>	6349
<i>9th</i>	25383.5	<i>175th.</i>	9687.5	<i>390th.</i>	8259.5	<i>605th</i>	6010.5
<i>10th</i>	25311.5	<i>180th.</i>	9678	<i>395th</i>	8227.5	<i>610th.</i>	5829.5
<i>11th</i>	25091	<i>185th</i>	9653	<i>400th.</i>	8201.5	<i>615th</i>	5600.5
<i>12th.</i>	24713.5	<i>190th.</i>	9609	<i>405th</i>	8186	<i>620th.</i>	5507
<i>13th</i>	24313.5	<i>195th.</i>	9490	<i>410th.</i>	8151	<i>625th</i>	5375
<i>14th.</i>	24076.5	<i>200th.</i>	9441	<i>415th</i>	8129.5	<i>630th</i>	5224.5
<i>15th</i>	23645	<i>205th.</i>	9405.5	<i>420th.</i>	8113.5		
<i>16th.</i>	23319	<i>210th.</i>	9380	<i>425th</i>	8082		
<i>17th</i>	23137.5	<i>215th.</i>	9370.5	<i>430th.</i>	8062		
<i>18th.</i>	22389	<i>220th.</i>	9348	<i>435th</i>	8034.5		
<i>19th</i>	22007	<i>225th.</i>	9334	<i>440th.</i>	8006.5		
<i>20th.</i>	21377.5	<i>230th.</i>	9315.5	<i>445th</i>	7969.5		
<i>25th.</i>	21166	<i>235th.</i>	9294.5	<i>450th.</i>	7954		
<i>30th.</i>	20364	<i>240th.</i>	9248	<i>455th</i>	7944		
<i>35th.</i>	20046.5	<i>245th.</i>	9162.5	<i>460th.</i>	7913.5		
<i>40th</i>	19479.5	<i>250th.</i>	9141.5	<i>465th</i>	7887		
<i>45h.</i>	18919.5	<i>255th.</i>	9047	<i>470th.</i>	7858.5		
<i>50th.</i>	18218	<i>260th.</i>	9022.5	<i>475th</i>	7819.5		
<i>55th.</i>	17263	<i>265th.</i>	9495.5	<i>480th.</i>	7804		
<i>60th.</i>	16017.5	<i>270th.</i>	8959.5	<i>485th</i>	7783.5		
<i>65th.</i>	15245	<i>275th.</i>	8988.5	<i>490th.</i>	7773.5		
<i>70th.</i>	14423.5	<i>280th.</i>	8955.5	<i>495th</i>	7748		
<i>75th.</i>	14003.5	<i>285th.</i>	8876	<i>500th.</i>	7729.5		
<i>80th.</i>	13292	<i>290th.</i>	8846.5	<i>505th</i>	7701.5		
<i>85th.</i>	12984.5	<i>295th.</i>	8841	<i>510th.</i>	7613.5		
<i>90th.</i>	12693	<i>300th.</i>	8830	<i>515th</i>	7488.5		
<i>95th.</i>	12245	<i>305th</i>	8812.5	<i>520th.</i>	7419		
<i>100th.</i>	12042.5	<i>310th.</i>	8698	<i>525th</i>	7285.5		
<i>105th.</i>	11658	<i>315th</i>	8859	<i>530th.</i>	7314.5		
<i>110th.</i>	11479.5	<i>320th.</i>	8666	<i>535th</i>	7202		
<i>115th.</i>	11175	<i>325th</i>	8647	<i>540th.</i>	7150.5		
<i>120th.</i>	10970.5	<i>330th.</i>	8614	<i>545th</i>	7121.5		
<i>125th</i>	10571.5	<i>335th</i>	8546	<i>550th.</i>	6996.5		

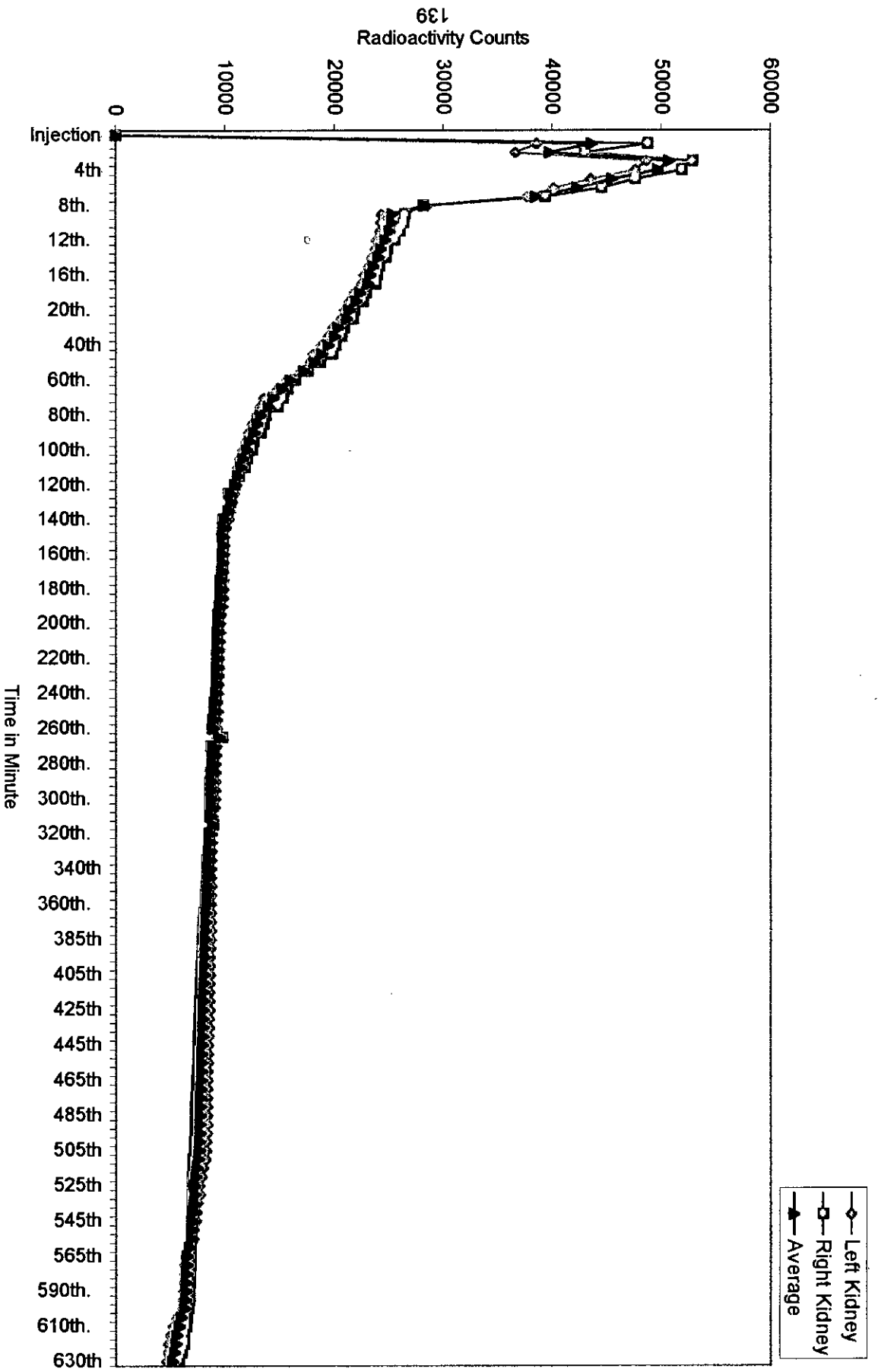


Figure :4.8 Pharamacokinetic Study of Tc 99m-DTPA in Average in Both Kidneys

4.3 Results of Target Organ of Liver

Biodistribution of ^{99m}Tc-Tin Colloid Within Different Organs

The detailed results of biodistribution of the ^{99m}Tc-Tin colloid in different organs are presented in table: 4.10. The biodistribution was highest in liver, followed by other tissues of the body. In liver of twenty patients, the biodistribution ranged between 46.06% to 70.22%, the average value being 62.58%. In other tissue of there remaining body it varied from 10.80% to 39.12%, the average being 20.82%. Most of the radiopharmaceutical remained concentrated in the liver, which indicates the high affinity of the radiopharmaceutical to the organ. The radiopharmaceutical is distributed within the spleen ranging from 5.57% to 8.36% and the average being 7.015%. The lowest biodistribution was recorded in the small intestine (SI) which indicated that the radiopharmaceutical has a lower affinity to the small intestine. It is observed from the data that biodistribution of the radiopharmaceutical in different organs did not vary significantly among the twenty patients. These were true incase of biodistribution of radiopharmaceutical for all the organ studied.

Table 4.10: Biodistribution of The Radiopharmaceutical in Different Organs (target organ:liver)

Patient	In Percentage Uptake								
	Kidney	Liver	Spleen	Bone Marrow	ULI	LLI	SI	Bladder	Other Tissue
1	1.86	65.34	6.55	3.17	2.29	0.72	0.65	0.71	18.71
2	2.02	59.35	6.93	3.50	2.28	0.74	0.72	0.69	23.77
3	1.81	66.57	6.95	3.95	2.45	1.05	0.74	0.74	15.74
4	1.77	52.85	6.48	3.42	1.93	0.73	0.69	0.75	31.38
5	1.68	63.60	6.68	3.36	2.06	0.70	0.62	0.67	20.63
6	1.78	58.02	6.13	2.78	1.97	0.65	0.62	0.68	27.37
7	1.77	55.89	6.57	3.70	1.85	0.80	0.63	0.71	28.08
8	2.00	70.02	8.36	4.37	2.35	0.75	0.68	0.67	10.8
9	1.81	64.18	6.68	3.29	1.90	0.72	0.64	0.71	20.07
10	1.62	57.40	7.57	3.36	2.23	0.78	0.73	0.66	25.65
11	1.47	46.06	5.57	3.70	2.03	0.83	0.58	0.64	39.12
12	1.44	62.57	7.06	2.99	2.08	0.70	0.64	0.66	21.86
13	2.13	65.67	6.97	4.34	2.22	0.75	0.63	0.67	16.62
14	1.66	65.12	7.99	3.80	2.11	0.74	0.66	0.67	17.25
15	1.80	62.40	7.63	3.71	2.00	0.74	0.71	0.74	20.27
16	1.58	68.29	7.09	3.09	1.94	0.70	0.64	0.62	16.05
17	1.89	65.45	6.56	3.18	2.29	0.72	0.65	0.72	18.54
18	2.39	70.22	7.50	3.69	2.53	0.90	0.83	0.89	11.05
19	1.65	64.18	8.00	4.39	2.34	0.78	0.67	0.68	17.31
20	1.54	68.42	7.02	2.99	1.98	0.77	0.63	0.61	16.04
Mean	1.7835	62.58	7.0145	3.539	2.1415	0.7635	0.668	0.6945	20.8155

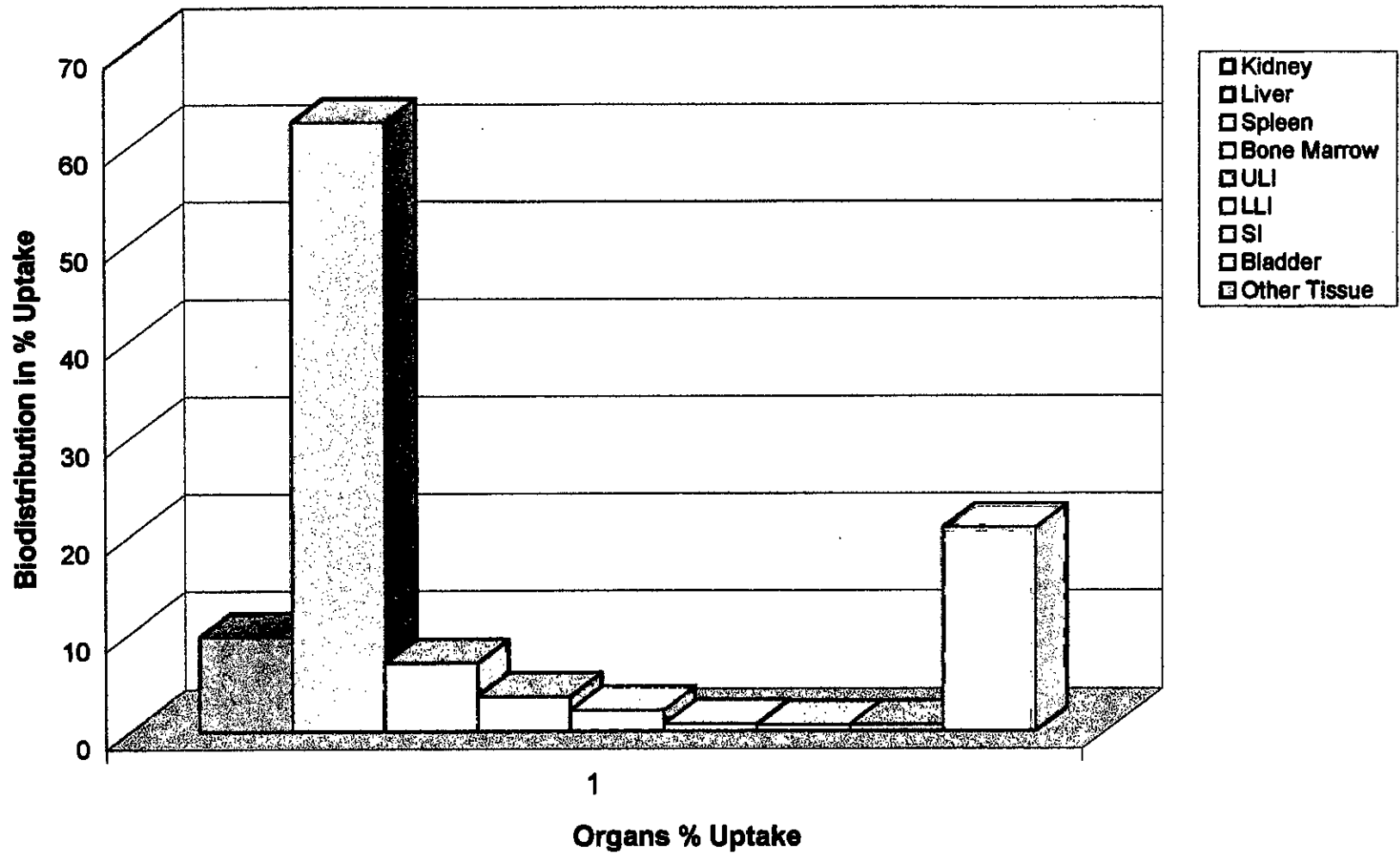


Figure:4.9 Biodistribution of Different Organs (Target Organ : Liver)

Cumulative Activity of ^{99m}Tc-Tin Colloid in Different Organs

The detailed result of cumulative activity of ^{99m}Tc-Tin colloid within the different organ of the twenty patients taking liver as target organ are shown in table 4.11. The highest activity was observed in liver and then comes, the other tissue of the body. The lowest activity was recorded in the small intestine the mean value of which is only 282.6405 μ Ci hr. The mean value of the cumulative activity of the radiopharmaceutical in liver was 26917.28 μ Ci-hr, which ranged from 20157.12 μ Ci-hr to 30335.04 μ Ci-hr. No significant variation among the twenty patients was observed. The cumulative activity of the radiopharmaceutical within liver was much greater in all the twenty patients. The cumulative activity of the ^{99m}Tc-Tin colloid in other tissue lies in between 4665.60 μ Ci-hr to 16899.84 μ Ci-hr and the average being 9239.6405 μ Ci-hr.

Absorbed dose of ^{99m}Tc-Tin Colloid in Different Organs

The absorbed dose of ^{99m}Tc-Tin colloid in different organs of twenty patients is presented in table:4.12. The highest amount of radiopharmaceutical was absorbed in the target organ liver itself followed by other tissue of the body. Lowest absorption was recorded in bladder. This indicated that bladder has lower affinity to the radiopharmaceutical and therefore the radiopharmaceutical concentrates a little within it .In liver the absorbed dose ranged from 0.927 rads to 1.391 rads. The average value was 1.2445 rads. Absorbed dose in different organs of the twenty patients did not vary significantly among themselves.

**Table 4.11: Cumulative Activity of The Radiopharmaceutical in Different Organs
(Target Organ: liver)**

Patient	In $\mu\text{Ci-hrs}$								
	Kidney	Liver	Spleen	Bone Marrow	ULI	LLI	SI	Bladder	Other Tissue
1	803.52	28226.88	2829.60	1369.44	989.28	311.04	280.8	306.72	8082.72
2	872.64	25639.2	2993.76	1512.00	984.96	319.68	298.08	311.04	10268.64
3	781.92	28758.24	3002.4	1706.40	1058.4	453.6	319.68	319.68	6799.68
4	764.64	22831.2	2799.36	1477.44	833.76	315.36	298.08	324.00	13556.16
5	725.76	27475.2	2885.76	1451.52	889.92	302.40	267.84	289.44	8912.16
6	768.96	25064.64	2648.16	1200.96	851.04	280.80	267.84	293.76	11823.84
7	764.64	24144.48	2838.24	1598.40	799.20	345.60	272.16	306.72	12130.56
8	864.00	30248.64	3611.52	1887.84	1015.20	324.00	293.76	289.44	4665.60
9	781.92	27725.76	2885.76	1421.28	820.80	311.04	276.48	306.72	8670.24
10	699.84	24796.8	3270.24	1451.52	963.36	336.96	315.36	285.12	11080.80
11	635.04	20157.12	2406.24	1598.40	876.96	358.56	250.56	276.48	16899.84
12	622.08	27030.24	3049.92	1291.68	898.56	302.40	276.48	285.12	9443.52
13	920.16	28369.44	3011.04	1874.88	959.04	324.00	272.16	289.44	7179.84
14	717.12	28131.84	3451.68	1641.60	911.52	319.68	285.12	289.44	7452.00
15	777.60	26956.8	3296.16	1602.72	864.00	319.68	306.72	319.68	8756.64
16	682.56	29501.28	3062.88	1334.88	838.08	302.40	276.48	267.84	6933.60
17	816.48	28274.40	2833.92	1373.76	989.28	311.04	208.80	311.04	8009.28
18	972.48	30335.04	3240.00	1594.08	1092.96	388.80	358.56	384.48	4773.60
19	749.84	26891.55	2828.36	1441.81	911.35	333.26	271.51	315.02	9867.65
20	821.69	27786.84	2937.28	1490.32	974.23	382.15	256.34	309.74	9486.44
Mean	777.1445	26917.28	2994.114	1516.0465	926.095	332.1225	282.6405	304.046	9239.6405

**Table 4.12: Absorbed Dose of The Radiopharmaceutical in Different Organs
(Target Organ: liver)**

Patient	In per 5mCi of Injected Dose in rads								
	Kidney	Liver	Spleen	Bone Marrow	ULI	LLI	SI	Bladder	Other Tissue
1	3.13E-03	1.289	2.77E-03	1.26E-03	2.57E-03	7.78E-05	5.05E-04	5.21E-05	8.89E-03
2	3.40E-03	1.179	2.93E-03	1.39E-03	2.56E-03	7.99E-05	5.37E-04	5.29E-05	0.011295
3	3.05E-03	1.323	2.94E-03	1.57E-03	2.75E-03	1.13E-04	5.75E-04	5.43E-04	7.48E-03
4	2.98E-03	1.05	2.74E-03	1.36E-03	2.17E-03	7.88E-05	5.36E-04	5.50E-05	0.01491
5	2.83E-03	1.264	2.83E-03	1.34E-03	2.31E-03	7.56E-05	4.82E-04	4.92E-05	9.80E-03
6	2.99E-03	1.153	2.59E-03	1.10E-03	2.21E-03	7.02E-05	4.82E-04	4.99E-05	0.013006
7	2.98E-03	1.111	2.78E-03	1.47E-03	2.08E-03	8.64E-05	4.89E-04	5.21E-05	0.01334
8	3.37E-03	1.391	3.54E-03	1.74E-03	2.64E-03	8.10E-05	5.29E-04	4.92E-05	5.13E-03
9	3.05E-03	1.275	2.83E-03	1.31E-03	2.13E-03	7.78E-05	4.98E-04	5.21E-05	9.54E-03
10	2.73E-03	1.141	3.21E-03	1.34E-03	2.50E-03	8.42E-05	5.68E-04	4.84E-05	0.012188
11	2.48E-03	0.927	2.36E-03	1.47E-03	2.28E-03	8.96E-05	4.51E-04	4.70E-05	0.018589
12	2.43E-03	1.243	2.99E-03	1.19E-03	2.34E-03	7.56E-05	4.97E-04	4.85E-05	0.010387
13	3.58E-03	1.305	2.95E-03	1.72E-03	2.49E-03	8.10E-05	4.90E-04	4.92E-05	7.90E-03
14	2.79E-03	1.294	3.38E-03	1.51E-03	2.37E-03	7.99E-05	5.13E-04	4.92E-05	8.19E-03
15	3.03E-03	1.24	3.23E-03	1.47E-03	2.25E-03	7.99E-05	5.52E-04	5.43E-05	9.63E-03
16	2.66E-03	1.357	3.00E-03	1.23E-03	2.18E-03	7.56E-05	4.98E-04	4.55E-05	7.63E-03
17	3.18E-03	1.3	2.78E-03	1.26E-03	2.57E-03	7.77E-05	3.76E-04	5.29E-05	8.81E-03
18	4.02E-03	1.39	3.18E-03	1.47E-03	2.84E-03	9.72E-05	6.45E-04	5.92E-05	5.25E-03
19	2.54E-03	1.29	2.44E-03	1.55E-03	2.21E-03	8.25E-05	4.71E-04	4.82E-05	0.019546
20	2.73E-03	1.368	2.53E-03	1.49E-03	2.33E-03	7.69E-05	5.19E-04	4.79E-05	0.0174628
Mean	3.00E-03	1.2445	2.90E-03	1.41E-03	2.39E-03	8.20E-05	5.11E-04	7.53E-05	1.09E-02

Radiation Absorbed Dose of ^{99m}Tc-Tin Colloid in Liver

The radiation absorbed dose in the liver of the twenty patients ranged between 0.1909 rads/ mCi to 0.2816 rads/mCi (Table: 4.13), the mean value being 0.2482 rads/mCi. A little variations were observed in radiation absorbed dose in twenty patients but this variation is not highly significant. This sort of variation is observed due to the difference in age group of patients. This would be evident from the Figure: 4.10 and 4.11. The patients were categorized into three different age groups; seven were in the age group of 21-30 years, seven being in the 31-40 years age group and six in the 41-50yrs age group. The radiation absorbed dose is found higher in the patients of lower age group of 31-40 yrs. The lower absorption of radiation dose is observed in the older age group of 41-50 years. The Π-Chart in Figure:4.11 shows a brief comparison in the radiation absorption of radiopharmaceutical between the three different age groups. 37% of patients showed highest radiation absorption who are in the younger group. This was followed by middle aged patient group which is 33% and the older group includes only 30%. This study indicates that the radiation absorption was higher in young age patients who are normally much healthier and stronger.

**Table 4.13 : Radiation Absorbed Dose of The Radiopharmaceutical in Patients
(Target Organ: Liver)**

Patient	In per mCi of Injected Dose in rads	
	Age Group	Absorbed Dose
1	21-30	0.2635
2	31-40	0.2403
3	21-30	0.2683
4	41-50	0.2150
5	31-40	0.2567
6	41-50	0.2351
7	41-50	0.2268
8	21-30	0.2816
9	31-40	0.2589
10	41-50	0.2327
11	41-50	0.1909
12	31-40	0.2526
13	21-30	0.2648
14	21-30	0.2626
15	31-40	0.2521
16	21-30	0.2749
17	21-30	0.2638
18	31-40	0.2415
19	31-40	0.2450
20	41-50	0.2368
Mean		0.2482

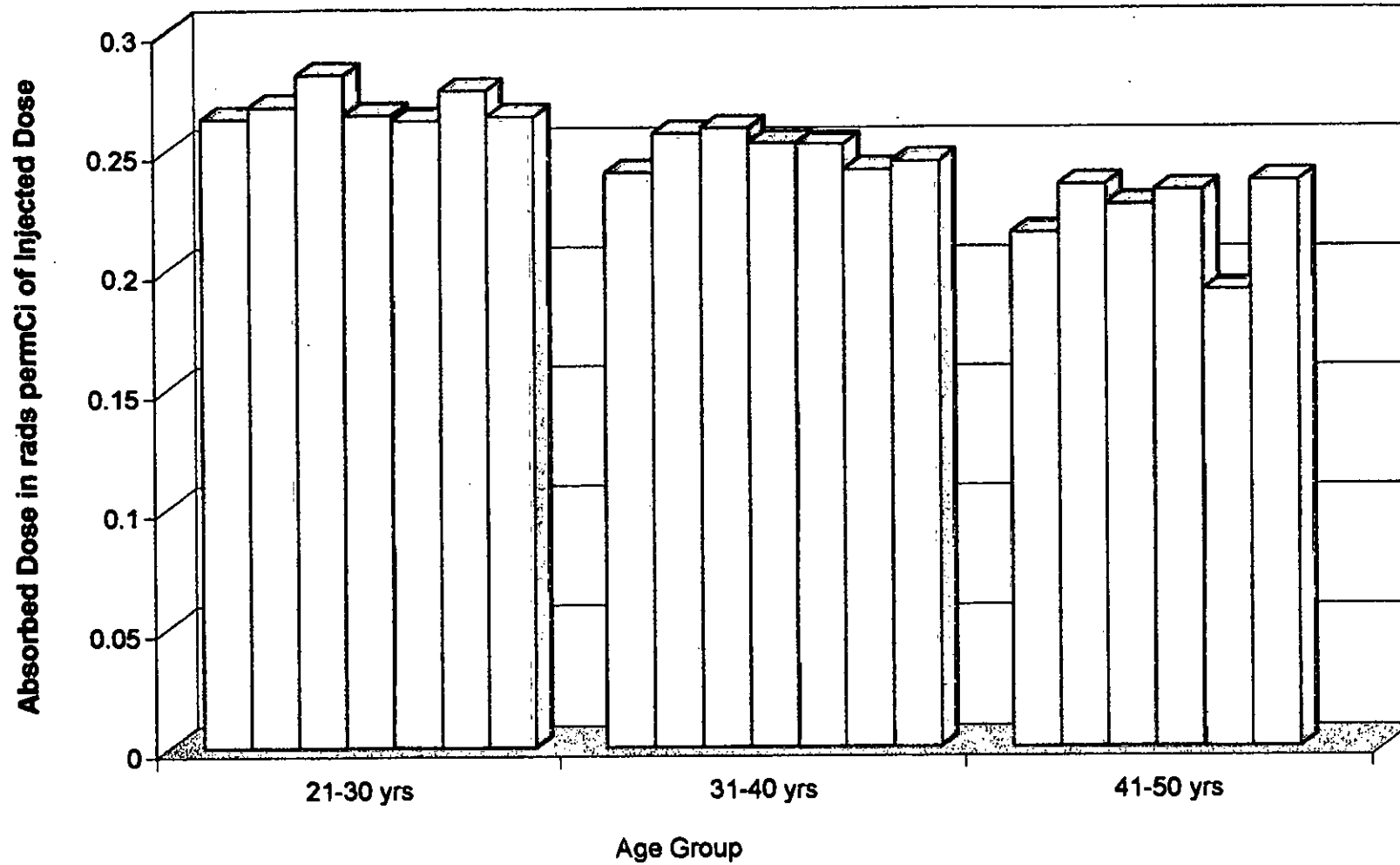


Figure:4.10 Radiation Absorbed Dose in Patient According To Different Age Group As (Target Organ:Liver)

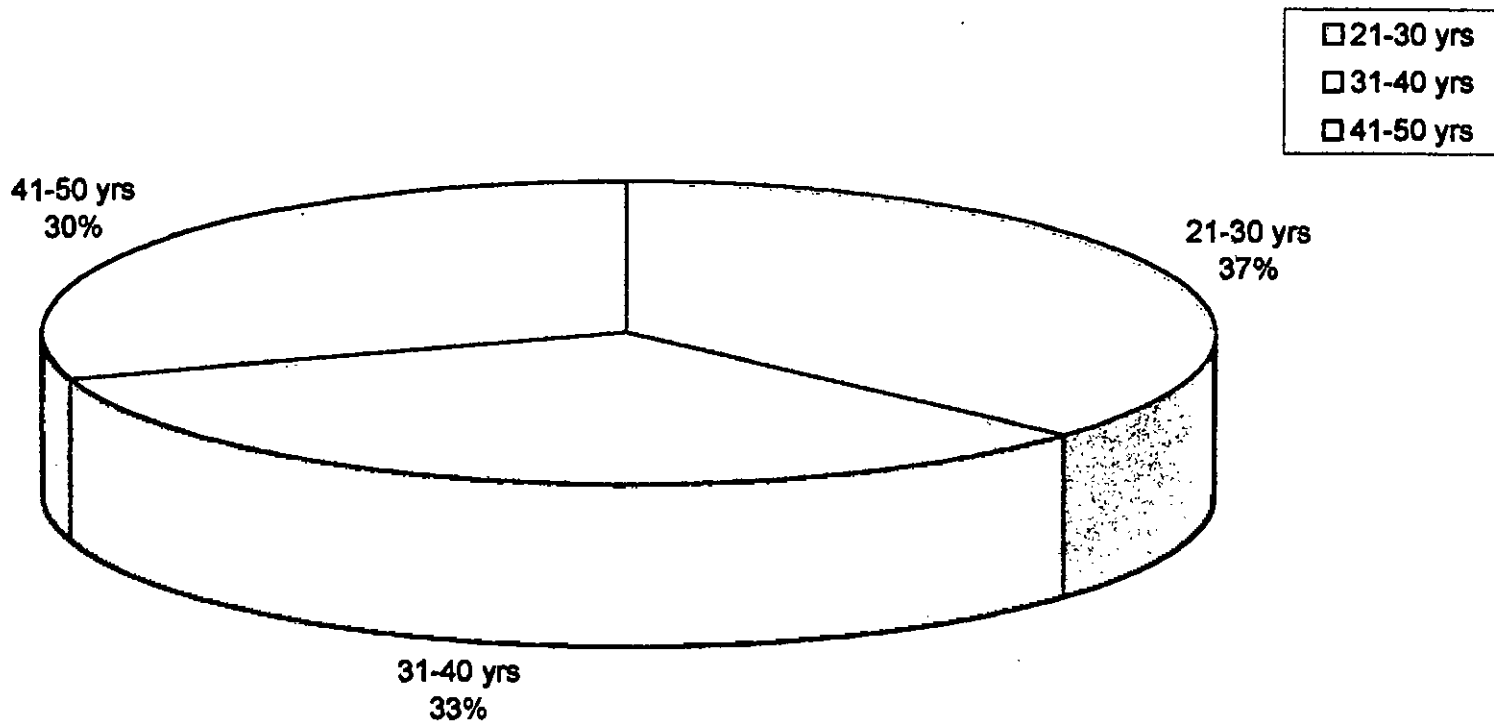


Figure:4.11 Radiation Absorbed Dose in Patients According to Different Age Group(Target Organ: Liver)

Comparison Between Biodistribution of ^{99m}Tc -Tin Colloid and Radiation Dose Absorbed

Figure: 4.12 shows the biodistribution of the radiopharmaceutical and the dose absorption in liver alone due to the injected dose of 5mCi of the radiopharmaceutical. It is evident from the figure that there is similarity in the trend of the distribution and dose absorption by liver. The patient who showed higher distribution of the radiopharmaceutical had a higher amount of radiopharmaceutical dose absorption in the liver. Similar trend was observed in case of lower biodistribution in the patients with lower dose absorption with a minor exception of one or two patients.

Table 4.14 : Radiation Absorbed Dose by Liver Vs Biodistribution of Liver

Patient	In per 5mCi of Injected Dose in rads	In Percentage Uptake
	Dose Absorbed	Biodistribution
1	1.289	65.34
2	1.179	59.35
3	1.323	66.57
4	1.050	52.85
5	1.264	63.60
6	1.153	58.02
7	1.111	55.89
8	1.391	70.02
9	1.275	64.18
10	1.141	57.40
11	0.927	46.06
12	1.243	62.57
13	1.305	65.67
14	1.294	65.12
15	1.240	62.40
16	1.357	68.29
17	1.300	65.45
18	1.390	70.22
19	1.290	64.18
20	1.368	68.42
Mean	1.2445	62.58

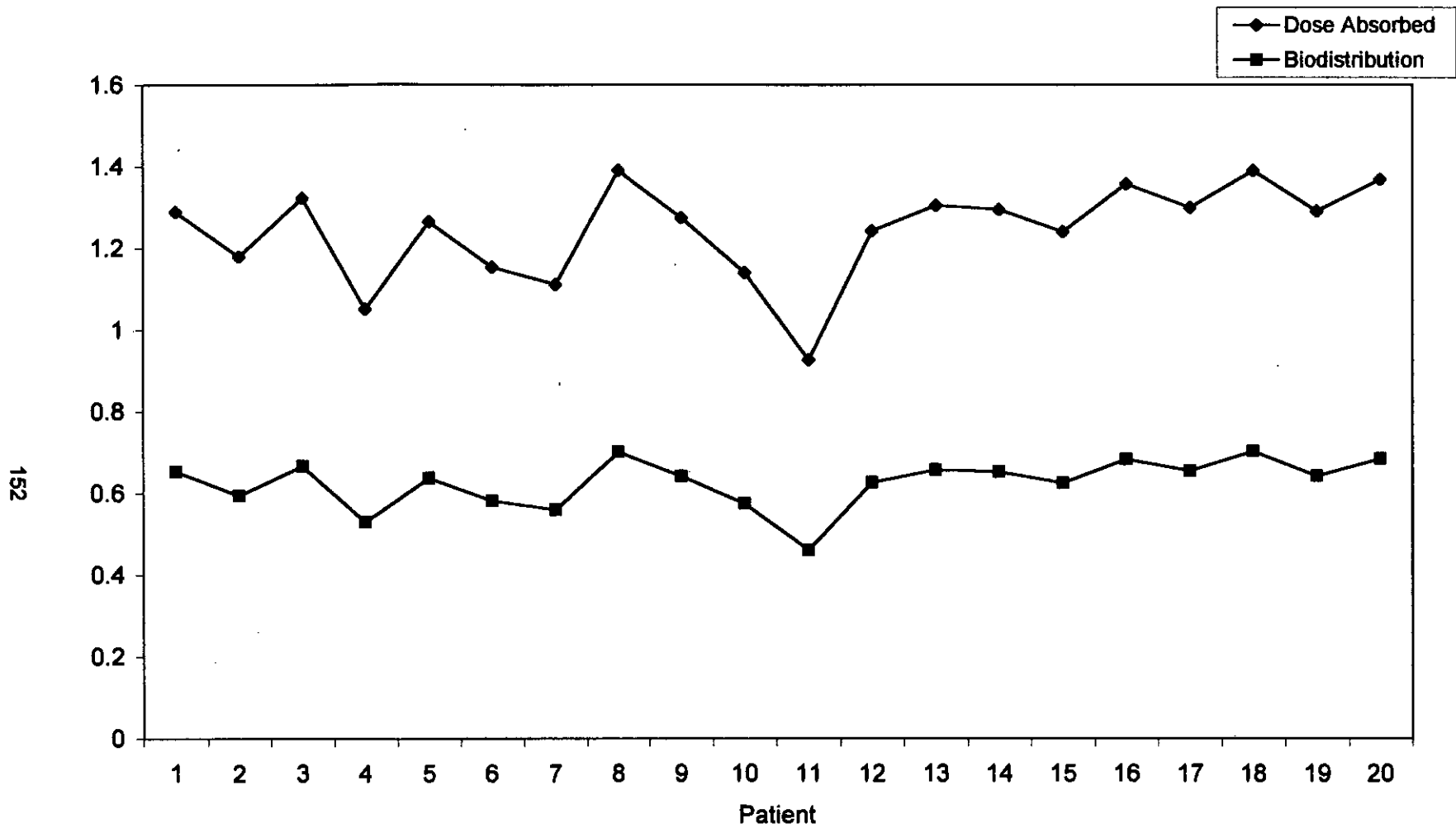


**Figure:4.12 Radiation Dose Absorbed by Liver
Vs
Biodistribution of Radiopharmaceutical
Within The Liver**

4.4 Discussions

^{99m}Tc - DTPA is introduced in individual human bodies to study the renal function in-terms of it's biodistribution and also in-terms of measuring the cumulative activity, the dose absorbed by different organs of the body and also the radiation absorbed dose in the whole body. For interpretation of the clinical findings pharmacokinetics studies were also performed in kidneys of twenty patients of different age group. Data of pharmacokinetic distribution of radiation dose from Tc-99m DTPA were measured in twenty individuals who had undergone diagnostic processes.

The radiation absorbed dose in adults for Tc-99m DTPA was very much within the limit as obtained by other workers ^[1]. In agreement with the result obtained by other investigators, after injection the radiopharmaceutical penetrates the capillary walls entering extra cellular fluid after certain time. The DTPA does not enter cells because of lipid insolubility and negative charge. The plasma decay in-terms of the half-life was recorded at 9,90 and 600 minutes. Similar observation was reported by Datz 1998 ^[91].

Dose estimates for the patients, studied at different times included in this study are in reasonable accord for individual organ doses between different patients. Similar observation was reported by Mardirossian G. et al 1996^[92] while studying radiation absorbed dose from Indium-111-CYT-356.

In the present study the radiation absorbed dose varied within different age groups —the highest being in the younger groups of 21-30 years age. The higher age groups although showed lower total absorbed dose, it was not significantly different from dose recorded by the mid age groups.

^{99m}Tc -Tin Colloid is introduced in individual human bodies to study the liver function in terms of it's biodistribution and also in terms of

measuring the cumulative activity, the dose absorbed by different organs of the body and also the radiation absorbed dose in the whole body. Data of pharmaceutical distribution and radiation dose from ^{99m}Tc -Tin Colloid were measured in twenty individuals who underwent diagnostic processes by introducing the radiopharmaceutical intravenously. Dose estimates for the patient studied at different times included in this study are in reasonable accord for individual organ doses between different patients. Similar observation was reported by O'Connor et al 1996 ^[72].

The radiation absorbed dose in adults for Tc-99m Tin Colloid was very much within the limit as obtained by other workers^[13].

CHAPTER 5

CONCLUSION

CHAPTER 5

Conclusion

The physical aspects of radionuclide distribution within the human body are of great importance. The precise information in distribution of dose decays in close proximity to every cell, is necessary to assess the cellular doses accurately. This also ensures a precise therapeutic perception and reduces access potential risks to patients. The calculation of deposited radiation energy by the internally administered radionuclides is obtained by internal radiation dosimetry. The result helps to observe the radiation effects on an organ. The inhomogeneous distribution of radioactivity within an organ is studied by the bio-distribution calculations, led further uncertainties in dose specification for that organ. The present study tries to determine the absorbed dose of radiopharmaceuticals, ^{99m}Tc -DTPA and ^{99m}Tc -Tin Colloid, which are in common use in the field of nuclear medicine and the distribution of the same in respective organs of the body. There is also an attempt to observe the pharmacokinetic study of ^{99m}Tc -DTPA within kidney. The resultant observation explains the effect of the used radiopharmaceutical in human body and shows that the used radiopharmaceutical leaves the organ under study, giving three half-lives. Though a few works have been done in this spectrum outside Bangladesh that are mentioned the Chapter 2, this study is obviously one of the first work in this field in Bangladesh, especially the method of determining the absorbed dose of radiopharmaceuticals by internal dosimetry. It was thought that, because of the poor socio-economic condition of Bangladesh, the prescribed injected dose might be hazardous to the patient. Observed results provides a chance to compare itself with the traditional and

is in good agreement with the result of other worker. Moreover, the absorbed doses in different organs as obtained in this work are well within the limits prescribed by other reserchers of nuclear medicine society.

In order to further confirmation and evaluation of the obtained results, extensive studies are necessary. For the reason, the research program may be extended to observe effects of injected radiopharmaceuticals that are now in use for brain or bone imaging. The pharmacokinetic study can also be performed on these cases. Moreover the long term deleterious effect of radiopharmaceuticals on human body and also on fetus or environment can be a new era in the field of nuclear medicine in Bangladesh.

CHAPTER 6

References

CHAPTER 6

References

1. **Gopal B, Saha**, "*Physics and Radiobiology of Nuclear Medicine*" Chapter.5 pp.40.Springer-Verlag New York, Inc.1993.
2. **Herman Cember**, "*Introduction to Health Physics*" 2nd Edition-Revised And Enlarged,Pergamon Press Ltd. Oxford,UK. Chapter.7, pp.117, 1980.
3. **Robert Granier and Denis-Jean Gambini**, English Translator **Roy Lisker**, "*Applied Radiation biology and Protection*" Ellis Harwood, England, 1990
4. **Abel. J. Gonzalez**, "*Biological Effects of low Dose of Ionizing Radiation: A Fuller Picture*" Quarterly Journal of the IAEA; Vol:36, Bulletin 4, PP. 37-47 IAEZ 1984.
5. **S. Khalilullah**, "*Radiation Injury and its Management: A Guideline of Physicians*" Appendix of the Medical Preparatory Plan of the TRF; AERE Dhaka Publication, PP.1-5, September 1986.
6. **Alan Martin and Samuel A, Harbison**, "*An Introduction Radiation Protection*" 3rd Edition, Chapman and Hall, London, 1986.
7. **Eric J. Hall** "*Radiobiology for Radiologist*" 3rd Edition, Harper & Row Publisher, Philadelphia, 1992.
8. **K. Sriram**," *Nuclear Measurement Techniques*" Affiliated East West Press Pvt, Ltd, New Delhi, India 1986.
9. **Herman Cember** "*Introduction to Health Physics*" 3rd Edition, Pergamon Press Ltd, UK, 1995.

10. "IAEA-RCA Course on Safety Aspects in the Industrial Application of Radiation Sources, Bombay, December 2-13, 1991: Lecture Notes" Division of Radiobiological Protection, Bhabha Atomic Research Centre, Bombay, India, 1991.
11. **Born. M.** "Atomic physics", 8th Edition, Hafner. Darien Conn. 1970.
12. **Fried Lander, G, Kennedy. J.W. Maclas, E.S., and Miller. J.M.** "Nuclear and Radiochemistry" 2nd Edition, John Wiley & Sons, New York, 1981.
13. **James A. Sorenson and Michael E. Phelps** "Physics of Nuclear Medicine" 2nd Edition Grune & Straton, Inc, Harcourt Brace Jovanovich Publishers. 1987.
14. "Clinical Nuclear Medicine", Edited by **Maisey M.N., Britton K.E., Gilday D.L.**, Chapman and Hall Ltd. 1985.
15. **J.T. Andrews & Jean Milne**, "Nuclear Medicine", John Wiley & Sons. Inc. 1977.
16. "Freeman & Johnson's Clinical Radionuclides Imaging", Edited By: **Leonard M. Freeman**, 3rd Edition, Grune & Straton, Inc, 1984.
17. **Cassen B., Curtis L, Reed C.W. and Libby R.** "Instrumentation for ¹³¹I use in medical" Nucleonics. 9 (2): 46-50, 1951.
18. **Mayneord W. V, Evans H. D, and Newbery S.P.** "An Instrument For The Formation of Visual Images of Ionizing Radiations" J. Sci, Instrum 32:45-50, 1955.
19. **Bender M.A., Blau M.** "Autofluoroscopy: The Use of a Non-scanning Device For Tumor Localization With Radioisotopes (abstract)" J. Nucl. Med. 1. 105, 1960.
20. **Bender M.A., Blau M.**, "The autofluoroscope, in Progress in Nuclear Radioisotope Scanning" Oak Ridge TW, Oak Ridge Institute of Nuclear studies, 1962.

21. **Harper P.V, Lathrop K.A, McCardle R.J, Andros G.,** “ *The Use of ^{99m}Tc As Pertechnetate For Thyroid, Liver and Brain Scanning, in Medical Radioisotope Scanning*”, Vienna, I. A. E.A. 1964.
22. **Eckleman W, Meinken G, Richards P.** “ *The Chemical State of ^{99m}Tc in Biomedical Products, II. The Chelation of Reduced Technetium with DTPA* “. J. Nucl Med.13: 577,1972.
23. **Rollo F.D., Cavalieri R.R., Born M., et at,** “*Comparative evaluation of ^{99m}Tc Glucoheptonate, Pertechnetate and DTPA As Brain Agents*”, Radiology 123: 379,1977.
24. **Taplin G.V., Johnson D.E., Dore E.K., et at:** “ *Suspensions of Radioalbumin Aggregates For Phatoscanning The Liver, Spleen and Lung*”,J. Nucl. Med 5: 259m 1964.
25. **Subramanian G., Mc Afee J.G., Bell E.G., et al** “*Tc-99m, Labeled Polyphosphate As A Skeletal Bone Imaging Agent*”, Radiology 102: 701,1972.
26. **Subramanian G., Mc Afee J.G., Blair R.G., et al,”** *Tc-99m EHDP: A Potential Radiopharmaceutical For Skeletal Imaging*” , J. Nucl Med 12: 947, 1972.
27. **Stern H.S., McAfee J.G., Subramanian G.,** “*Preparation, Distribution And Utilization of Tc-99m, Sulfer Colloid*”, J Nucl Med 7: 665, 1966.
28. **Wistow B.W., Subramanian G., Gogne G.M.** “ *Experimental And Clinical Trials of New Tc-99m Labeled Hepatobiliary Agents*”, Radiology 128:793, 1978.
29. **Medical Science Series; Edited by: Webbs,** “*The Physics of Medical Imaging*” Institute of Physics Publishing, Bristal and Philadelphia, 1998.
30. **B.H. Brown and R. H. Smallwood,** “ *Medical Physics and Physiological Measurements*”, Blackwell Scientific Publications 1981.

31. **Administration of Radioactive Substances Advisory Committee:**
Notes For Guidance On The Administration Of Radioactive Substances To Presents For The Purposes Of Diagnostic , Treatment or Research;
 [London: Department of Health: 1993]
32. **Fisher D.R, M.E Frajier and T.K. Androws (Jr)** “ *Energy Distribution And Relative Biological Effects Of Internal Alfa Emitters* “ *Radiet. Prot. Dosim*, 13 223-7, 1985.
33. **Humm J.L.and Chin L.M.** “ *Cellular dosimetry* “ *Dosimetry of Administered Radionuclides* Edited:S.J. Adelstein (Washington DC. Americal College of Nuclear Physicians) PP-306-30, 1990.
34. **Humm J.L.and Chin L.M.** “ *A Model Of Cell Inactivation By Alfa Particle Internal Emitters*” *Radiate, Res* 134, 143-50,1993.
35. **Bubeck B., W. Brandau, E. Weber, Ernst et al,** “ *Pharmacokinetics Of Technetium-99m- MAG₃ In Human*” *J Nucl Med* 1990; 31: 1285-1293.
36. **Malik Juweid, Robert M. Sharkey, Lawrence C, Swayne, Gary L, Griffiths, Robert Dunn and David M. Golderberg,** “*Pharmacokinetics, Dosimetry and Toxicity of Rhenium-188-Labeled Anti Carcinoembryomic Antigon Monoclonal Antibody, MN-14, in Gastroin-testinal Cancer*”, *J.Nucl Med.* vol 39, No:1, , pp, 34-42 January 1998.
37. **M.Baldwin, S.Zoghbi, Y. Zea-Ponce, Y.Gao, W.Y.Zhang, T.I.Neameyer,I, George Zubal, D.S. Charney,P.B. Hoffer and R.B, Innis,** “*Whole-Body Biodistribution , Radiation absorbed Dose and Brain SPECT Imaging with Iodine-123-β-CIT in Healthy Human Subjects*” , *JNucl Med*, Vol;35, NO:5, pp 764-770,1994.

38. **B.L Holman, R.S Hellmom, S.J.Goldsmith, I.G. Mena, J, Leveille, P.G.Gherardi. J.L. Moretti, A. Bischofpelaloye, T.C.Hill, P.M. Rigo, R.L Vantteertum, P.J,Ell, U. Brell, M.C. De Roo and R.A. Morgan,** “*Biodistribution , Dosimetry and Clinical Evaluation of Technetium-99m Ethyl Cysteinate Dimer in Normal Subject and in Patients With Chronic Cerebral Infarction*”, J.Nucl Med. Vol.30, pp 1018-1024, 1989.
39. **C, Rossetti, G. Vanoli, G. Paganelli, M, Kwiathowshi, F. Zito, F. Colombo,** “*Human Biodistribution, Dosimetry and Clinical Use of Technetium (III)-99m-Q12*”, J.Nucl Med Vol: 35, pp1571-1580, 1994.
40. **Masyuki Nakajo, Hasashi Kobayashi, Kunisada Shimabukura et al,** “*Biodistribution and Invivo Kinetic of Iodine-131 Lipiodal Infused via The Hepatic Artery of Patient With Hepatic Cancer*”, Nucl Med. Vol: 29, No: 6, pp: 1066-1077, June 1988.
41. **C. Mohan Thonoor, Margaret W. Couch, David M. Greer, Kathleen D. Thomas and Clyde M. Williams,** “*Biodistribution and Radiation dosimetry of Radioiodinated-SCH 23982 A Potential Dopamine D-1 Receptor Imaging Agent*”, J Nucl Med Vol, No 10, pp1668-16674, 1988.
42. **F.J. Wackers D. S. Berman, J. Maddahi, D.D, Watson, G.A Better, H.W, Strauss, C.A. Boucher, M. Picard, B.L. Halman et al ,** “*Technetium-99m hexakis 2-Methoxyisobutyl Isonitrile: Human Biodistribution , Dosimetry, Safety and Preliminary Perfusion Imaging* “, J Nucl Med , Vol 30, No. 03, pp 301-311, 1989 .
43. **P.D. Mozley, J.B. Stubbs, K. Plossl, S.Dresel et al.,** “*The Biodistribution and Dosimetry of a Technetium-99m Labeled Tropane for Imaging Dopamine Transporters*”, Scientific Abstract of 45 the Annual Meeting, Toronto, Onterio, 7-11, June 1998.

44. **S. Vallabhajosula, R.E. Zimmerman, M. Picard, P Stritzke, I, Mena, R.S. Hellman, R.S. Tikofsky, M.G. Stabin, R.A. Morgan and S.T. Goldsmith**, "*Technetium-99m ECD: A New Brain Imaging Agent: In Vivo Kinetics and Biodistribution Studies in Normal Human Subject*", J Nucl Med. Vol 30 No 5, pp 599-604, May 1989.
45. **Michael Stabin, Andrew Taylor Jr, Dennis Eshima, and Wesley Wootter**, "*Radiation dosimetry for Technetium-99m-MAG₃, Technetium-99m-DTPA, and Iodine-131-OIH Based on Human Biodistribution Studies*", J Nucl Med Vol 33, No 1, pp 33-40, 1992.
46. **Andrew Taylor Jr. and Dennis Eshima**, "*Effects of Altered Physiologic States On Clearance and Biodistribution of Technetium-99m-MAG₃, Iodine-131 OIH And Iodine-125 Iothalamate*", J Nucl Med Vol 29, No 5, pp 616 to 622, May 1988.
47. **Brian C. Lentle, Janet Williams and David Coupland**, "*Variable in Radiotracer Kinetics and Biodistribution*", J Nucl Med Technology, T19-2 ;94, 1991.
48. **H.M. Deloar, T. Fujiwara, M. Shidalar, T. Nakamura**, "*Internal Dosimetry By TLD Method And Comparison With The Result Of Whole Body PET*", J Nucl Med. Scientific Abstract of 45th Annual Meeting, Toronto, Ontario. June 1998.
49. **Glenn D. Flux, Steve Webb, Robert J. OH, Sarah J. Chittenden and Robert Thomas**, "*Three-Dimensional Dosimetry for Intra Lesional Radionuclide Therapy Using Mathematical Modeling And Multimodality Imaging*", J Nucl Med Vol 38, No 7, pp 1059-1066, 1997.
50. **Terry Smith, Kenneth Evans, Mark F. Lythgoe, Peter J. Anderson and Isky Gordon**, "*Radiation Dosimetry of Technetium-99m-DMSA In Children*", J Nucl Med. Vol 37, pp 1336-1342, 1996 .

51. **S. Murty Guddu, Roger W. Howell And Dandamudi V. Rao,** *"Cellular Dosimetry: Absorbed Fractions for Monoenergetic Electron And Alpha Particle Sources and S-values for Radionuclides Uniformly Distributed in Different Cell"*, J Nucl Med Vol 35, No 2 , pp 303-316, 1994 .
52. **G. Mike Makrigrigos, S. James Adelserin and Amin L Kassis.** *"Limitations of conventional Internal Dosimetry at the Cellular level"*, J Nucl Med Vol 30, No 6 pp 1856-1864, 1998.
53. **Roger W, Howell, S. Murty Goddu and Dhandmudi V. Rao,** *"Design and performance characteristics of an experimental Cesium-137 Irradiator To Simulate Internal Radionuclide Dose Rate Pattern"*, J Nucl Med, Vol 38, No 5, pp 727-730, 1997.
54. **K.S. Kolbert, G. Sgouros, A.M. Scott,** *"Implementation and Evaluation of patient- Specific Three-Dimensional Internal Dosimetry"*, J Nucl Med Vol 38, No 2, pp 301-308, 1997.
55. **Huan B. Giap, Daniel J. Macey and Donald A Podoloff,** *"Development of SPECT-Based Three-Dimensional Treatment Planing System For Radioimmunotherapy"*, J. Nucl Med Vol 36, No 10, pp 1885-1894, 1995.
56. **George Sgrouros, Glenn Barest, Josh Thekkumthala, Chen Chui, Radhe Mohan, Rodney E. Bigler and Pat B. Zanzonico,** *"Treatment Planning for Internal Radionuclide Therapy: Three- Dimensional Dosimetry for Non Uniformly Distributed Radionuclides"*, J Nucl Med , Vol 31, No 11, pp 1884-1891, 1990.
57. **Graham M.M., Peterson L.M., Muzi M. Graham B.B., SPence A.M., Link J.M., Krohn K.A.,** *"1- [Carbon-11]-Glucose Radiation Dosimetry And Distribution In Human Imaging Studies"*, J Nucl Med, Vol 39, No:10, pp 1805-10, October 1998.

58. **John M.H. de Klerk, Erik B. van Dieren, Alfred D. van het Schip, Anne Itoedstra, Bernard A. Zonnenderg, Ait Van Dijk, Derk H. Rutgers, Geert H. Blijham and Peter P van Rijk,** “ *Bone Marrow Absorbed Dose of Rhenium-186-HEDP and the Relationship with Decreased Platelet Counts*” *J. Nucl Med*, Vol 37, No 4, pp 151-159, 1996.
59. **M.K O'Connor, L.K.Kvols, M.L. Brown, J.C. Itung, R.J. Irayostek, D.S Cho and R. J. Vetter,** “ *Dosimetry and Biodistribution of an Iodine-123-Labeled Somatostatin Analog in Patients with Neuroendocrine Tumors*” *J Nucl Med*, Vol 33, No 9, pp 1613-1619, 1992.
60. **John R. Votaw, M. Sib Ansari, N. Scott Mason, Dennis Schmidt, Tomas de Panulis, George Itolburn, Jeff A. Clanton, Delicia B. Gotaw, Ronald G. Manning and Robert M. Kessler,** “ *Dosimetry of Iodine-123 Epidepride: A Dopamine D2 Receptor Ligand*”, *J Nucl Med*, Vol 36, No 7, pp 1316-1321, 1995.
61. **Cheryl M. Culver and Howard J. Dworkin,** “ *Radiation Safety Considerations for Post-Iodine-131- Thyroid Cancer Therapy*”, *J Nucl Med*, Vol 33, No: 7, pp 1402-1992.
62. **Ciaran Nicholl, Ashour Mohammed, William E. Hull, Bernd Bubeck And Michael Eisenhut,** “ *Pharmacokinetics of Iodine-123-IMBA for Melanoma Imaging*” *J. Nucl Med* Vol 38, pp 127-133, 1997.
63. **Bernd Budech, Wolfgang Brandau, Erust Weber, Tilman Kälble, Niranjana Parekh and Peter Georgi,** “ *Pharmacokinetics of Technetium-99m-MAG3 in Human*” *J Nucl Med*, Vol 31, No 18, pp 1285-1293, 1990.
64. **Hans Herzog, Frank Rösch, Gerhard Stöcklin, Christoph Lucders, Syed M. Qaim and Ludwig E. Feinendegen,** “ *Measurement of Pharmacokinetics of Yttrium-86 radiopharmaceuticals With PET and*

Radiation Dose Calculation of Analogous Yttrium-90 Radiotherapeutics
J Nucl Med , Vol 345 No 12, pp 2222-2226,1993.

65. **W. krhwinhel, H, Herog and L,E, Feineddegen,** “ *Pharmacokinetics of Thallium-201 in Normal Individuals After Routine Myocardial Scintigraphy*” T Nucl Med, Vol:29, No: 9, pp 1582-1586,1988.
66. **Richard J. Quinn and Grahame J. Elder,** “*Poor Technetium-99m-DMSA Renal Uptake with Near Normal Technitium-99m-DTPA Uptake Caused by Tubulointerstitial Renal Disease*”, J Nucl Med, Vol 32, pp 3273-2274, 1991
67. **David Groshar , Oscar M. Embom, Aley Frenkel and Dov Front,** “*Renal Function and Technetium-99m- Dimercapsuccinic Acid Uptake in Single Kidneys: The Value of In Vivo SPECT Quantitation*” ,J Nucl Med Vol: 32, NO: 5, PP 766-768,1991.
68. **Paul Shreve, Ping-Chun Chiao, H. David Humes, Markus Schwaiger and Milton D. Gross,** “*Carbon-11-Acetate PET Imaging in renal Disease*” J Nucl Med, Vol 36, No 9, pp 1595-1601,1995.
69. **J.V. Nally Jr., H.S. Clarke Jr., B.K. Gupta, M.L. Gross, L.R. Low, W. J. Potvin, J.P. Windhan, GP Grecos,**” *Captopril Renography in Two Kidney and One Kidney GoldblaH Hypertension in Dogs*” J Nucl Med, Vol 28, No 7, pp 1171-1179. July 1987.
70. **Charles D. Russell, Daniel Young, J.D. Billingsley and Eva V Dubovsky,** “*Technical Procedures for Use Of New Kidney Agent Technetium-99m-MAG₃*” J.Nucl Med Technology, Vol 19, No 3, pp 147-152,1991.
71. **John R, Buscombe, Andrew J.W. Hilson, Margaret L. Hall, Caroline E,Yownsend, Gill Clarke and Peter J. Ell,**“*Dose Three-Dimensional Display of SPECT Data Improve the accuracy of ^{99m}Tc-DMSA Imaging of Kidneys?*” J Nuel Med Technology, Vol 23 No 1, pp 11-17, 1995.

72. **M.K.O'Conner, P. MacMathuna and P.W.N, Keeling,** "Hepatic Arterial and Portal Venous Components of Liver Blood Flow: A Dynamic Scintigraphic Study", *J Nucl Med*, Vol 29, No 04, pp 466-472, 1988.
73. **F. Mut, S. Glickmans D. Marciano, R.A Hawkins,** "Optimum Processing Protocols for Volume Determination Imaging with Technitium-99m-Sulfur Colloid". *J Nucl Med* Vol: 29, No: 11, pp 1768-1775, 1988.
74. **H.D. Fawcett, B.A. Sayle,** "SPECT Versus Planar Scintigraphy: Is SPECT Worth It?" *J Nucl Med*, Vol 30, No 1, pp 57-59, January 1998.
75. **Ken Wintch and Art Meyers,** "Positive Liver SPECT Images Correlated With Normal and Equivocal CT Studies: Two Case Studies", *J Nucl Med*, Vol 22, No 2, pp 65-67 June, 1994.
76. **H. Bauser and W. Rouge,** "The Electret Ionization Chamber: A Dosimeter For Long Term Personnel Monitoring", *Health Physics*, Vol: 34, pp 97-102, 1978.
77. **J.R. Greening,** "Fundamentals of Radiation Dosimetry", 2nd Edition, Medical Physics Handbooks. 15, Institute of Physics Publishing (IOP) Bristol, London, 1992.
78. **Dosimetry in Radiotherapy, Vol-2** "Proceedings of a Symposium, Vienna, 31 August-4 September, 1987", IAEA, Vienna, pp 339-342, 1988.
79. **H.E Johns and J.R, Cunningham,** "The Physics of Radiology", 4th Edition, Charles C. Thomas Publisher USA, 1980.
80. **Alan Martin and Samuel A, Harbison,** "An Introduction to Radiation Protection", 3rd Edition, Chapman and Hall London, 1986.
81. **Donald R. Bernier, Raul E. Chrishtian, James K. Langan, L. David Wells,** "Nuclear Medicine Technology and Techniques", 2nd Edition, The C.V. Mosby Company, 1989.

82. **Kotegov K.V., Paulov O.N., Shredor V.P.**, "*Technetium in Emleus*
H.J., Sharpe A.G. (Eds): *Advances in Inorganic Chemistry and
Radiochemistry*", Vol 12, New York Academic Press, 12: 72, pp 72, 1969.
83. **Peacock R.D.**, "*The Chemistry of Technetium and Rhenium, Topics in
Inorganic and General Chemistry*", Monograph 6, New York, Elsevier,
1966.
84. **MIRD Dose Estimate Report No. 3**, "*Summary of Current Radiation
Dose Estimates To Human With Various Liver Conditions From ^{99m}Tc
Sulfur Colloid*", J Nucl Med, 16:108 A, 1975.
85. **Harper P.V., Beck P., Charleston D, et al**, "*Optimization Of A Scanning
Method Using ^{99m}Tc*", Nucleonics, 22:50, 1964
86. **Stern H.S., McAfee J.G., Subramanian G.**, "*Preparation, Distribution
and Utilization of Technetium-99m Sulfur Colloid*", J Nucl Med, 7: 665, 1966.
87. "*Measurement of Radioactivity in Food and The Environment, A Guide
Book*", Technical reports Series No. 295, IAEA, Vienna, 1989.
88. **Johns H.E. and Cunningham J.R.**, "*The physics of Radiology*", 4th
Edition, Charles C. Thomas Publisher, USA, 1980.
89. **Khalilullah S.**, "*Radiation Injury and it's management: A Guideline for
Physicians*", Appendix of the Medical Preparatory of the TRF: AERE
Dhaka Publication; pp1.5, September 1986.
90. **Horowitz Y.S. (Editor)**, "*Thermoluminescence and Thermoluminescent
Dosimetry*", CRC Press, Inc. Boca Roton, Florida, USA, 1984.
91. **Datz Frederik L.**, "*Handbook of Nuclear Medicine*", 2nd Edition, pp146
Mosby - Year Book, Inc. USA, 1993.
92. **Mardirossian G., Brill A. B., Dwyer K. M., Kahn D. and Nelp W. ,**
"*Radiation Absorbed Dose From Indium-111-CYT-356*", J Nucl Med, 37:
1583-1588, 1996.

CHAPTER 7

Appendix

APPENDIX

SPECIFICATION OF ATOM LOB 100 DOSE CALIBRATOR (MODEL NO.086-250) :

Physical Characteristics

Dimensions	Bench Cabinet	Rack Mounting
Height	7.75 in (19.7 cm)	6.93 in (17.6 cm)
Width	17.12 in (43.5cm)	19.0 in (48.3cm)
Depth	15.75 in (40.0cm)	15.75 in (40.0 cm)
Weight	37 lb (17 kg)	
Temperature Range	+ 10 to 45 ⁰ C	

Constituent Assemblis

Power Supply	Type 1083A
H.V. & Input	Type 5175A
Analyser/Ratemeter	Type 1080A
Scaler/Timer	Type 1082A

Electrical Supply

Mains Input Supply Voltage	100-125V, 2000V ac, 50-60Hz
Fuse (rear panel)	1A
<i>Internal (Power Supply 1083A) Supplies</i>	+ 24V, 600mA
	- 24V, 600mA
	+ 5V, 4A
Fuses (rear panel)	+ 5V line: 5A
Overload Protection	Automatic current trip

High Voltage Output

Range	< 100V to 2kV Standard, Different ranges up to 4k V by internal links.
Polarity	Positive
Current	150 μ A max. at 4kV. 0. 5mA at 2kV.
Regulation	100mV typical, 0-200 μ A.
Temperature stability	0.01% per °C typical
Mains stability	0.003% per 1% mains variation
Ripple	25mV typical
Control	Output continuously variable over specified range: 10-turn Helipot with lockable dial, ON/OFF switch.
Resetting Accuracy	$\pm 1V$
Indication	Meter display, calibrated in volts. Display accuracy: $\pm 3%$ of full scale
<i>Input (Sockets on rear panel)</i>	
S.C.	Carries H.V. to scintillation probe and input signal to amplifier.
G.M.	Carries H.V. to Geiger-Muller probe and input signal to 100 mV trigger circuit.
DIRECT	Direct input to amplifier (as for S.C. but without H.V.)
HEAD AMP.	Carries $\pm 24V$, 100mA Supply to head unit and quench probe input.

Pin Allocation

A	Gate -1) Input Control (OV inhibits internal
B	Gate-2) to Scaler (OV inhibits external
C	OV (E)
D	$\pm 24V$
E	-24V
F	0-10V Analogue Output from 4.7kQ impedance
G	Quench probe input

Scaler Input

NIMS compatible input to Scaler i.e. Positive >2.5V pulses. Maximum rate 1MHz.

Outputs

<i>In Channel</i>	Positive pulse for each detected pulse occurring between the upper and lower threshold i.e. amplitude within the selected channel. Also G.M. & TEST.
<i>Over Channel</i>	Positive pulse for each detected pulse occurring above the upper threshold i.e. amplitude greater than the selected channel.
<i>Amplifier</i>	
Input Impedance	250pF charge collection capacity in parallel with 0.5 MQ.
Sensitivity	Variable: linear control with 15: 1 range, Switch provides for energy selection over 150: 1 range. Maximum sensitivity 4.3mV or 1.075×10^{-12} Coulombs.
Input Polarity	Normally negative going input (internal link adjustment provides for positive going input).
Shaping	Double differentiation, single integration 1 μ s equal time constants.
Gain Stability	0.05% per $^{\circ}$ C
Linearity	1%

Note: The energy calibration is referred to input pulse height; non-linearity in the detector output will be reflected in the energy readings.

Analyser (Pulse Amplitude Discriminator)

Mode	Differential or Integral operation
Channel Centre	1.5V fixed
Temperature Stability	100 μ V per $^{\circ}$ C
Channel Width (Total Width)	Switched: 2,5,10,20,30,&60% relative to channel centre (INT). position of switch provides analyser threshold at 1.5V.
Channel Width Stability	0.05% per $^{\circ}$ C
Output	Outputs to scaler and ratemeter

**LINEAR
RATEMETER**

Ranges
Back Bias

40,100,400,1000,4000,10,000 c.p.s
Meter and Recorder outputs of up
to full scale on all ranges can be backed-
off to zero.

Scale Expansion

Continuously variable control provides
up to 10: 1 expansion of meter and
recorder outputs.

Accuracy of
Indication
Stability
Recorder Output

± 3%

± 0.1% per °C (non-expanded output.
Alternative outputs selected by rear
panel switch.

Galvonometric recorder: 1mA from 10V
source- impedance variable from 5KΩ to
15 KΩ by rear panel control.

Potentiometric Recordeers: 100mV from
100Ω source-Contro provies 67mV to
200mV output.

**DIGITAL RATE
METER**

Sample times:

1,3,6,10,30,100,300,10³,3x10³,10⁴ s.

SCALER

Decades
Count Stop

6: (1,2,4,8 BCD counter)
OFF, 100, 400, 10³, 4x10³-----10⁶
counts.

TIMER
Decades
Time Stop
Time Source

6: (1,2,4,8 BCD counter)
OFF, 10, 30, 60, 300, 10³, 3x10³---10⁵s
10Hz clock obtained by dividing down a
1MHz crystal controlled oscillator.
(100 Hz on Digital Ratemeter)

PRINT OUT FACILITIES

Optional plug-in print out boards available as follows:

Addo-x Print Out	Type 5153A
ASR 33 Print Out	Type 5160A
Keinzle D4 & D44 Print Out	Type 5151A

The Detailed Specification of SPECT Patient Handling System with Carbon Fibre Pallet:

Orbiting Motion

Rotating mechanics provides 455° of circular orbit at radius of rotation from 7 to 32 cm (2075 to 1205 inches). Step-and-shoot operation under computer control. Start angle, angle of rotation, direction of rotation and time-per-view selectable.

Patient –Positioning Table

The table accepts a range of interchangeable low-attenuation pallets with resilient pads. The central longitudinal axis of the pallet is aligned transversely to the rotational axis of the detector. Longitudinal adjustment is approximately 30 inches(76 cm). Pallet height is electromechanically adjustable from approximately 34.0 to 44.0 inches (86.4 to 111.8 cm) from floor to top of pallet. table can also be used in in conventional nuclear medicine procedures or moved away from the detector stand.

Net Weight

Approximately 474 lbs(215 kg),less pallet

Environmental requirements

Refer to the environmental requirements specified in the operation instructions for the ORBITER Detector Stand .

Power Requirements

Receives all power from the detector stand.

The Detailed Specification of DOT with Digitrac® :

Persistence

Display

Digitally emulated persistence display of acquired image with selectable growth and decay rates in a format 128x128 bits by 8 bits deep. Analyzer spectrum and optional ECG waveform also displayed in this mode.

Study Start

Start delay selectable from 0 to 999 seconds in steps of one-second

Stop Control

increments, or when count rate threshold selectable from 0 to 999,000 counts per second in 1000-count increments is crossed. Preset count termination selectable in one-count increments from 1 to 9,999,999 accumulated counts. Preset time termination selectable in 0.001-second increments from 0.001 to 999.999 seconds. Preset information density (ID) termination selectable in one-count increments from 1 to 9,999 counts per square centimeters; user selectable size and position of the ID region of interest. Number of sequential or dynamic frames acquired selectable in one-frame increments from 2 to 99 frames.

Count/Time

readout

Annotation of count accumulation in each two scalers to a maximum of 9,999,999 counts in one-count increments. Annotation of elapsed clock time to a

maximum of 999,999 seconds in 0.001-second increments.

Analyzers

Three independent analyzers, each with photopeak energy range selectable from 50 to 510 keV and window width selectable from 0 to 99% of its selected selectable energy. Parameters entered through preset isotope selections or manually.

Off-peak imaging achieved by directly entering the shift as a percentage of the photopeak energy level.

The high count-rate mode can be automatically enabled at a selectable system deadtime from 0 to 63.75% in 0.25% increments, with display of actual system deadtime.

Multichannel spectrum display with analyzer window positions and widths; display updated approximately every 2,048 detected events in enabled window channel. Display of system deadtime and analyzer photopeak correction.

Protocols

Up to 16 sets of definable parameters from standard and optional control pages (except DIGITRAC control pages) can be saved, and subsequently entered into the system by selecting the protocol.

Free Text And

Patient/Study

Data Annotation

Information can be entered as a free text using the keyboard, in the desired position relative to the acquired

clinical images; maximum capacity is 24 lines at 32 character spaces per line. This can be exposed on imager film either with or without the acquired image. Patient/study data of 11 parameters can be entered using the keyboard, and exposed on imager film as a "header" along the top and bottom edges of the film.

Dimensions And

Weight

Overall dimensions of terminal and keyboard: 14.5 inches (37cm) high, 18.5 inches (47cm) wide, and 19.5 inches (50cm) deep; 28.25 inches (72cm) deep with keyboard positioned against terminal. Net weight approximately 75 lbs (34 kgs), less optional cart.

Environmental

requirements

Normal operation requires an ambient temperature range of +50° to +80°F(+10° to +26.7°C), with a relative humidity between 20% and 80% noncondensing. The ventilation openings along the sides and rear of the terminal must not be obstructed. Refer to the operation manual received with the detector stand for additional temperature restrictions required for the detector.

Maintain a relative humidity of approximately 40% in the room whenever possible. This is particularly important in winter months when buildings are heated, since heating dries the air and reduces the humidity

significantly. Carpeting is not recommended because it compounds the problems with static electricity, which may interfere, with system functioning. If the equipment site must be carpeted, select a carpet with good anti-static characteristics, clearly specifying an extremely low residual static electricity level. Anti-static carpeting containing carbonized filaments to prevent static buildup is commercially available. Carpeting that is not anti-static must be treated with one of the commercially available anti-static fluids. these fluids are usually sprayed onto the carpet and re-application at periodic intervals to maintain a static-free environment. It should be noted , however, that spraying may not be sufficient to control static electricity at all times.

Power

Requirements

power required is approximately 1725 watts, which is obtained from the detector stand.

The Detailed Specification of ECAM Gamma Camera which is the latest version of "ORBITER" Gamma Camera:

<p style="text-align: center;"><u>System Configurations</u></p> <p>The Open ICON™ G3 Workstation is a powerful nuclear medicine computer available for E.CAM® and ICON P Configurations.</p> <p>A complete Open ICON Workstation With Power PC™ consists of:</p> <ul style="list-style-type: none"> • Power Macintosh® G3• 51 cm (20 inch) color monitor • Keyboard and mouse <p><i>Specification</i></p> <ul style="list-style-type: none"> • Power Macintosh G3/300 - Computer manufacture: Apple Computer, Inc. - Central microprocessor: Power PC 750 - Central microprocessor features: - Manufacturer: IBM/Motorola - Instruction set class: RISC - Clock rate: 300 MHz - 1 m Byte L2" backside" cache 150MHz dedicated 64-bit backside bus 	<ul style="list-style-type: none"> -System bus speed: 66MHz -Performance: -Integer: 13.2 SPEC int 95 - Floating point: 8.5 SPEC fp 95 - Main memory (Ram): 128 MB - internal storage devices (standard): - 4 GB disk drive - Built-in 24xspeed CD-ROM disk drive - Built-in Ethernet connection - 1.4 MB, 3.5 inch floppy disk drive - SCSI controller (supports up to six optional external storage options) - Three PCI slots • Precision high-resolution color display - 20-inch color View Sonic® monitor - Flicker-free, non-interlaced - 1152×870 pixel resolution • Keyboard and mouse - Alphanumeric keys - Numeric keypad - Function keys - Ergonomically designed mouse.
---	---

Technical Data

Physical Environmental and Power Data 51 cm (20 inch) Color Monitor

Picture tube	51 cm (20 in.)diagonal	keyboard	
	high contrast antiglare		
Resolution	(horizontal) 1,152 pixel	Height	4.1 cm (1.6in.)
	x (vertical) 870 pixels		
Input signals	red, green, blue, HD,VD	Width	47.5cm (18.7in)
Horizontal scan rate	68.7 kHz	Depth	19.5cm (7.7 in)
Vertical refresh	75 Hz	Weight	1.8kg (4.0lb.)
Vertical scanning	non-interlaced method	Mouse	
Controls front side	Power switch	Height	3.3cm (1.3 in.)
	(automatic degauss)	Width	6.1 cm (2.4 in)
	recall button control	Depth	10.7 cm (4.2 in.)
	button brightness	Weight	0.1 kg (4.0z)
	contrast horizontal and vertical size rotation	Power	
	horizontal and vertical convergence	MacintoshG3/	38.6cm (15.2in)
	color temperature	300	24.3cm (9.6in)
		Height	45.2 cm (17.8in)
		Width	15.00 kg (33.1lb.)
		Depth	100v-240V AC.
		Weight	50-60Hz single
		Power	phase
		Requirements	8 amps.
Tilt range	-5 ⁰ to +15 ⁰	<u>Environmental Requirements</u>	
Swivel range	± 90 ⁰	Normal operation requires an ambient temperature range of 10 ⁰ to 40 ⁰ C (50 ⁰ to 104 ⁰ F) with relative humidity not to exceed 80% non-condensing.	
Height	50.4cm (19.8 in.)		
Width	50.0cm (19.7 in)		
Depth	49.2 cm (19.4 in)		
Weight	26.5 kg (58.3 lb.)		

Technical Data

<i>System Description</i>	<i>System Configurations</i>
<p>ECAM™ systems are offered in four configurations to meet the specific clinical and productivity requirements of any nuclear medicine™ family of gamma cameras offers optimized imaging capabilities at all energies. The proprietary, energy-independent HD³ digital detectors deliver consistent high performance for single-isotope, dual-isotope and multi-peak-isotopes. The patient bed features significant comfort improvements and a 2.5 mm (0.1 in.) thick imaging pallet. The result is superb image quality for all emission tomography-whole body and general imaging procedures.</p>	<p><i>E. CAM Single-Head System:</i> The E.CAM Single-Head System utilizes an open gantry with caudal/cephalic detector tilt capability. The BICORE™ rapid insert collimator system includes optimized collimators for the entire energy range up to 511 keV. The system offers general purpose flexibility with unrestricted access for gurneys and wheelchairs and has the smallest footprint.</p> <p><i>E. CAM Dual-Head 180° System:</i> The E.CAM Dual-Head 180° System is optimized for both whole body and SPECT scanning with the detectors in opposing, making it the ideal system for ontological applications. The open gantry permits easy access to both detectors for imaging of patients on stretchers or in sitting or standing positions.</p> <p><i>E. CAM Dual-Head Variable-Angle System:</i> The E.CAM Dual-Head Variable-Angle System allows for 180° and 76°_(W.I.P) detector positions to optimize system sensitivity and throughput for very acquisition type. The system's full range of motion presents unsurpassed flexibility in patient positioning, including cauda/cephalic tilt, wheelchair tilt, wheelchair, and sitting and standing patient studies.</p> <p><i>E. CAM + Dual-Head Coincidence system:</i> The E.CAM +Dual-Head Coincidence System enables dual-head variable-angle and fixed 180° systems to perform whole body positron imaging. The system features Siemens propriatals and coincidence electronics and software.</p>

Technical Data

HD3 High-Definition Digital Detector NEMA Specification

Performance Standards

Intrinsic Spatial Resolution

FWHM in CFOV $\leq 3.8\text{mm}$

FWHM in CFOV $\leq 3.9\text{mm}$

FWHM in CFOV $\leq 7.5\text{mm}$

FWHM in CFOV $\leq 7.7\text{mm}$

Intrinsic Spatial Linearity

differential in CFOV $\leq 0.2\text{mm}$

differential in CFOV $\leq 0.2\text{mm}$

absolute in CFOV $\leq 0.4\text{mm}$

absolute in CFOV $\leq 0.7\text{mm}$

Intrinsic Energy Resolution (typical)

FWHM in UFOV $\leq 0.9.9\%$

Intrinsic Flood Field Uniformity uncorrected

differential in CFOV $\leq 2.5\%$

differential in CFOV $\leq 2.7\%$

integral in CFOV $\leq 2.9\%$

integral in UFOV $\leq 3.7\%$

Multiple Window Spatial

Registration $\leq 0.6\text{mm}$

Class Standards

Intrinsic Count Rate Performance in Air

Maximum count rate $\geq 240\text{kcps}$

20% count rate loss at $\geq 190\text{kcps}$

Intrinsic Spatial Resolution @ 75 kcps

FWHM in UFOV $\leq 4.1\text{mm}$

FWHM in UFOV $\leq 7.8\text{mm}$

Intrinsic Flood Field Uniformity @ 75 kcps

differential in CFOV $\leq 2.5\%$

differential in CFOV $\leq 2.7\%$

integral in CFOV $\leq 2.9\%$

integral in UFOV $\leq 3.7\%$

System Spatial Resolution without Scatter with LEHR Collimator

FWHM in CFOV $\leq 7.4\text{mm}$

FWHM in CFOV $\leq 14.1\text{mm}$

System Spatial Resolution without Scatter with LEHR Collimator

FWHM in CFOV $\leq 8.3\text{mm}$

FWHM in CFOV $\leq 15.5\text{mm}$

System Planar Sensitivity with LEHR Collimator

absolute $202\text{cpm}/\mu\text{Ci}$

SPECT Class Standards

Reconstructed Spatial Resolution with Scatter Using LEHR Collimator

center $\leq 9.5\text{mm}$

radial $\leq 10.00\text{mm}$

tangential $\leq 7.5\text{mm}$

HD3 High-Definition Digital Detector Physical Specifications

Field-of-view (FOV) 53.3×38.7cm(21×15.25 in)
Diagonal FOV 63.5cm(25 in)

Crystal

Size 59.1×44.5cm(23×17.4 in)
Diagonal 69.2 cm (27 in)
Thickness 0.95cm(0.37 in)

Photomultiplier Tubes

Total Number 59
Diameter 53-7.6cm(3in)6-5.1cm(2 in)
Type bialkali high efficiency box type
Array dynodes
hexagonal

Shielding

Back 9.5mm(0.375 in)
Sides 12.7mm(0.5in)
Min. and Max. in patient direction 27.9-36.4mm(1.1-1.435 in)

Brain Reach

Distance from edge of detector housing to edge of FOV 7.6cm(3 in)

Technical Data

<i>HD3 High-Definition Digital Detector</i>		<i>System Spatial Resolution without</i>	
<i>NEMA Specification</i>		<i>Scatter with LEHR Collimator</i>	
<i>Performance Standards</i>		FWHM in CFOV $\leq 7.4\text{mm}$	
<i>Intrinsic Spatial Resolution</i>		FWHM in CFOV $\leq 14.1\text{mm}$	
FWHM in CFOV	$\leq 3.8\text{mm}$	<i>System Spatial Resolution without</i>	
FWHM in CFOV	$\leq 3.9\text{mm}$	<i>Scatter with LEHR Collimator</i>	
FWHM in CFOV	$\leq 7.5\text{mm}$	FWHM in CFOV $\leq 8.3\text{mm}$	
FWHM in CFOV	$\leq 7.7\text{mm}$	FWHM in CFOV $\leq 15.5\text{mm}$	
<i>Intrinsic Spatial Linearity</i>		<i>System Planar Sensitivity with LEHR</i>	
		<i>Collimator</i>	
differential in CFOV	$\leq 0.2\text{mm}$	absolute	$\geq 202.\text{cpm/uCi}$
differential in CFOV	$\leq 0.2\text{mm}$	SPECT	Class
		Standards	
absolute in CFOV	$\leq 0.4\text{mm}$	<i>Reconstructed Spatial Resolution with</i>	
		<i>Scatter Using LEHR Collimator</i>	
absolute in CFOV	$\leq 0.7\text{mm}$	center	$\leq 9.5\text{mm}$
<i>Intrinsic Energy Resolution</i>	$\leq 0.9.9\%$	radial	$\leq 10.00\text{mm}$
<i>(typical)</i>			
<i>FWHM in UFOV</i>			
<i>Intrinsic Flood Field Uniformity</i>		tangential	$\leq 7.5\text{mm}$
<i>(uncorrected)</i>			
differential in CFOV	$\leq 2.5\%$	<i>HD3 High-Definition Digital Detector</i>	
		<i>Physical Specifications</i>	
differential in CFOV	$\leq 2.7\%$	Field-of-view (FOV)	53.3x38.7cm
		Diagonal FOV	(21x15.25in.)
			63.5cm (25 in.)

integral in CFOV	$\leq 2.9\%$	<i>Crystal</i>	
integral in UFOV	$\leq 3.7\%$	Size	59.1x44.5cm(23 x17.4in)
Multiple Window Spatial	$\leq 0.6\text{mm}$	Diagonal	69.2cm (27 in)
Registration		Thickness	0.95 cm (0.37 in)
Class Standards		<i>Photomultiplier</i>	
<i>Intrinsic Count Rate</i>		<i>Tubes</i>	
<i>Performance in Air</i>		Total Number	59
Maximum count rate	$\geq 240\text{kcp/s}$	Diameter	53-7.6cm (3 in)6-5.1 cm (2 in)bialkali high- efficiency
20% count rate loss at	$\geq 190\text{kcp/s}$	Type	box type dynodes
Intrinsic Spatial Resolution @ 75 kcps		Array	hexagonal
FWHM in UFOV	$\leq 4.1\text{mm}$	<i>Shielding</i>	
FWHM in UFOV	$\leq 7.8\text{mm}$	Back	9.5mm (0.375 in)
<i>Intrinsic Flood Field Uniformity</i> @ 75 kcps		Sides	12.7mm (0.5 in)
differential in CFOV	$\leq 2.5\%$	Min. and Max. in patient direction	27.9-36-4mm (1.1-1435 in)
differential in CFOV	$\leq 2.7\%$	<i>Brain Reach</i>	
integral in CFOV	$\leq 2.9\%$	Distance from edge of detector	housing to edge of 7.6 cm (3in) FOV
integral in UFOV	$\leq 3.7\%$		

Technical Data

<i>Acquisition Parameters</i>	<i>Static</i>	<i>Gated Planar</i>	<i>Dynamic</i>	<i>Whole Body</i>	<i>SPECT</i>
Matrix Size	Up to 1024	up to 128	up to 256	up to 1024	up to 128
Max # of View/ Frames. Etc.	20 views 2 detectors 4 windows (3 scalers)	64 frames 1 detector 4 windows (3 calers)	32 phases 2 detectors 4 windows (3 scalers)	1 view 2 detectors 4 windows (3 scalers) max. 224cm/min.	360 views 2 detectors 4 windows (3 scalers) min 1° steps
Motion				max 202 cm length	
Stop Conditions	time, counts	time, counts beats	time/frame	scan length	time/view 1 st view by counts
<i>LCD Flat Panel Display</i>		<i>ECG Input</i>		<i>Analyzer Control</i>	
• Rotation Angle	• TTL Signal Input	• Send and Receive from DICOM-Compliant NM processing Workstation(wip)		• 6 Energy Windows Provide UP to 4 Energy Images.	
• Detector Radius	• 0 to + 5 Volt	• ICON-Direct Interface via ICON ACR-NEMA v.2 File Format		• off-Peak Window Setting	
• Detector Tilt	Negative and positive Trigger	• Optional Interfile v.3.3		• Energy Spectrum Display	
• Patient Bed Position		<i>Max. Acquisition Count Rate</i>		• User-Definable Isotope Settings.	
• Patient Bed Height	<u>ECG Gating</u>	• 240 kcps per Detector		<i>Predefined Acquisition Protocols</i>	
• Gantry Lateral Position	• F/W or B/W Framing in Planar Mode.	• 480 kcps Total		• Analyzer setting	
• Analyzer Energy setting	• F/W or B/W by Percentage Framing in SPECT Mode	<i>Zoom Selections</i>		• Motion Parameters	
• Collimator	• Buffered Bear Window	• 1, 1.23, 1.45, 1.78 2.2.29, 2.67, 3.2		• Study Parameters <i>Maximum Number of Images Displayed</i>	
• Zoom Setting	• Bad beat Rejection	<i>Hardware</i>			
• Attenuation Source "On" Indicator	• Number of Frames per R-R Interval of Milliseconds per Frame	• 43cm(17 in) Monitor		64x64	1088
		• keyboard		128x128	320
		• Monitor		256x256	80
				512x512	20
				1024x1024	5
				256x512	40
				256x1024	20
				512x1024	10

<p>Cont.....</p> <ul style="list-style-type: none"> • Elapsed Time • Time Remaining 	<ul style="list-style-type: none"> • Automatic or manual Selection of Beats Acceptance window • Integrated EGG Port Conveniently plugs into Bed. Eliminating Any cable obstruction. 	<p>SPECT Acquisition Model</p> <ul style="list-style-type: none"> • 90° for Variable-Angle Model only (76°WIP) • continuous • Acquire During step
<ul style="list-style-type: none"> • View Number • Count Rate • Patient Positioning Monitor, -256 Matrix. -Window and Persistence Adjustment <p>Acquisition Memory</p> <ul style="list-style-type: none"> • 64 MB <p><i>Flat Panel Display Modes</i></p> <p>Gantry Display</p> <ul style="list-style-type: none"> • Acquisition Display <ul style="list-style-type: none"> • Patient Positioning Display • Zoom Setup Display 	<p>Local Storage</p> <ul style="list-style-type: none"> • > 2GB Local Disk for Storage of Patient Data. <p>Connectivity</p> <ul style="list-style-type: none"> • Ethernet Networking Protocols • Thin wire(10BASE2) Unshielded Twisted Pair (UTP or 10 ASET) • Thick wire 10BASE5) 	<ul style="list-style-type: none"> • Step and shoot • Circular • Auto color

<i>Collimator</i>	<i>High Sensitivity</i>	<i>LEAP</i>	<i>High- Resolution</i>	<i>Ultra- High Res.</i>	<i>Fan beam</i>
	^{99m} Tc	^{99m} Tc	^{99m} Tc	^{99m} Tc	^{99m} Tc
Hole Shape	Hex	Hex	Hex	Hex	Hex
No. of Holes	28	90	18	146	64
Hole length(mm)	24.05	24.1	24.05	35.8	35
Septal Thickness (mm)	0.36	0.20	0.16	0.13	0.16
Hole Diameter(mm across the flats)	2.54	1.45	1.11	1.16	1.53
Sensitivity@10cm(cm m / μ Ci)	1063	350	202	100	300
Geometric Resolution @10 cm(mm)	14.6	8.3	6.4	4.6	8.8/8.3 *
System Resolution @10 cm(mm)	15.2	9.2	7.5	6.3	9.6/8.7 *
Septal Penetration(%)	1.5	1.9	1.5	.8	1
Focal length@ exit Surface(mm)	n.a	n.a	n.a	n.a	445
Weight in lb	42	49	45	56	100
Weight in kg	18.9	22.1	20.4	25.2	45.0

<i>Gad SPECT</i>	<i>Whole Body SPECT</i>	<i>System Options</i>	<i>E.CAM single-Head</i>	<i>E-CAM Dual-Head 180⁰</i>	<i>E-CAM Dual-Head Variable Angle</i>
Up to 128 60 vws/16 frames detectors windows (1 scaler) min. 1 ⁰ steps Time/view Acceptable beats	up to 128 360 views 2 detectors 4 windows (3 scalers) min. 1 ⁰ steps max. 5 SPCTs time/view	<i>System</i>			
		Left of Right Sided			
		Access Patient Bed	•	•	•
		Profile Attenuation			
		Correction		•	•
		ECAM ⁺			
		Coincidence			
		Imaging Package		•	
		Variable- Angle			
		Upgrade	•		
		Dual-Head Upgrade	•		
		<i>Collimator</i>			
		Low-Energy			
		High-Sensitivity	•	•	•
		Low-Energy All Purpose	•	•	•
		Low-Energy High-Resolution	•	•	•
		Low-Energy Ultra-High-Resolution	•	•	•
		Medium-Energy High-Energy	•	•	•
		Extra High- Energy	•	•	•
		Fan beam	•	•	•
		Pinhole	•	•	•
		<i>Accessories</i>			
		WholeBody SPECT			
		Acquisition	•	•	•
		Remote Access	•	•	•
		ECG Trigger Unit	•	•	•
<i>E.CAM⁺ Nal Coincidence Package</i>					
• PET-based HD3					
Detector Technologies					
• Ultra-Hith-Efficiency 5/8 in. Nal Crysals					
• Iterative Reconstruction					
• Fully Intergated Software					
• Predefined Acquisition and reconstruction Protocols • Multiple Rotations per Field-of-View.					

<i>Collimator</i>	<i>Pinhole</i>		
	^{99m} Tc	¹²³ I	¹³¹ I
Hole Shape	Round	Round	Round
Number of Holes	1	1	1
Hole Diameter (mm)	4,6,8	4,6,8	4,6,8
Cone Length (approx. in mm)	200	200	200
Diameters at Base of Cone (approx. in mm)	300	300	300
Sensitivity @ 10cm with 4mm (cpm/Uci)	123	111	67
Sensitivity @ 10cm with 4mm (cpm/Uci)	271	243	133
Sensitivity @ 10cm with 4mm (cpm/Uci)	478	426	221
Geometric Res. @ 10 cm with 4mm (mm)	6.2	6.3	7.5
Geometric Res. @ 10 cm with 6mm (mm)	9.3	9.3	10.6
Geometric Res. @ 10 cm with 8mm (mm)	12.3	12.4	13.6
System Res. @ 10 cm With 4mm (mm)	6.6	6.6	7.6
System Res. @ 10 cm With 6mm (mm)	9.5	9.5	10.7
System Res. @ 10 cm With 8mm (mm)	12.5	12.5	13.7
Weight in lb.	165	165	165
Weight in kg	74.3	74.3	74.3

Collimator Server(w/o collimators)

Height	132.1cm (4ft. 4in.)
Width	110.5cm (2ft.7.5in)
Depth	110.5cm (2ft.7.5in)
Weight	120.2kg (265lb)

Medium-Energy		High-Energy	Extra High-Energy	
¹¹¹ In	⁶⁷ Ga	¹³¹ I	^{99m} Tc	¹⁸ F
Hex	Hex	Hex	Hex	Hex
32	32	8	7	7
32.84	32.64	50.80	50.50	50.50
0.66	0.68	2	3.4	3.4
2.07	2.07	3.4	2.5	2.5
450	226	104	52	52
9.6	9.1	12.6	8.1	10.6
10.2	10.1	13.1	8.9	10.8
1.9	1.6	3.5	< 0.1	3.4
n.a	n.a	n.a	n.a	n.a
96	96	245	260	260
44.10	44.10	111.10	117.0	117.0

Technical Data

<i>Gantry and Detectors</i>		<i>Patient Bed</i>	
Height	193.0cm (6ft. 4in.)	Width	88.9cm (35.4in.)
Width	167.6 cm (5.ft6 in)	Length	251.5cm (99 in)
Depth	59.4 cm (5 ft 2.75 in.)	Weight	253kg (562lb)
Axis of Rotation (From Floor)	99.00 cm (39 in)	Height	109.2 cm (43.in)
Weight High-Energy Collimator (HE Coll.)	1755 kg (3900lb.)Dual Det. 110 kg (2600 lb) single Det		

Gantry and Detectors		Patient Bed	
Min. Patient Opening(HE Coll.)	9.0 cm(3.5 in.)	Pallet Material	Aluminum
Min. Patient Opening(HR Coll.)	14.0 cm(5.5in.)	Pallet Thickness	2.54mm(0.1in.)
Max.Patient Opening(HE Coll)	62.0 cm (24.4in.)	Pallet Width SPECT	35.6cm(14in.)
Max. Patient Opening(HR Coll)	67.0 cm (26.4 in.)	Pallet Width Whole Body	63.5cm(25 in.)
Average Auto contour Distance	1.1cm(0.45 in.)	Attenuation @140keV	< 7%
Max.Radial Seed	120 cm/min. (47.2 in./min.)	Max. Patient Weight	180kg(400lb.)
Max. Lateral Position Left	5.1 cm (2 in.)	Max. Deflection of Patient Pallet	< 3.2mm (< 0.125 in.)
Max. Lateral Position Right	22.9cm (9 in.)	Vertical Motion Range	48.3-110.5cm (19.0-43.5 in.)
Max. Lateral Speed	22.9cm/min. (47.2 in./min.)	Max. Scan Length in Whole Body Mode	202cm(79.5 in.)
Single-Head,Duel-Head 180°and Duel-Head Variable Angle		Maximum Vertical Speed	120 cm/min. (47.2 in./min.)
Max. CW Rotation Det.1(as seen from patient bed side, detectors at 180° opposed position start with detector 1 on top).	440°	Horizontal Motion Accuracy	0.4mm(0.016in.)
Max. CCW Rotation Det.1(as seen from patient bed side, detectors at 180° opposed position start with detector 1 on top).	30°	Horizontal Motion Range	164.5cm (5ft.4.75 in.)

<i>Variable –Angle E.CAM</i>			
Max. CW Rotation Det.1(as seen from patient bed side, detectors at 90° cardiac position start with detector 1 on top)	350°	Maximum	240 cm/min.
		Horizontal Speed	(94.5 in./min.)
Max. CCW Rotation Det.1(as seen from patient bed side, detectors at 90° cardiac position start with detector 1 on top)	120°	Minimum	0.1 cm/min.
		Horizontal Speed	(0.040 in./min.)
Ring Rotation Range	470°	<i>Rear Pallet Support</i>	
Rotational Accuracy	0.1°	Width	35.6 cm (14 in.)
Max. Rotational Speed	3 RPM	Length (with bar in)	110.9 cm (43.7 in.)
Min. Rotational Speed	0.33 RPM	Length(with bar out)	163.1 cm (64.2 in.)
Centre of Rotation	≤ 0.25 pixel(64x64 matrix)	Weight	49 kg(109 lb)
Max. Caudal Tilt(Outward)	90°	<i>Electronic Enclosure</i>	
Max. Caudal Tilt(Inward)	20°	Height	105.4 cm (41.5 in.)
		Width	55.9 cm(22 in.)
		Depth	52.3 cm (20.25 in.)
		Weight	99kg(220 lb.)

System Environment Requirement

Floor Loading Single-Head, Duel-Head 180°and Duel-Head Variable Angle	0.073kg/sq.cm(150lb./sq.ft.)
Power Rating	50-60Hz 3.0 kVa,30 Amp. Single Phase Service
Heat Dissipation	7200 Joules/hr. (6800 BTU/hr.)
Temperature Range	15.5°-35°C (60°-95° F)
Max. Temperature Variance	4.4° C/hr. (8°F/hr.)
Humidity	15-80% non-Condensing

